Master of Science Thesis

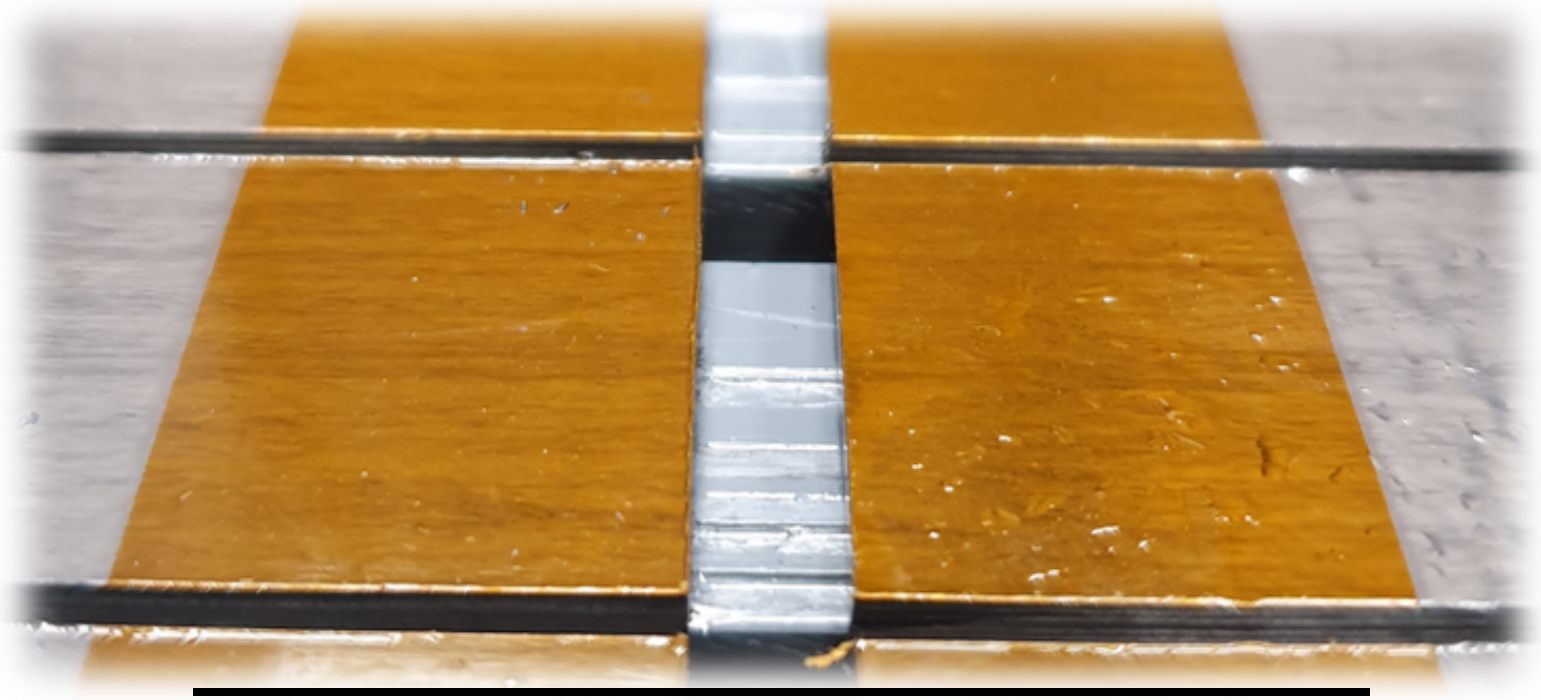

Investigating the Degree of Crystallinity in Ultrasonically Welded Thermoplastic Composite Joints

Alexander de Bruin

July 20, 2020

TU Delft

Faculty of Aerospace Engineering

Delft University of Technology

Investigating the Degree of Crystallinity in Ultrasonically Welded Thermoplastic Composite Joints

Master of Science Thesis

For obtaining the degree of Master of Science in Aerospace Engineering
at Delft University of Technology

Alexander de Bruin

July 20, 2020

Faculty of Aerospace Engineering · Delft University of Technology

Delft University of Technology

DELFT UNIVERSITY OF TECHNOLOGY
DEPARTMENT OF AERODYNAMICS

The undersigned hereby certify that they have read and recommend to the Faculty of Aerospace Engineering for acceptance the thesis entitled **"Investigating the Degree of Crystallinity in Ultrasonically Welded Thermoplastic Composite Joints"** by **Alexander de Bruin** in fulfillment of the requirements for the degree of **Master of Science**.

Dated: July 20, 2020

Supervisors:

Dr. I. Fernandez-Villegas

Prof. C.A. Dransfeld

Dr. M. Nijemeisland

Preface

I would firstly like to thank Dr. I. Fernandez-Villegas for giving me the opportunity to research this very interesting topic. Her guidance and her close attention to my results motivated me to contribute to her composite welding research group, and not only see this as a requirement that I have to fill in order to receive my MSc. degree. I would also like to thank all the researchers in the group for their frequent help. Secondly, I would like to thank Prof. C.A. Dransfeld for all of his guidance during the research. His expertise provided new perspectives for me to explore, and broadened my field of view.

I would also like to thank the staff of the Delft Aerospace Structures & Materials Laboratory who have helped me during my project. I would like to particularly thank Dr. M. Nijemeisland, who helped me to develop certain aspects of my methodology and interpret my results.

Finally, I would like to thank all those who are close to me. My parents have shown a lot of patience over my years as a student and have always supported me. I thank my girlfriend Nena, who kept me sane as I was dealing with the difficulties associated with my thesis. And of course, I am thankful for my friends. A special shout-out goes to Val, without whom I would still be attempting to fix Latex and Matlab bugs to this day!

Summary

Ultrasonic welding (USW) is a fusion bonding technique that works by applying high-frequency low-amplitude vibrations to the weld area. It can be used to join thermoplastic composites, and is attractive for the aerospace industry because consistently high strength joints can be made under very short times (0.1-1 second) compared to other methods. To be used industrially for this purpose, its complex heating mechanisms need to be better understood. Another aspect which is not well understood yet is how the crystallinity of the polymer matrix will be affected by the welding process. This MSc. thesis therefore researches the effect of USW on the degree of crystallinity (DOC) of uni-directional carbon fibre reinforced Lower Melting Polyaryletherketone (LM PAEK), a relatively new high performance thermoplastic composite.

The same topic was investigated in N. Koutras' state-of-the-art research for carbon fibre reinforced PPS, but only analysed the energy director (ED) from the weld interface. The research presented in this paper aimed to also investigate locations through the thickness of the joint away from the weld interface, to see how the degree of crystallinity varied and if it was influenced by the carbon fibres. A methodology was developed to achieve this aim, by using adherends with co-consolidated polyimide films. The films facilitated thermocouples to be inserted between the adherends' composite plies, and created a section that could be removed after welding for Differential Scanning Calorimetry (DSC) analysis. However, the temperature measurements suggest that the inclusion of thermocouples and polyimide films interfered with the temperature evolution in the joint during welding, and therefore affected the final DOC results.

Three locations in the joint were investigated; the weld interface, between the 1st and 2nd composite ply, and between the 4th and 5th composite ply. Two sets of welding parameters were used; one with a high force and amplitude, and the other with a low force and amplitude. It was unexpected that the DOC did not have a clear relation with cooling rate as was hypothesized based on polymer crystallisation theory and the state of the art. Instead, it is suspected that the final DOCs were affected more by crystal melting and superheating during the heating phase rather than re-crystallisation during cooling. This was supported by a noticeable trend between the DOC and the integration of the temperature curves over their time in the molten phase. Higher integrations generally resulted in lower DOCs. However, scatter in the results makes it difficult to be sure that this trend applies to all the weld cases. Further research and improvements to the methodology are suggested in order to confirm this

speculation and better understand the crystallisation kinetics of LM PAEK composite during USW.

Table of Contents

List of Figures

List of Tables

List of Abbreviations

CF	Carbon Fibre
CTE	Coefficient of Thermal Expansion
DASML	Delft Aerospace Structures & Materials Laboratory
DOC	Degree of Crystallinity
DSC	Differential Scanning Calorimetry
ED	Energy Director
H	High welding force and amplitude
L	Low welding force and amplitude
LM PAEK	Low Melting Polyaryletherketone
LSS	Lap Shear Strength
PEEK	Polyetheretherketone
PEI	Polyetherimide
PPS	Polyphenylene sulfide
Pre-Preg	Pre-impregnated fibres
TCL	Transcrystalline layers
TPC	Thermoplastic Composite
T_g	Glass transition temperature
T_m	Melting temperature
UD	Uni-direction (fibres)
USW	Ultrasonic Welding
WAXD	Wide Angle X-Ray Diffraction
XRD	X-ray diffraction

Chapter 1

Introduction

Ultrasonic welding is a fusion bonding technique that has already enjoyed extensive industrial use for neat thermoplastic polymer products, but is not yet mature enough for industrial use on thermoplastic composites. This limits its current use as a joining method in the aerospace industry, despite promising advantages for processing ease and final joint result. This MSc. thesis report addresses a specific engineering problem for the ultrasonic welding process:

We do not know what the state of crystallinity is of a thermoplastic composite joint formed by Ultrasonic Welding.

The material chosen for the subject of this research is carbon fibre uni-directional Low Melting Polyaryletherketone (LM PAEK) composite, provided by Toray Advanced Composites [2]. LM PAEK is a relatively new polymer matrix by Victrex that has similar mechanical properties to other high performance thermoplastics such as PEEK and PEKK, but with a lower processing temperature that saves energy in production [3].

1.1 Motivation for Research

The benefit of thermoplastics have been known for a very long time, and the motivation for increasing their use in aircraft over thermosets involve their impact toughness, chemical resistance, low water uptake and thermal stability. However, a list of drawbacks such as high melt viscosity and challenging repair strategies have made their implementation slow over the years leading up to the current millennium [4, 5]. In 1993, a paper [6] stated that TPC were proposed as substitutes for thermosetting composites, for which manufacturing process models already existed [7], due to their properties and processing opportunities. In the year 2000, a review on the advances of fusion bonding techniques [8] claimed that TPC were then regarded as candidates for primary structures.

Fast forwarding a mere 14 years, an article on Composites World that summarises a market report by Composites Forecasts & Consulting LLC shows that TPC was then already present in almost every part of the aircraft market, having increased in demand by roughly 400% [9]. Popular civil aircraft such as the Airbus A340-600, A380, and Boeing 787 entering services respectively in 2002, 2007 and 2009 all use a significant amount of TPC skins, ribs, angle brackets, clips and cleats. Furthermore, their presence in the aircraft cabin interiors market is expected to double or triple by 2023. It is therefore evident that the development and maturing of thermoplastic manufacturing and joining techniques is very important to support this foreseen growth in market demand.

It is well accepted that traditional joining techniques for metals, particularly mechanical fastening, are ill suited for both thermoset and thermoplastic composite structures. The low plasticity of both the fibres and polymer matrix compounds stress concentrations, along with other issues such as delamination and differential thermal expansion. The importance of joining is even greater for TPC, because the higher melt viscosity of the resin makes it difficult to mould large integral parts using infusion processes. It is then much more cost-effective to mould smaller parts and join them together [8].

One common joining category is called fusion bonding, and takes advantage of thermoplastic polymers' ability to melt and cool back to solid form. Even at the start of this millennium, fusion bonding of polymers was already considered to be a long established technology with a significant market share in the 60s [10]. The three main methods of fusion bonding that became most applicable to TPC structures are: resistance welding, induction welding, and ultrasonic welding (USW) [11]. These three proved advantageous over other methods such as spin welding or vibration welding, because of the opportunity to localise the heat to the welding interface, which makes for a more controllable process [8]. For welding reinforced composites, both resistance welding and induction welding are being used industrially, but USW it is not matured enough to be used industrially [11]. Given it's numerous advantages over other joining methods, further maturing it is of interest to the future of the TPC market. One of the aspects that is not yet well understood is how the USW process affects the crystallinity in the joint.

1.2 Research Questions & Sub-questions

How does the Ultrasonic Welding process affect the degree of crystallinity at the weldline and adjacent plies of Carbon Fibre Reinforced LM PAEK composites?

1. **How is the temperature evolution and cooling rate distributed through the plies starting from the weldline?**
    - How can thermocouples be introduced into the joint?
    - How do the amplitude and force parameters affect this?

2. **How can samples be extracted from the joint and be prepared for measurements in DSC analysis?**
    - How can the effect of the fibres be included in the sample?
    - How does the sample extraction system interfere with the temperature measurements and DSC analysis?

3. **How is the degree of crystallinity distributed through the plies starting from the weldline?**
    - How do the amplitude and force parameters affect this?
    - How comparable can the results be to the latest research, considering differences in methodology?

4. **What correlations can be found between the cooling rates and the degrees of crystallinity?**
    - Are these correlations affected by the location through the plies, and the amplitude and force parameters?

1.3 Structure of Report

This report first gives a brief literature review in chapter 2 that serves as background information regarding USW and polymer crystallinity, as well as discussing the state of the art. The final methodology is described in chapter 3, with supplementary information about the development of the methodology in appendices A and B. The experimental results are presented in chapter 4. Then, the results are analysed and discussed with relation to the research questions in chapter 5. Finally, conclusions and recommendations for further research are given in chapter 6.

Chapter 2

Literature Review & Research Questions

The first stage of this thesis research was an extensive literature study, to identify the state of the art and knowledge gaps that could be contributed to by new research. This chapter presents a condensed version of that literature review, containing the most necessary topics to understand the work carried out in this research. First, ultrasonic welding (USW) is put into context, by explaining the use of thermoplastic composites (TPCs) in the aircraft industry and their respective joining methods. Then, USW is explained. Next, an introduction to polymer crystallinity is given along with suitable characterisation methods. Then, the state of the art research for crystallinity in ultrasonically welded joints is summarised. Finally, the research questions and hypotheses are given.

2.1 Ultrasonic Welding of Thermoplastic Composites

This section will examine what is known about the USW process for both unreinforced and reinforced thermoplastic polymers. First, the state of the art will be explained including the current limitations. Then, the working principle and the welding stages will be explained. Finally, the main welding parameters will be listed and explained.

2.1.1 State of the Art

For over 50 years already, ultrasonic welding has been a very popular method to industrially weld unreinforced thermoplastic polymer products [10, 12, 13]. In the current day, there is still a motivation to optimize the method because of its potential as an eco-friendly manufacturing process [14]. The myriad of advantages of USW makes it a very promising process for use in the aerospace industry:

- Consistent and high strength quality joints are attainable [15, 16, 13]
- It is the fastest joining technique for TPCs, with rates between 0.1-1 second compared to 30-90 seconds for resistance and induction welding [15, 10, 17].
- No foreign material is required at the interface; a distinction from resistance welding and glass-fibre induction welding which require a metal mesh or susceptor that stays in the weldline [12, 13, 18]
- It is easily automated and well suited for mass production [15, 19, 20, 21]
- Although it has high power requirements, the fast process results in lower energy consumption compared to resistance and induction welding [11]
- It requires minimal labour work and no elaborate ventilation systems [16, 15]

However, for welding reinforced composites, it is not matured compared to resistance and induction welding which are both used industrially [11]. Despite the extensive research in recent years, the complex heating mechanisms are not yet fully understood [12, 22]. A better in-depth understanding is required to reach a higher technology readiness level, which is a necessary step to upscaling the process for industrial use [13]. This will also help efforts to develop a reliable finite element model, whose challenges include obtaining accurate measurements of temperature distribution at the weldline and adherends [22]. These temperature measurements are important in order to calculate the cooling rate, which if outside of the known process-property envelope, will make it difficult to predict the final mechanical performance [23]. For semi-crystalline polymers, this also has an effect on the final crystallinity, which not only affects the mechanical performance but also chemical resistance. The effect of crystallinity will be discussed in detail in the next section.

2.1.2 Working Principle of USW

Two thermoplastic polymer parts can be welded together by applying high-frequency (10-70 kHz) but low-amplitude (10-250 μm) mechanical vibrations transverse to the welding interface [15, 17, 12, 13]. Figure 2.1 labels the different components of the welder to allow this process. The generator first converts the mains line power supply into a high voltage signal at the required welding frequency. The transducer converts the electrical energy of the generator to mechanical vibrations via the use of piezoelectric discs. These vibrations can be amplified by the booster, and by the welding horn depending on the cross section. The welding horn is also known as the sonotrode, whose tip makes contact with the polymer parts to be welded and transfers the ultrasonic vibrations. The vibrations applied by the sonotrode force the polymer to undergo sinusoidal strain. Since polymers have viscoelastic properties, energy is dissipated through intermolecular friction and hysteresis [8]. The viscoelastic heating can be calculated through equation 2.1 [15]:

$$Q_{avg} = \omega \epsilon_0^2 E'' / 2 \tag{2.1}$$

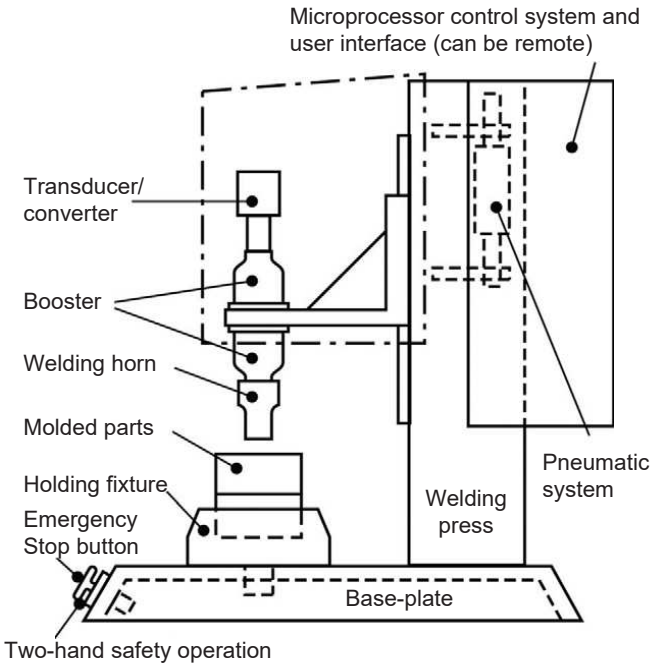

Figure 2.1: Diagram of a typical Ultrasonic Welding setup [15]

Q_{avg} is the average heating rate, E'' is the loss modulus, ω is the frequency, and ϵ_0 is the applied strain. While viscoelastic friction is the main thermal source for USW [21], heat is also generated through surface friction [17, 24].

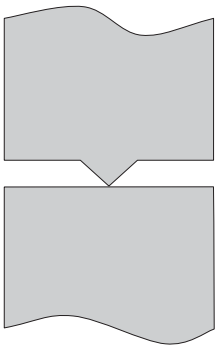

Figure 2.2: Basic form of a triangular energy director at the welding interface [15]

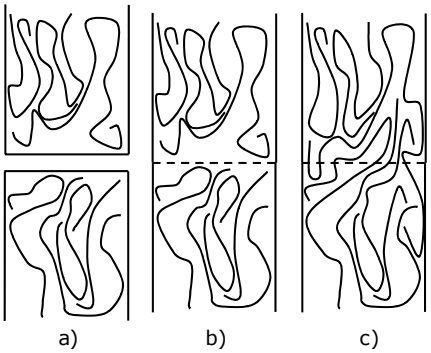

Figure 2.3: Fusion of two polymer interfaces, being distinct in (a), achieving intimate contact in (b), and autohesion in (c) [8]

To focus the ultrasonic energy at the welding interface, energy directors are used. This is an essential consideration in the joint design of both unreinforced and reinforced polymers, because there is otherwise potential for excessive uncontrolled energy dissipation [10, 20, 21]. Traditional energy directors for unreinforced polymers take the form of triangular protrusions

made from the same polymer, and are moulded onto the interface (figure 2.2). Many different configurations have been researched, but the most important principle is that the lower stiffness of the protrusion allows it to undergo preferential deformation and thus viscoelastic friction.

For TPCs, flat energy directors have proven to be an effective and straightforward alternative, or even improvement, to traditional triangular ones [25, 12, 13]. The reinforcement in the adherends make them much stiffer than any neat resin introduced. Therefore, a flat film of neat resin will undergo preferential deformation, and heat first visco-elastically [17, 12, 13, 16, 19]. A diagram of a flat ED in position prior to welding is shown below in figure 2.4.

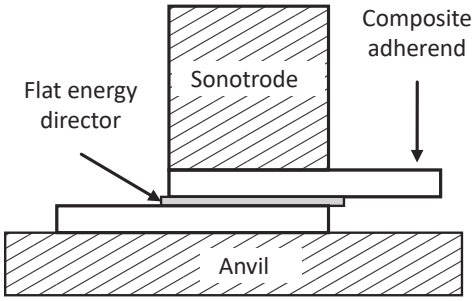

Figure 2.4: Flat energy director in position prior to welding [13]

2.1.3 Stages of the Welding Process

Power and displacement data from modern microprocessor-controlled ultrasonic welders has been used to distinguish 5 stages of the USW process, which are also visualised in figure 2.5 [13, 12, 17].

1. **Heating of ED:** The ED is heated but there is low displacement and little observable physical changes at the interface. The dissipated power continuously increases until a maximum.
2. **Gradual melting of ED:** The ED starts to melt as surface friction triggers viscoelastic friction (which is maximised around Tg [22]). The dissipated power decreases step-wise while the displacement remains constant.
3. **Flow of molten ED:** The ED is now molten and can flow, thus the sonotrode displaces downwards and squeezes it out. The power increases during this stage.
4. **Gradual melting of resin on first composite ply:** this is the requirement for autohesion to occur. Therefore, this is the minimum stage that must be reached for a proper weld, while simultaneously being the stage that maximum LSS is achieved. The sonotrode displacement continues while the dissipated power plateaus.
5. **Flow of resin on first composite ply:** A sensitive stage, since excessive flow of the resin in the adherends can cause fibre disruption and a decrease in LSS. The displacement continues to squeeze molten polymer from the interface while the power drops.

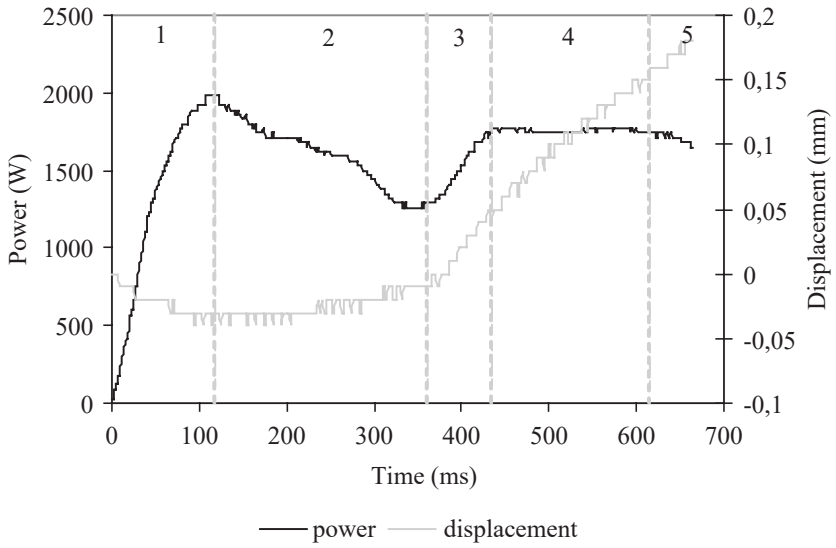

Figure 2.5: Power/Displacement-Time curve for different stages of the USW process (CF/PEI) [12]

2.1.4 Welding Parameters

The main parameters that can be controlled in modern ultrasonic welders and will impact the final weld quality are: frequency, force, amplitude, time, and displacement. The frequency is usually fixed per machine, and can range between 15 and 70 kHz [26, 27]. Lower frequency welders have a higher power capability, and are thus better for welding structural components [15]. A sufficiently high force is important to properly transfer the vibrational energy from the sonotrode to the adherends by maintaining contact. The trigger force is the initial force, the build-up rate can vary the force over the weld cycle, and the hold force is the final maintained force after vibrations stop. A sufficiently high amplitude is necessary to initiate melting uniformly and avoid premature solidification. Since the applied strain is directly proportional to the amplitude of the vibration, a higher amplitude results in faster heating [28, 24]. If welding process is time-controlled, then the sonotrode will vibrate for as long as the chosen time. If the process is displacement-controlled, then vibration will continue until the sonotrode has travelled to the defined displacement. This method gives the best guarantee that the same amount amount of material is melted each time, and that a desired joint thickness is reached. For both time and displacement controlled welding, there is an optimum value where joint strength is maximised, after which there is either minimal improvement or material degradation [15].

2.2 Polymer Crystallinity

One distinct feature of thermoplastic polymers that opens opportunities to alter their performance is their crystallisation behaviour. This section will first start by highlighting the

importance of crystallinity for both neat and reinforced polymers, and then explaining the science and kinetics behind the crystallisation process. Transcrystallinity due to the reinforcing fibres will then be explained, before giving an overview of the main analysis techniques.

2.2.1 Relevance of Crystallinity

The ability of thermoplastic polymer molecules to crystallise has been recognised since the inception of polymer science [29]. The degree of crystallinity, the size, and the arrangement of the crystallites strongly influence the physical and mechanical properties of both neat polymers and reinforced polymers. Thus, understanding and controlling this crystallinity is of enormous technological importance [29, 30, 7, 31]. While some common polymers such as polycarbonate and acrylic are amorphous, the high performance polymers used for structural TPC in the aerospace industry such as PEEK (polyetheretherketone), PEKK (polyetherketoneketone), and PPS (polyphenylene sulfide) are all semi-crystalline. The heating and the cooling stage that controls the crystallinity is one of the three major steps in TPC manufacturing [7], and provides a means to control the mechanical properties and environmental resistance [32]. It is essential in the design of processing operations in order to ensure final part quality [33, 34].

Most literature, backed by [32, 5, 8, 6], will agree that an increase in the degree of crystallinity will result in:

- Higher modulus
- Higher shear strength
- Higher tensile strength
- Higher chemical/environmental resistance
- Higher thermal resistance
- Lower fracture toughness (such as Mode 1 fracture)

2.2.2 Crystallisation Kinetics

Since this is well understood as a fundamental topic in polymer science, the book Introduction to Polymers [29] has mostly been used to gather this section's information. Crystallisation refers to the process whereby an ordered phase forms from a disordered phase. To understand how polymer molecules crystallise from the melt, we must first consider the thermodynamics of the crystallisation process. The equation 2.2 below shows the relation between the Gibbs free energy (G) of a system and the enthalpy (H), entropy (S) and thermodynamic temperature (T):

$$G = H - TS \tag{2.2}$$

The system is in equilibrium when the Gibbs free energy is at a minimum. Starting from the melt (or a state where the polymer chains are free to move), the polymer chains are randomly

coiled and entangled, so the system will have a high entropy and a low Gibbs free energy. When the chains are cooled from a melt, then they are given the chance to orient themselves into crystal formations. There will be a large reduction in enthalpy (latent heat), although an increase in entropy. If the change in enthalpy is greater than that of the entropy multiplied by the melt temperature, then crystallisation is thermodynamically favoured. This theory only applies to quasi-static processes, so when the chains cool very slowly from the melt. This is rarely the case in most industrial processes, where fast cycle times are favoured. Therefore the cooling rate becomes an important parameter.

There are two main ways that a polymer can crystallise: from solution below the melting point, or from the melt. Solution crystallisation still follows the principles of thermodynamic theory explained above, and is capable of producing polymer single-crystals by precipitation from a dilute solution. In melt crystallisation, the kinetics of molecular chain entanglements is the driving factor. Considering the polymer matrices in TPC and the welding process, only melt crystallisation will be considered in this report.

Semi-crystalline polymers are generally only *semi*-crystalline because of the vast number of chain entanglements in the melt, making it practically impossible for all of them to align even under slow cooling. The first stage of crystallisation is nucleation. As the melt is cooled to the melting point, some of the tangled chains align themselves into small regions called nuclei that are only stable below the melting temperature. Although nucleation can theoretically take place homogeneously at random points in the melt, in reality it happens heterogeneously on foreign bodies such as container boundaries or dust particles. It has also been observed that a higher degree of undercooling (faster cooling rate) results in more nuclei.

The second stage of crystallisation is growth. Starting at a nucleation point, the long chains fold in on themselves and form crystallites called lamellae, that extend radially from the nucleation point. If not hindered by geometry or boundaries, then the collective region is spherical in geometry and is thus called a spherulite. They are the dominant feature of melt-crystallised polymers [35], and are visualised below in figure 2.6. For a constant temperature of crystallisation, the radius will grow linearly with time until the boundary reaches another spherulite. However, the temperature of crystallisation itself and molecular mass will dictate the growth rate as well. The growth rate is slow just below Tm, and decreasing the temperature will increase the thermodynamic driving force for crystallisation. However, it will decrease after an optimum because the increasing viscosity will hinder chain movement. Upon inspection with SEM, the spherulites seem very similar to the morphologies of poly-crystalline metals, as shown below in figure 2.7. However, a key distinction is that each crystal in a metal is a single crystal, whereas each spherulite in a polymer has both crystal and amorphous regions. Even a single chain can be part of both crystal and amorphous regions, and are called tie molecules if they bridge lamellae together. There are even more specific features, such as lamellar thickness, twisting and dislocations, but is considered to be too detailed for the scope of this project.

The crystal morphology is also dependent on whether the melt crystallises under stress or flow. For most industrial manufacturing processes, cooling from the melt will rarely happen stress-free. It is generally observed that crystals nucleate along a central backbone and will grow transverse to the direction of applied stress. This gives the crystals an orientation, and

marks a difference from the spherulites reported earlier.

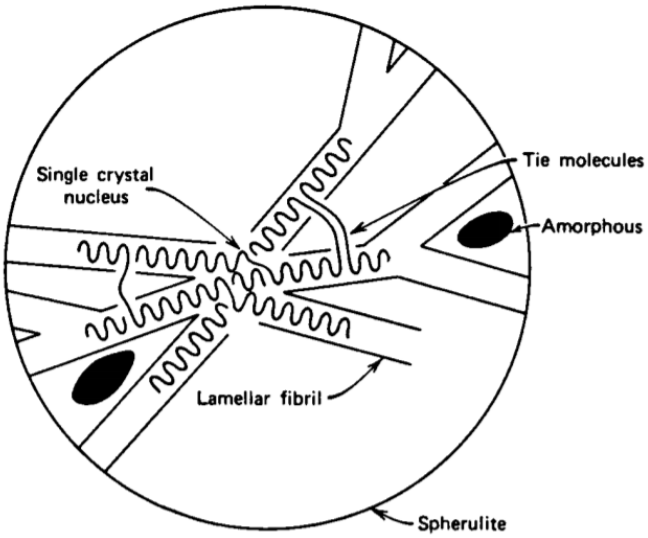

Figure 2.6: Labeled diagram of spherulite features [36]

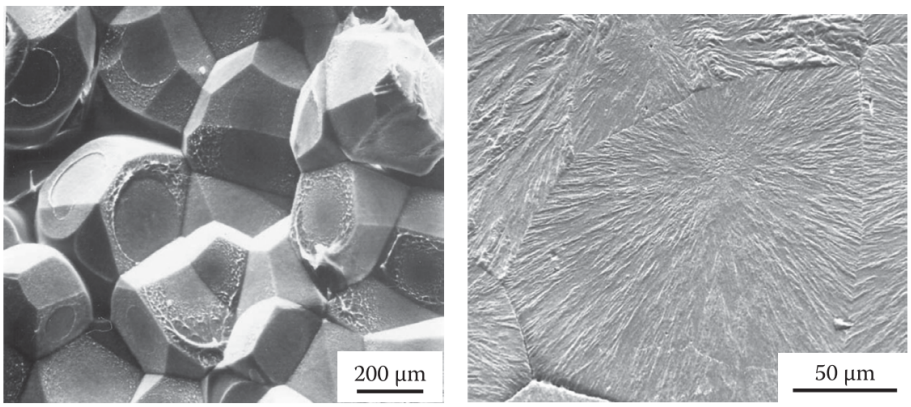

Figure 2.7: Scanning electron micrographs of polypropylene spherulites [29]

It should also be noted that although thermoplastic polymers can be remelted and cooled, the melting temperature (or temperature range) can depend on both its thermal history as well as the the rate of heating. This will thus also change the crystallisation kinetics [6]. It is generally found that a higher degree of crystallinity (and lamellar thickness, though this is not discussed in detail here) will postpone the melting point. Furthermore, just because Tm has been reached and the polymer is in the melted phase, it does not mean that all the crystals have melted yet. If any crystals still remain once cooling initiates, then they can act as nucleation sites [34].

The higher the degree of crystallinity, the higher the density of the polymer. This is because the more the chains align and fold in on themselves (packing), the less space there is between

them. This space is referred to as the free volume, and becomes the basis for the mechanical and chemical behaviour of the polymer. Less free volume means there is less space for foreign chemicals to ingress into the chains, making it more environmentally stable. However, it also means that there is less space for chains to move when absorbing energy from an impact, hence the lower toughness.

2.2.3 Transcrystallinity

Transcrystallinity is a unique crystal morphology that has been observed in fibre reinforced polymers. Since foreign bodies tend to act as nucleation sites, the reinforcing fibres become heterogeneous nucleating agents. When nucleation occurs with a high enough density along the interphase between matrix and fibre, the crystal growth is restricted laterally to the fibre axis, and forms a columnar transcrystalline layers (TCLs) along the fibre. Figure 2.8 below shows a single flax fibre in bulk resin, and how TCLs form along its length whereas the surrounding bulk polymer is dominated by spherulites.

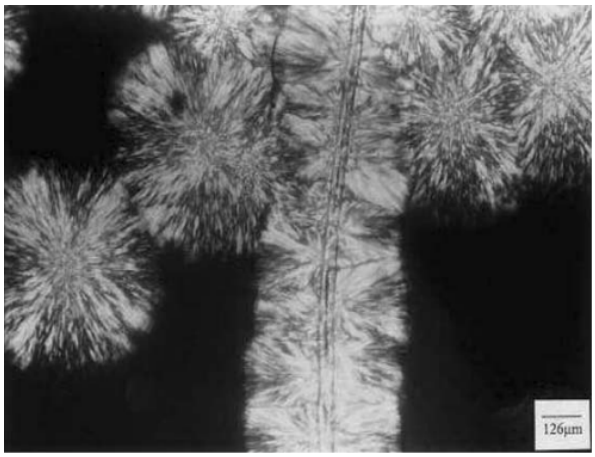

Figure 2.8: Transcrystalline layers forming along the fibre length until they reach spherulites in the bulk resin [37]

Transcrystallinity has already been researched for over half a century, after first being discovered in 1952. A review paper from 2005 [31] summarised a large number of research papers over the years and provides an excellent insight into our understanding of he phenomenon. Research has been conducted on carbon fibres reinforcing higher performance thermoplastics such as PEEK and PPS, as well as natural fibres in softer plastics. However, the formation mechanisms are still not well understood, and its general effects have been debated, making prediction very difficult. Many researchers have reported a significant impact on mechanical properties, especially because of the anisotropy of the crystallites. However, some argue negligible or even negative effects.

It has been observed that TCL is not guaranteed for all TPC, and that it is highly specific to both the fibre, the matrix, as well as the fibre-matrix combination. It is generally agreed

to be dependent on:

- Epitaxy (deposition of crystalline overlayer onto crystalline substrate) between fibre and matrix
- Mismatch of thermal coefficients
- Thermal conductivity of fibre
- Chemical composition of fibre surface
- Surface energy of fibre and substrate
- Crystallinity and molecular weight of substrate
- Processing conditions (temperature, cooling rate, flow field)

For carbon fibres, the surface morphology and thermal conductivity of the fibres may be the leading variables. Small scale grooves on the surface may act as nucleation sites, such as pitch-based carbon fibres (commonly used in aerospace) that features edge-planed grooves. For PAN carbon fibres, it may be attributed more to the thermal conductivity mismatch [38]. This mismatch is greater for fibres with a higher conductivity, that creates supercooling at the fibre-matrix interface because of the lower conductivity of the matrix, which increases the nucleation rate. It was also found that high stiffness fibres induced TCL better than high strength fibres, which strengthens the mismatched expansion during a change in temperature. Interestingly, it was reported that a TCL is observed more strongly for a high cooling rate and low temperature of crystallisation [31].

Even without considering transcrystallinity explicitly, researchers acknowledge that the presence of fibres will modify the crystal morphology and possibly limit the final crystallinity [6, 33]. Differential Scanning Colorimetry measurements in [32] revealed that the limitation on growth reduced the effects of heat treatment on composites compared to neat resins. Data by [34] showed that the crystallisation rates of neat PEEK and reinforced PEEK was actually comparable. If the (carbon) fibre and resin weight fractions are equal, then a competition is triggered between the effects of increasing nucleation sites but decreasing growth space [39]. A dominant fibre fraction is enough to counter the effects of extra nucleation, as [38] found that a 60% fibre fraction limits the growth space too much for the property differences to be profound between unreinforced and reinforced PEEK.

2.2.4 Determination of Crystallinity

The characterisation of polymers is an analytical branch that has produced numerous methods for determining the crystallinity in polymers. While the term 'crystallinity' can be used broadly, it consists of two main categories:

- **Degree of crystallinity (DOC):** The volume ratio of crystal regions to amorphous regions, expressed as a percentage.

- **Morphology of crystallinity:** The shape, size and orientation of crystal/crystallite structures.

This research focuses on the degree of crystallinity, so techniques to analyse the morphology will not be discussed. Some very simple methods can already give an indication of the degree of crystallinity. For example, highly crystalline polymers will be less transparent than more amorphous ones because of diffraction of light through crystal planes [16]. Furthermore, crystal formation increases the polymer density, thus testing the flotation of the sample in a density-gradient column can give an estimate of the degree of crystallinity. However, this assumes that there are zero voids and a homogeneous density, which is rarely the case for manufactured specimens. This section will explain DSC, which is the most commonly used method to calculate the degree of crystallinity.

Differential Scanning Calorimetry is a very important thermoanalytical technique within polymer science to study melting, crystallisation, polymerisation and glass transition [29]. It is considered to be the most popular technique for polymer characterisation, for its advantages; a modest sample size requirement, and its ability to provide quantitative data on reaction kinetics with ease, speed and flexibility [40]. Furthermore, it can be applied to any material that shows a transition over a temperature range, including fibre reinforced composites. It has been used in the studies [41, 7, 32, 33, 5, 40, 37, 39, 23, 16] to measure the degree of crystallinity.

The general working principle is measuring the difference in heat flow to a sample compared to a reference sample as a direct function of time or temperature. There are two types of DSC:

- **Power Compensation / Heat flow DSC:** the sample and the reference are mounted in individual micro furnaces with their own heat sources. The power is kept constant, and the measured heat is compensated by electrical energy. Visualised by figure 2.9 (a).
- **Heat Flux DSC:** the sample and reference are both heated from the same heat source. The temperature difference is measured, and converted to a power difference. The heat flux is kept constant. Visualised by figure 2.9 (b).

The DSC machines will output a plot of heat flow against the temperature. The sign convention of the two methods are opposite to each other because of the differing mechanism. The first small change in heat flow shifts the baseline and corresponds to the glass transition temperature, T_g, due to the absorbed energy to mobilize the amorphous chains [42]. The first major peak corresponds to the cold crystallisation temperature, T_cc, and the second major peak is the melting temperature, T_m. If the polymer contains multiple crystal types/phases, then multiple peaks will represent the crystallisation temperature [5].

For the majority of simple applications, both types of DSC give good data that are comparable. However, each has some slight strength and weaknesses. Power Compensation DSC may be slightly more suitable for measuring the DOC, since ΔH accuracy is higher [42]. The

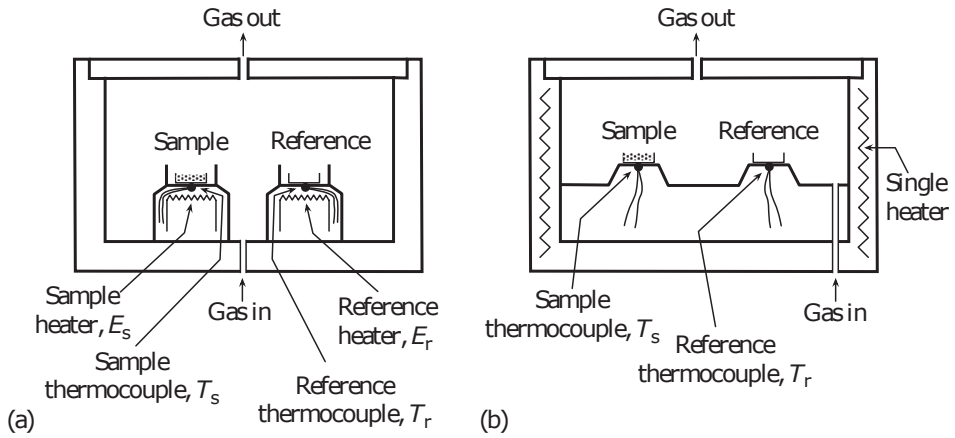

Figure 2.9: Diagrams representing the general physical architectures of (a) Power Compensation DSC and (b) Heat Flux DSC [29]

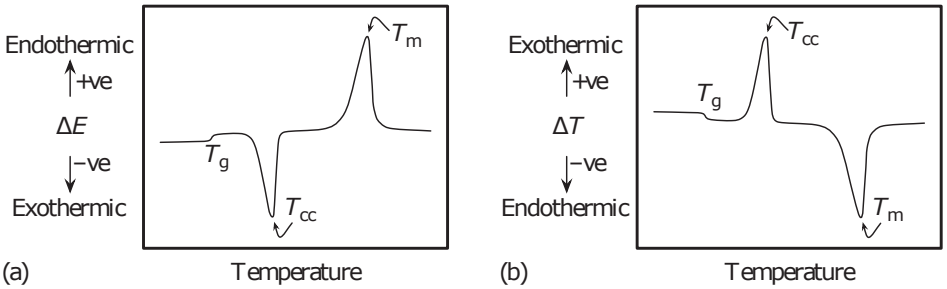

Figure 2.10: Example output curves for (a) Power Compensation DSC and (b) Heat Flux DSC [29]

sample size is limited by the sample pan of the specific machine, but generally a smaller sample (between 5-10 mg) will give a better resolution due to more uniform heating. It is very important that a good physical, and thus thermal, contact is established between the specimen and the pan. Since temperature is measured from the bottom of the pan, a bad thermal contact may result in a heat flow discrepancy or lag between the pan and the sample.

Using DSC to measure the DOC is an indirect method. What is actually measured is the heat of fusion. The sample is first heated from ambient at a controlled rate until T_m to compare the heat of fusion against a reference ideal crystal. The heating phase will recrystallise the sample during the scan, therefore yielding a higher DOC than the true value. Thus, for an amorphous or low expected DOC material, it may be necessary to subtract the exothermic heat of crystallisation from the total heat of fusion. The DOC can be calculated by equation 2.3. For a highly crystalline sample, there may be a secondary endothermic heat of reaction due to an additional crystallization phase. The DOC in this case can be calculated by equation 2.4. [40].

$$\%DOC = \frac{\Delta H_m + \Delta H_c}{\Delta H_f \left(1 - W_f\right)} \times 100\% \tag{2.3}$$

$$\%DOC = \frac{\Delta H_m + \Delta H_a}{\Delta H_f \left(1 - W_f\right)} \times 100\% \tag{2.4}$$

H_m is the endothermic heat of fusion, H_c is the exothermic heat of cold-crystallization, H_a is the endothermic heat of premelt heat of crystallization from the secondary crystallisation phase, and H_f is the heat of fusion for the material's 100% crystalline form. These equations have been modified to include the fibre reinforcements in TPCs, by W_f representing the fibre weight fraction.

Fast scan DSC (FDSC), also called Flash DSC, works on the same principles of power compensated DSC but at much faster heating and cooling rates. For example, Mettler-Toledo now offers chip-based FDSC machines capable of heating rates up to 3 million °C/min and cooling rates up to 2.4 million °C/min [43]. However, the fast rates are partly achieved by measuring samples that are much smaller than for standard DSC, and must be melted onto the chip sensors for effective thermal contact. Having to melt the sample may erase its thermal history to a degree. Therefore, the FDSC is most useful to first use its fast heating or cooling rate to emulate a production process, and then to measure the crystallinity afterwards instead of measuring the as prepared crystallinity. Furthermore, this will be harder to achieve for a composite sample due to the fibre content.

2.3 Ultrasonic Welding and Crystallinity

Polymer crystallinity theory can help predict how USW will affect crystallinity. As for all manufacturing methods, the processing conditions will define the microstructure, type, shape and size of the crystalline structures [8]. The very fast heating rates of USW also result in very fast cooling rates, because of the temperature gradient in the laminate and the contact with the sonotrode. In addition to this, the carbon fibres are especially good thermal conductors along their length and will transfer heat away from the weld region [16]. While researching welding of PPS composite, [11] predicts that this heat transfer should result in lower crystallinity levels, especially compared to resistance and induction welding. This section will summarise the state-of-the-art research, and the methodology that was used to support it.

2.3.1 State of the Art

The only research in open literature on the effects of USW on the crystallinity in the joint is by N. Koutras [16], from the same department at the faculty of Aerospace Engineering at the Delft University of Technology. Koutras' experimental tests assessed The DOC and crystallite size of CF/PPS laminates at the welding interface, for varying welding force and amplitude. A specific methodology was used to obtain the temperature and crystallinity measurements, as summarised below:

- Single thermocouples were embedded into the centre of the EDs prior to welding to measure the temperature evolution.
- Flash DSC was used to emulate the heating and cooling rates of USW on ED material, and subsequently calculate the degree of crystallinity.
- The ED was sandwiched between two Kapton films prior to welding, for extraction and analysis in DSC and WAXS. This is visualised in figure 2.11.

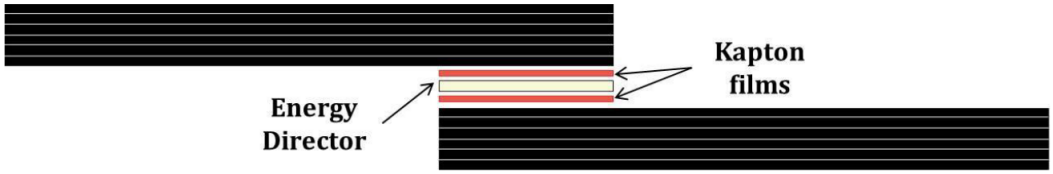

Figure 2.11: Isolation of the energy director using Kapton films [16]

The results are summarised as follows:

- Thermocouple measurements at the weldline reveal that the cooling rate can be reduced by lowering both the welding force and amplitude.
- Flash DSC experiments found that the crystallisation of (neat) PPS is suppressed at a critical rate of 20°C/s, or 1200°C/min. Final DOC was only 0.5%
- DSC and WAXD found the starting (press consolidated) DOC 26% and crystallite size 115.6 Å. For high welding force and amplitude, the resulting weldline was predominantly amorphous (and transparent), DOC 2.4% and crystallite size 25.5 Å. Reducing the welding force and amplitude, and thus the cooling rate, DOC and size up to 14.6% and 41.3Å respectively were obtained.
- Using a low welding force and amplitude still resulted in cooling rates greater than critical one to suppress PPS crystallisation. The crystal formation despite this may be attributed to the high strain rate of USW, but this effect was not tested separately in this research.

2.3.2 Effect of Methodology in the State of the Art

It could be argued that the experimental steps taken in Koutras' research do not adequately represent the interactions that take place in an USW process. The use of Kapton films as part of the methodology was an effective way of ensuring a simple removal of the samples. However, the Kapton films probably interfere with the heat transfer from the weldline to the adjacent plies, and the author acknowledges this. Furthermore, the isolation of the ED from adjacent plies means that the fibres were not analysed as part of the sample. Given the apparent effect that carbon fibres can have on DOC and crystal morphology, discussed in

section 2.2.3, the sample may be missing important interactions. The Flash DSC experiments were also performed with neat resin, which was melted prior to testing. This provides valuable insight into the crystallisation kinetics of the material, but the altered thermal history means that the sample no longer represents an as-manufactured laminate.

Another concern is the suspicion of how thermocouples can themselves act as energy directors and preferentially heat up [11, 12, 13]. This could also contribute to unrealistic temperature distributions. However, given that infrared cameras and other methods cannot be used due to lack of accessibility, this has left researchers little choice, and has been the method of temperature logging in all the literature discussed.

2.4 Research Question Hypotheses

Prior to the start of the experimental campaign, the following hypotheses were made based on polymer crystallisation theory and the state of the art:

1. It was predicted that the maximum temperature, heating rate, and cooling rate will all decrease through the plies away from the weldline. This is logical because the heat generated by USW is focused on the ED, which will experience the greatest temperature and heating/cooling rate. The heat from the ED will then spread to the neighbouring plies, but with insufficient time to homogenise, thus creating a temperature gradient. A higher amplitude and force was expected to produce a higher peak temperature, and higher heating and cooling rate.

2. It was predicted that a methodology could be developed that would allow extraction of samples from the weldline, as well a chosen number of adjacent composite plies. However, it was also foreseen that a practical sample extraction system would require introduction of foreign materials into the joint that may interfere with the temperature evolution and degree of crystallinity.

3. It was predicted that the degree of crystallinity at the weld interface would be much lower than the original degree of crystallinity prior to welding, and increase through the plies away from the weldline. Welding with a higher amplitude and force was expected to reduce the degree of crystallinity.

4. A general trend was predicted: the higher the cooling rate, the lower the degree of crystallinity. This was based on polymer crystallisation kinetics theory, and the results from the latest research. No prediction was made as to whether or how the presence of carbon fibres for samples containing composite plies would affect the degree of crystallinity compared to the neat polymer weldline.

Chapter 3

Experimental Methodology

The development of the methodology was a substantial part of the project that took place in the Delft Aerospace Structures & Materials Laboratory (DASML). It included the trial of multiple concepts that tested ways to measure the temperature during welding, and extract samples for DSC testing. The final developed methodology will be described in this chapter. First, the materials are defined and the working principle of the methodology is illustrated. Then, the steps to manufacture the coupons and energy director are laid out. This is followed by descriptions of the welding setup and procedure, the sample extraction, and DSC procedure. Finally, the data post processing steps are explained.

3.1 Material Definition

LM PAEK carbon fibre composite was provided by Toray Advanced Composites, in the form of a rolled uni-directionl pre-preg sheet, 305 mm wide. LM PAEK neat polymer was provided by Victrex, in the form of a film roll, 700 mm wide. The thickness was not consistent across its width, ranging from 30 - 50 μm. The film's properties are assumed to be identical to the polymer matrix of the composite, since Victrex also supplies the polymer matrix to Toray Advanced Composites. The properties for the composite and polymer are summarised below in table 3.1:

Table 3.1: Properties of LM PAEK T700 Composite and Neat Polymer [1]

T_g	147°C
T_m	305°C
Processing Temperature	365°C
Resin Content (wt)	34%
Crystallization Enthalpy	130 J/g

The 25 μm thick polyimide films were manufactured by DuPont, from here onwards called Kapton film. This was the thinnest film available in the DASML, chosen so that it would add only minimal extra thickness to the coupons. The commonly reported upper temperature limit for Kapton is 400°C [44].

The thermocouples used for temperature logging were K-type, 100 μm diameter wires, and glass-braid insulated. These were the thinnest thermocouples available and chosen to minimise the extra thickness added to the composite joint. The upper (short term) temperature limit of the thermocouples is 1300°C [45].

3.2 Methodology Working Principle

The final methodology of this research was a modification of the state-of-the-art Kapton film method [16], explained in chapter 2. Instead of only isolating the energy director, the Kapton films were moved away from the weldline and into the composite plies, in order to include the carbon fibres into the analysis. Figure 3.1 is a diagram that illustrates the concept. The first step (a) is to pry the composite plies open at the location of the embedded Kapton film, and insert a thermocouple. The second step (b) is the welding process, which will join the coupons at the welding interface but leave the plies adjacent to the Kapton film un-joined. Finally, the third step (c) is to remove the joint section from between the Kapton films, and cut out a sample for DSC analysis. These steps will be explained in more detail in section 3.3.

Three positions of the Kapton films were used in experiments, notated as: **0ply**, **1ply** and **4ply**. The 0ply case is the most similar to the state of the art, as the energy director was sandwiched directly between the Kapton films. Only one thermocouple was used, which was placed at the welding interface. For DSC analysis, only the energy director was analysed. For the 1ply case, the Kapton film is embedded one composite ply on top of the energy director, and one ply below. Two thermocouples were placed, one at each Kapton film location, on the side of the film closest to the welding interface. For the 4ply case, the scenario was the same as for the 1ply case, but ± 4 composite plies away from the welding interface. These cases are visualised in figure 3.2 for added clarity.

A detailed description of the trials of the other concepts that led to this final methodology is given in appendix A. Since LM PAEK composite had not yet been supplied at that stage of the project, the trials were carried out with UD CF/PEEK (polyetheretherketone). They involved removing the Kapton films prior to welding, and embedding the thermocouples during consolidation. The temperature measurements from welding the coupons of these trials also provided useful data that pointed out potential limitations of the final methodology. These results are given in appendix B, but will be used in the discussion in chapter 5.

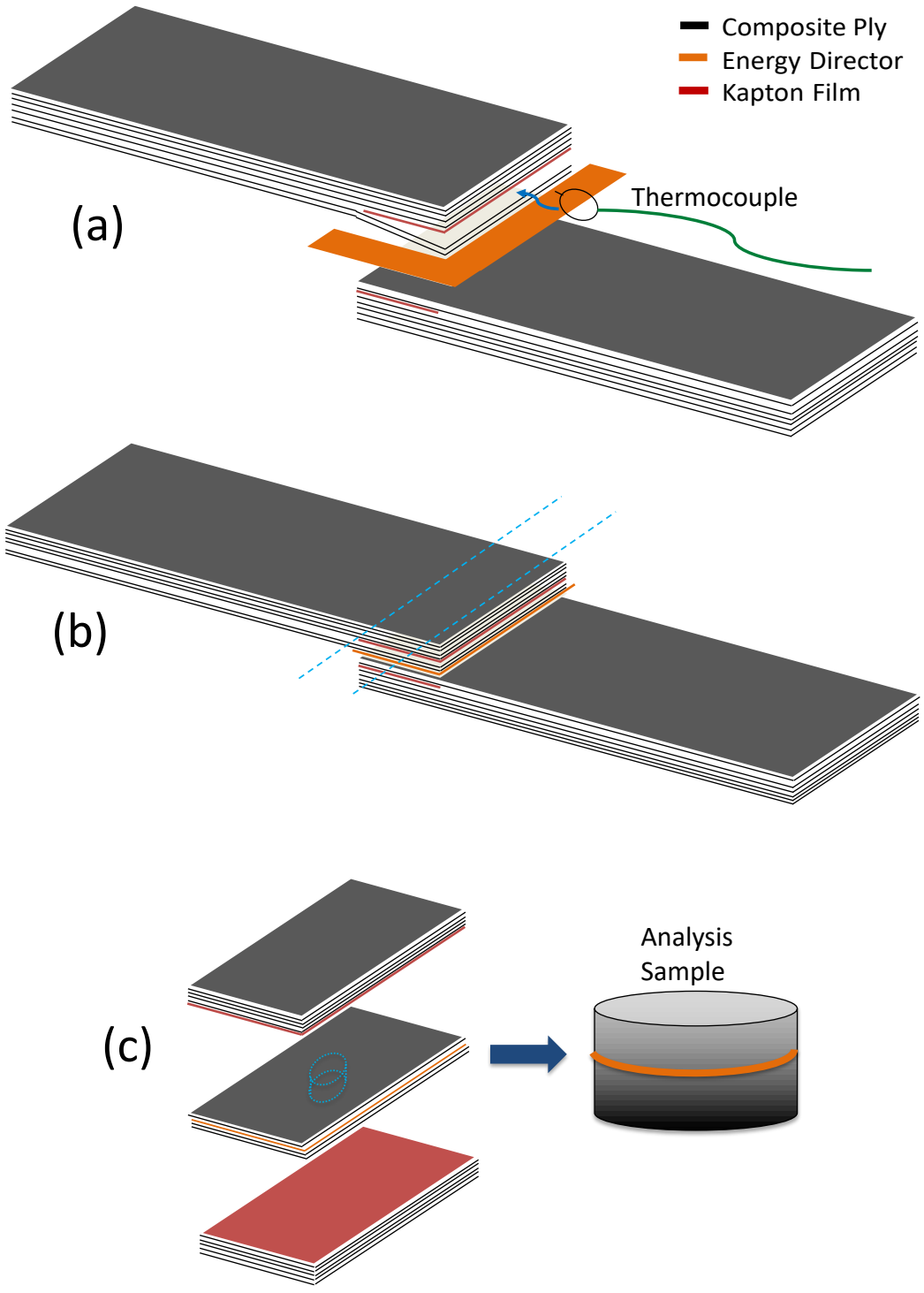

Figure 3.1: (a) Separating composite plies at the Kapton location to insert the thermocouple, (b) Joined coupons after welding, and (c) Removing the joint section from between the Kapton films and cutting out a sample for analysis

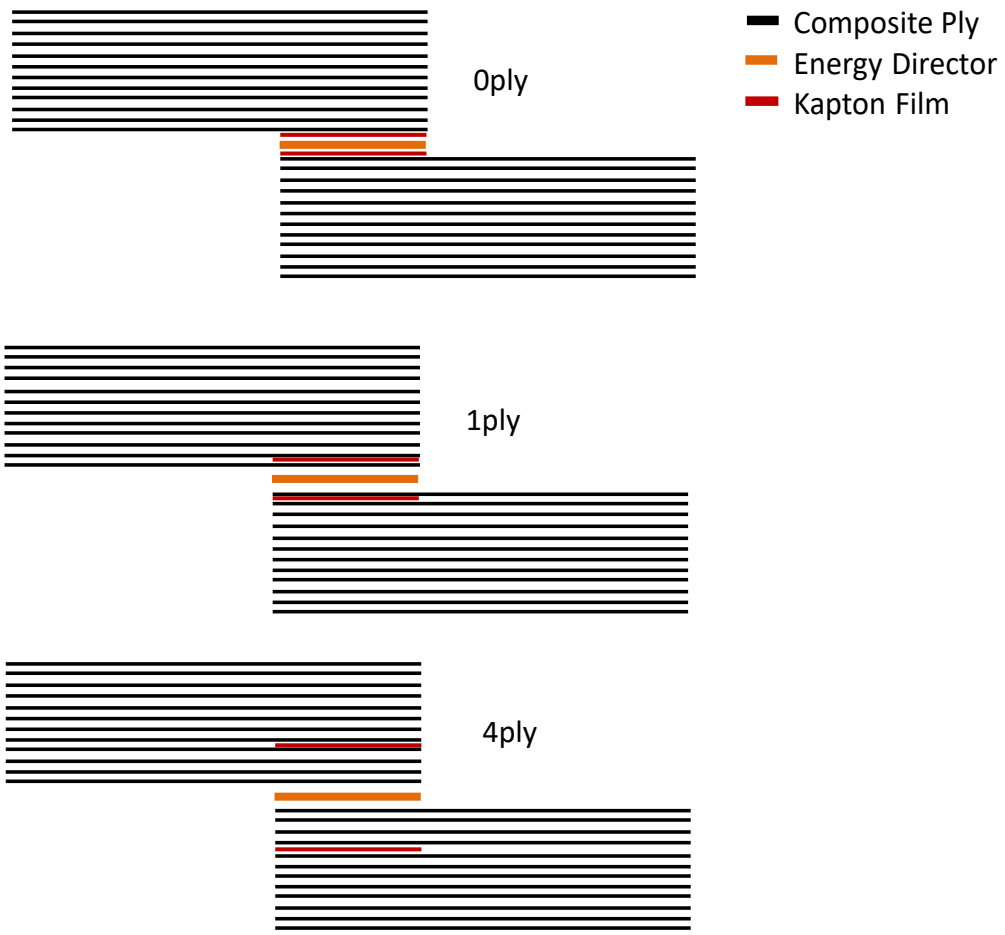

Figure 3.2: The three Kapton positions

3.3 Coupon & Energy Director Manufacturing

First, the steps taken to manufacture the laminates are listed:

1. **Cutting the materials:** The pre-preg roll was cut into square sheets of 305 mm x 305 mm using a hand operated guillotine cutter. The Kapton film was cut into rectangles of 280 mm x 20 mm using a precision knife, and treated with a single Marbocote release agent coating on one side. This coating ensured that the Kapton film consistently separated from the neighboring composite ply closest to the weld interface. This was done so that Kapton film would not interfere with the heat transferring from the weld interface.

2. **Laying up the materials:** The pre-preg sheets were laid up in in a $[0,90]_{3s}$ configuration, and welded in the corners using a RINCO ultrasonic hand welder to prevent them from sliding against each other in the press. The Kapton film ran across the centre of the laminate, as visualised in figure 3.3. Its position between the pre-preg sheets depended on whether the laminate was for 0ply, 1ply, or 4ply cases. The side with the Marbocote coating faced the side of the layup closest to the welding interface. The film was oriented such that the cut coupons will have 0^0 fibres running along their lengths on the outer plies.

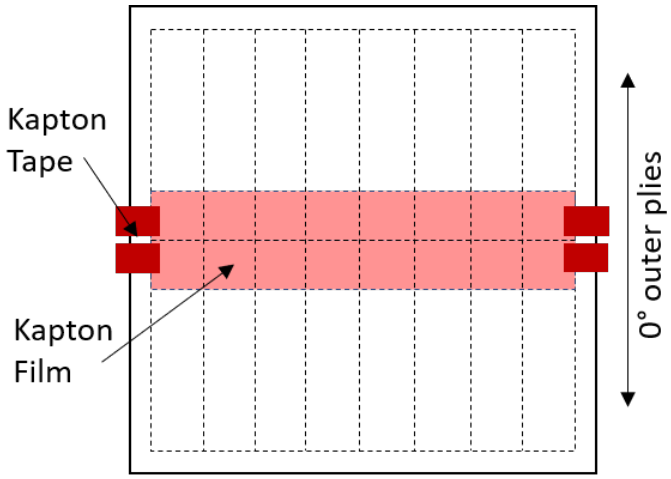

Figure 3.3: Top view of laminate layup

   The Kapton film was fixed in position using Kapton tape on the outer edges of the laminate. Since the Kapton film position is not visible after consolidation of 1ply and 4ply laminates, the tape was aligned such that a centre line for cutting could be identified after consolidation. Finally, aluminium foil was folded over all edges to contain any resin flow-out.

3. **Preparing the pressing stack:** The layup was sandwiched between a steel-graphite layup stack of 300 mm x 300 mm, shown in figure 3.4. The steel plates in contact with the layup were first coated with three layers of Marbocote release agent.

Figure 3.4: Side view of layup in stack for pressing

4. **Consolidating the laminate:** The stack was consolidated in a Joos hot platen press using the cycle shown in figure 3.5. Figure 3.6 shows a consolidated 0ply laminate, which reflects the orientation shown in figure 3.3.

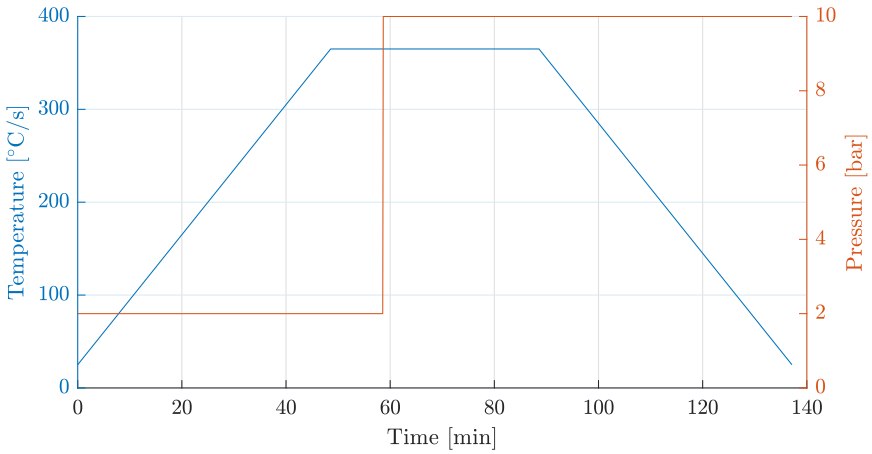

Figure 3.5: Laminate press cycle

5. **Trimming the edges:** The aluminium foil was removed and the Kapton tapes were used to mark a centre line across the laminate. From this centre line, the area of the edges to be trimmed were marked such that the remaining area will fit the nesting scheme shown by the dashed lines in figure 3.3. The edges were trimmed using a CARAT laser-guided diamond-coated circular saw. The edges were smoothed using a utility knife and sand paper.

6. **Cutting the coupons:** The remaining cuts were made with a digitally automatable PROTH column cutter, equipped with a 2mm thick diamond-coated circular blade. First the centre line was cut, and then all the coupons were cut to 101.6 mm x 25.4 mm; the dimensions for lap shear coupons. Figure 3.7 shows the ends of 0ply coupons with the Kapton film, after the cutting process.

7. **Cleaning the coupons:** The edges were once again smoothed with a utility knife and sanding paper. The cooling fluid from the CARAT and PROTH cutters left an oily residue on the coupons, so they were wiped with isopropyl alcohol both on the outer surface and the inner surfaces separated by the Kapton film.

The energy directors were manufactured as follows:

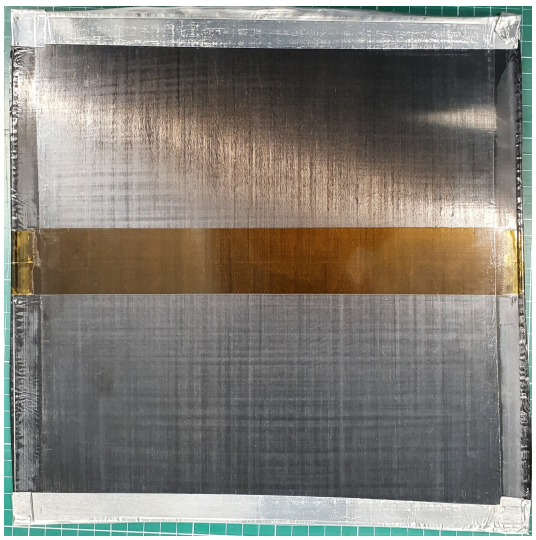

Figure 3.6: Consolidated 0ply laminate with aluminium foil removed from the left and right edges

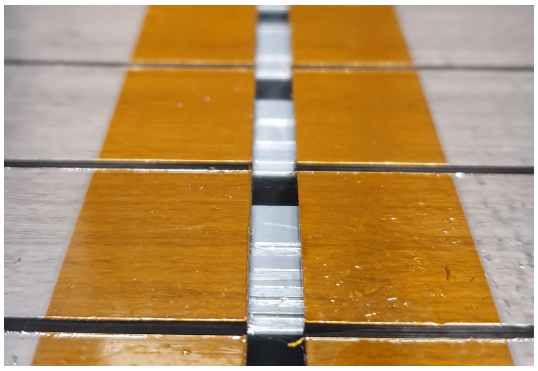

Figure 3.7: Cut 0ply coupons

1. **Preparing the film:** 6 sheets of film of dimensions 300 mm x 300 mm were cut from the roll using a precision knife. Each sheet was cleaned with isopropyl alcohol and checked for dust. If it was excessively static, a steel object was used to remove some static charge.

2. **Preparing the pressing stack:** The sheets were laid on top of each other, and then sandwiched in the same pressing stack used for the composite laminate (figure 3.4).

3. **Consolidating the thicker film:** The stack was consolidated in a Joos hot platen press using the cycle shown in figure 3.8.

4. **Cutting the energy directors:** The consolidated thicker film was cut into 30 x 30 mm EDs using a precision knife and scissors. The thickness of each ED was measured with a digital caliper to determine consistency. Any EDs which were outside the range of 0.31-0.33 mm (particularly along the edges of the film) were discarded.

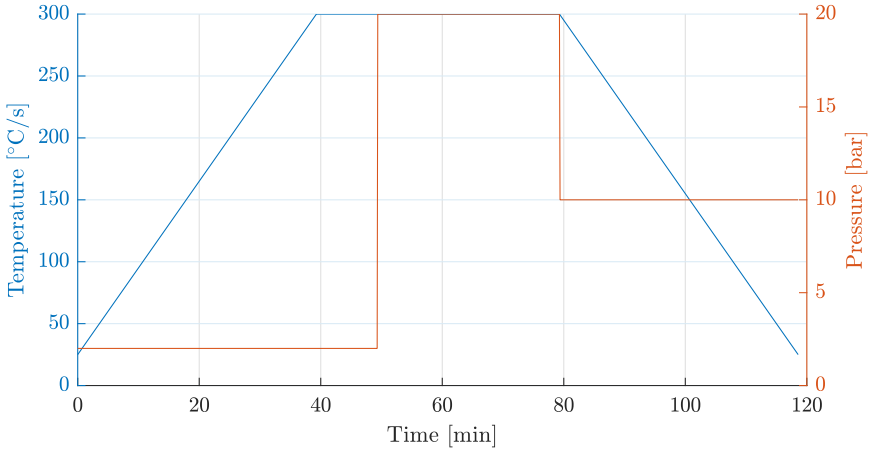

Figure 3.8: Energy director press cycle

3.4 Welding Setup and Parameters

All coupons were welded in a Hermann HiQ DIALOG 20 kHz ultrasonic welder. The fixture at the base of the welder was a custom manufactured jig, designed to clamp coupons for lap shear joints. The titanium sonotrode has a rectangular contact area of 30 mm x 16 mm. The welder is configured with a digital acquisition module, which can be connected to up to 5 thermocouples to sample temperature at 1000 Hz for 10 seconds. A photograph of the setup is shown in figure 3.9.

The welding process was displacement-controlled, and two sets of welding parameters were used; a higher force and amplitude, and a lower force and amplitude. These are respectively referred to as 'H' for high, and 'L' for low, as shown in table 3.2. The 'force' refers to the trigger force, welding force, and consolidation force, which are all given the same value. These chosen force and amplitude values are copied from the state of the art [16], however, the displacement values had to be re-determined because of the change in material and layup. The displacement values for both parameter sets were determined by welding to 0.3 mm (approximately the thickness of the energy director), and then reading the power-displacement curves generated by the welder software. A photo example of the screen is shown in figure 3.10. After the displacement curve starts to increase from zero, it progresses linearly until a point where it changes gradient. This point gives a first approximation of the optimal displacement that produces the highest quality weld. All the welding parameters are summarised in table 3.2.

The displacement values were tested to examine the joint quality. Since this research did not focus on finding the parameters that create the highest quality welds, the aim was to create welds of good enough quality. Coupons (without any Kapton film embedded) were welded at the approximate optimum value as well as one increment of 0.02 mm above and below it. All these welded coupons were lap shear tested until failure. The fracture surfaces were examined for excessive fibre disruption, or insufficient melting of the energy director. If these features were not present, then the weld quality was deemed sufficient.

Figure 3.9: Hermann Ultrasonic Welder fitted with lap-shear joint fixture

The approximate optimum values suggested by the power-displacement curves produced fracture surfaces that indicated sufficient weld quality. In figure 3.11, small white patches of still intact ED could be seen on the fracture surfaces of both interfaces, however this is reportedly a common occurrence when using this sonotrode and fixture. The lap shear strength for H and L were 35.8 MPa and 46.1 MPa respectively, which were stronger than the joints welded below and above the chosen displacement values.

Figure 3.10: Power-displacement curves shown on the Hermann Ultrasonic Welder screen. The approximate optimum is indicated by the red circle on the blue curve.

Table 3.2: Welding parameters

	H (high)	**L (low)**
Frequency	20 kHz	
Holding Time	4 s	
Trigger/welding/hold Force	1000 N	300 N
Amplitude	86.2 μm	51.8 μm
Displacement	0.12 mm	0.10 mm

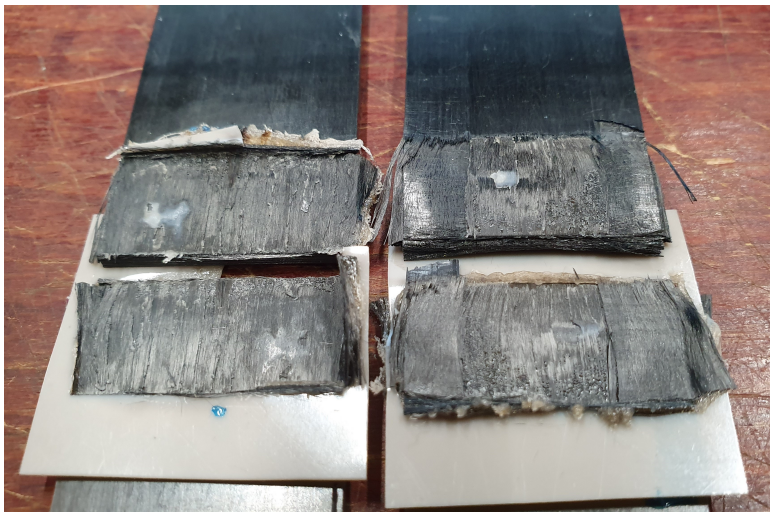

Figure 3.11: Fracture surface of welded joints using H parameters (left) and L parameters (right).

3.5 Welding Procedure

The welding procedure is defined as all the steps taken to setup the coupons, thermocouples and energy directors. The procedure between 0ply and 1ply/4ply differed slightly in regards to how the thermocouples were positioned. For 0ply, only one thermocouple was placed at the weld interface. For 1ply and 4ply, thermocouples were inserted into both the top and bottom adherends because preliminary testing showed that the temperature evolution through the plies above and below the weld interface differed from each other significantly. The procedure is described below:

1. **Cleaning the welder:** The sonotrode was cleaned between each weld with PSF sealant remover on a 3M Scotchbrite pad. The clamping surfaces on the fixtures were cleaned if there was residue from previous welds.
2. **Preparing the thermocouples:** Wires were cut to no longer than 0.5 m, then stripped on one end using a precision knife and connected to terminals. The other end was stripped and formed into a 0.7 mm diameter ring, then wound into a 1 mm tip which was welded using an arc welder.
3. **Setting up coupons, thermocouples, and ED in fixture:**

   0ply

   i The bottom adherend was clamped with the Kapton film facing upwards, and the top adherend was clamped with the Kapton film facing downwards.

   ii The thermocouple was taped on top of the bottom adherend, with its tip centred in the welding area and the free end trailing away from the interface, as shown in figure 3.12a.

   iii An ED was placed over the welding area and taped (such that the welding area was free of tape), as shown in figure 3.12b.

(a) Taping the thermocouple

(b) Taping the energy director and thermocouple

Figure 3.12: 0ply welding procedure

1ply & 4ply

i The bottom adherend was clamped with the side closest to the Kapton film facing upwards, and the top adherend was clamped with the side closest to the Kapton film facing downwards.

ii The plies separated by the Kapton film in both the bottom and top adherends were pried, and the tips of the thermocouples were placed inside in the centre of the weld areas as shown in figure 3.13a.

iii An ED was placed over the welding area, and was taped together with the thermocouple as shown in figure 3.13b.

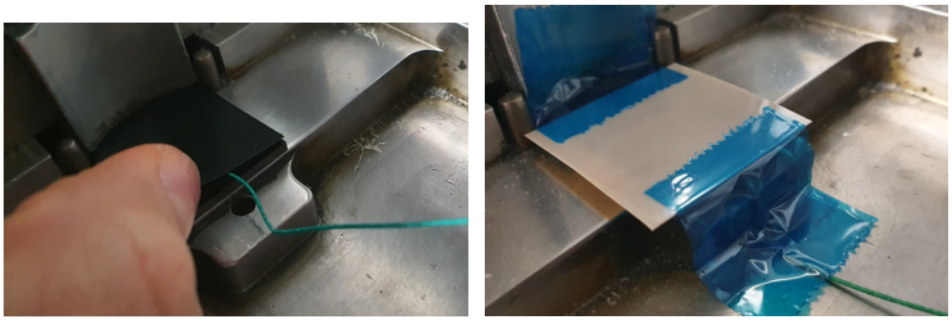

(a) Inserting the thermocouple **(b)** Taping the energy director

Figure 3.13: 1ply welding procedure

4. **Configuring the welding parameters:** With the welder switched on, the software was used to configure the chosen welding parameters (H or L).

5. **Connecting the thermocouples:** The thermocouple terminal(s) were connected to the terminal blocks leading to the digital acquisition module. The computer that controls the module was switched on, and the Labview program started up.

6. **Welding the joint:** The weld was initiated and the welder automatically followed the configured parameters. After completion, the adherends were unclamped and removed from the fixture.

3.6 DSC Sample Extraction

The samples had to fit into 5mm diameter aluminium sample pans.The DSC machine manual recommends (polymer) sample weights of between 5-10 mg for crystallinity analysis. From the preliminary tests, it was seen that greatly varying the sample weights led to variations in crystallinity measurements between samples. Therefore, the aim was to try to keep the sample sizes as consistent as possible during cutting. The process differed slightly between 0ply, 1ply, and 4ply, and is described below:

0ply

1. The joined adherends were snapped away from each other, and the weldline (remaining ED) was carefully peeled away from the adherend that it was still attached to, as shown in figure 3.14a.

2. Two holes were punched out of the weldline using a 4 mm diameter hollow punch tool. Care was taken to choose the region closest to the centre of the weld area, while avoiding any stuck Kapton or incompletely melted ED. This was done so that the extracted samples were as representative as possible of the areas that experienced the temperatures measured by the thermocouples. A removed sample is shown in figure 3.14b.

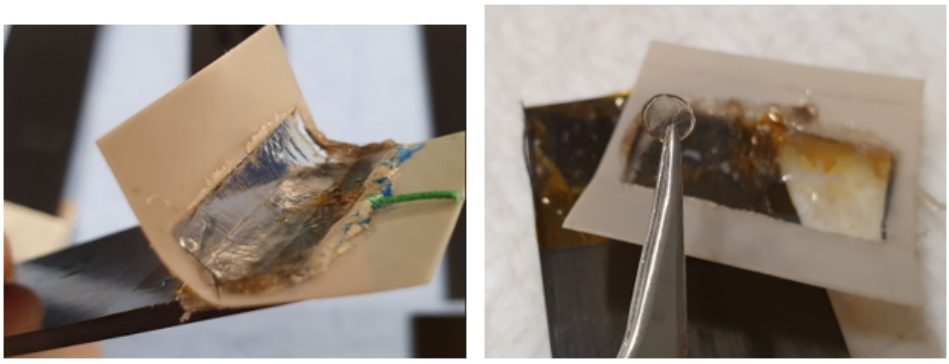

(a) Peeled ED after welding **(b)** Punched out DSC sample

Figure 3.14: 0ply DSC sample extraction

1ply

1. The joined adherends were snapped away from each other, which exposed the sample section (weldline ±1 ply) as shown in figure 3.15a. The sample section was then snapped off from the adherends as shown in figure 3.15b.

2. One hole was punched from the removed section, also with a 4 mm hollow punch tool. Since the thermocouples were often welded into the section, the sample was taken from the most centre part of the weld area while avoiding the thermocouples.

4ply

1. The joined adherends were snapped away from each other to expose the sample section (weldline ±4 plies), shown in figure 3.16a.

2. The broken off section was too thick for the hollow punch, so the samples had to be shaped by hand. First, the section was clamped and sawed to obtain a small square from the centre of the weld area (once again avoiding the thermocouples). This process is shown in figure 3.16b.

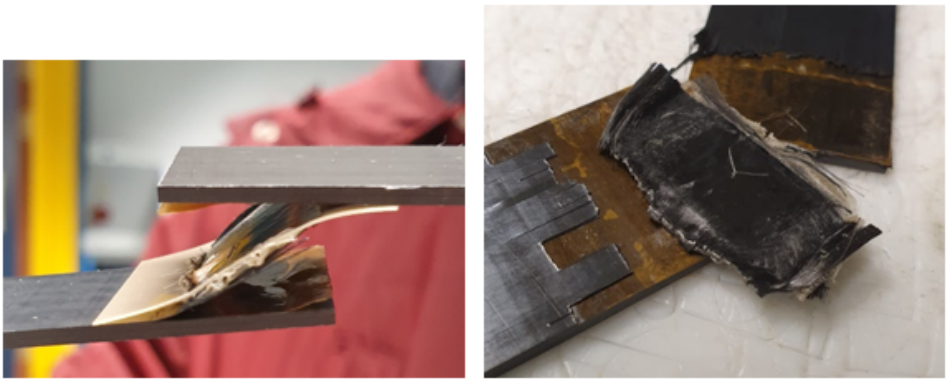

(a) Sample section separated from adherends **(b)** Sample section completely removed

Figure 3.15: 1ply DSC sample extraction

3. The sawed sample was filed down to a round cylinder that roughly matched the diameter of the 0ply and 1ply samples. A side view of the sample is shown in figure 3.16c, indicated by the blue circle.

(a) Removed sample section **(b)** Sawing the sample section **(c)** Side view of filed sample (blue circle)

Figure 3.16: 4ply DSC sample extraction

3.7 DSC Procedure

DSC analysis was carried out in a heat flux TA DSC 250 machine equipped with an autosampler and cooling using liquid nitrogen. The weld samples were weighed and placed into aluminium TZero sample pans with non-hermetic lids. The cycle was run with a heating rate of 10°C/min, as shown in figure 3.17.

The heat sample heat flows were recorded and plotted against temperature in the TRIOS software. The software includes an analysis tool that can integrate the curves to calculate the change in enthalpy over the cold crystallisation (exothermic) peak, and melting (endothermic) peak. These peaks were integrated over a baseline determined by eye, that ideally remained

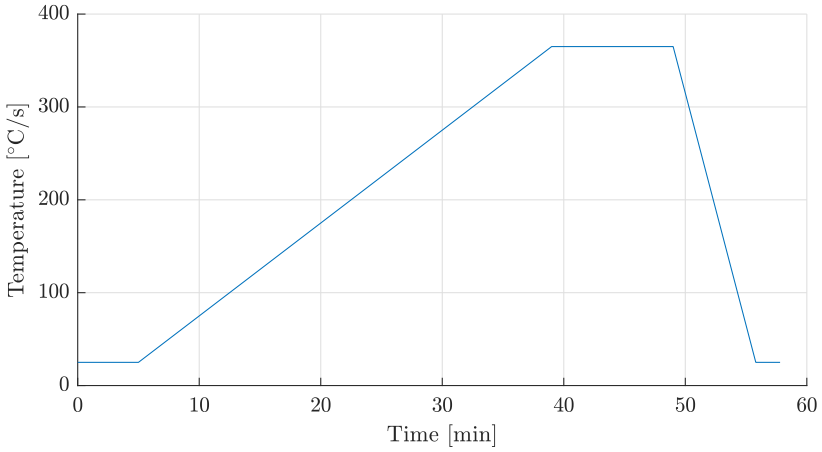

Figure 3.17: DSC cycle

linear between the onset of the cold crystallisation peak to the outset of the melting peak. An example of an integration, with annotations, is given below in figure 3.18:

Since the enthalpies needed to calculate the degree of crystallinity occur only in the heating phase, the cooling phase was programmed to a much higher rate to save time. For comparison, three samples of un-welded energy director and composite (taken from the un-welded end of the coupon) were also analysed. The analysis tool was used slightly differently for these samples. No cold crystallisation peaks were present, and their melting peaks showed an initial dip before the onset of the main peak. For the integration to capture both of these features, the baseline was defined to run linearly between the onset of the initial dip, to the outset of the main peak. An example of this is shown in figure 3.19:

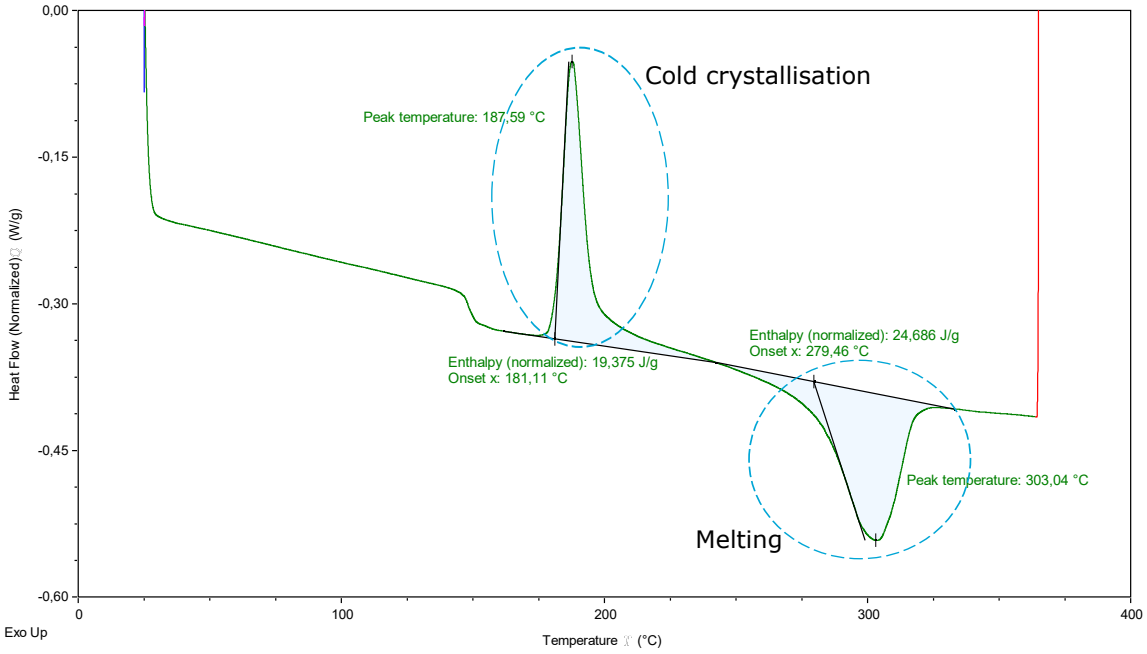

Figure 3.18: DSC heating curves for 1ply L trial 1

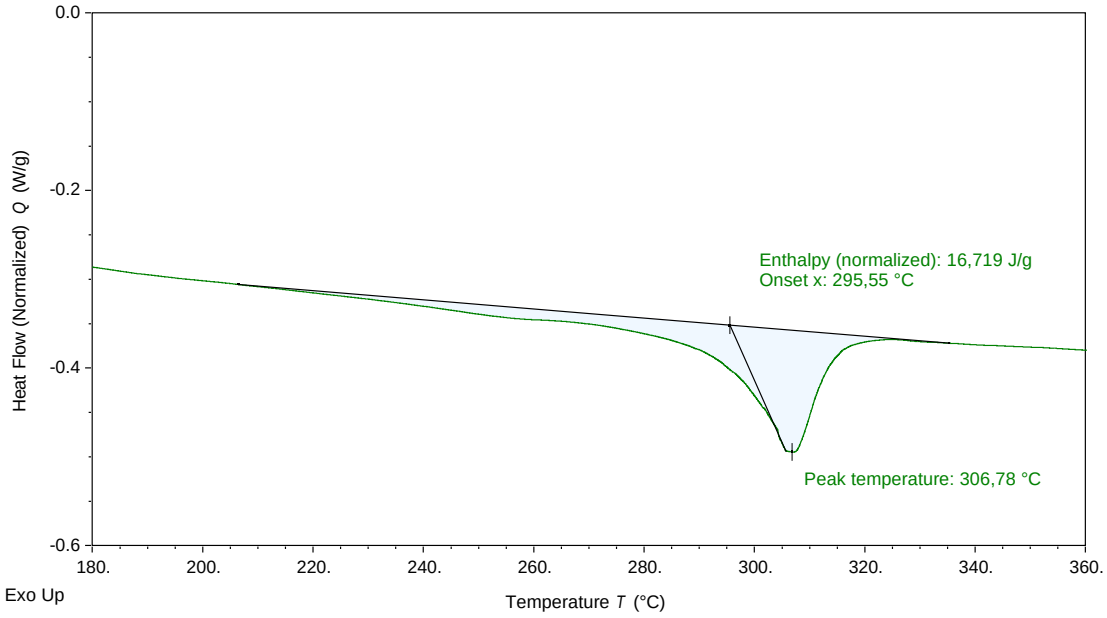

Figure 3.19: DSC heating curves for un-welded composite sample 1

3.8 Degree of Crystallinity Calculation

In order to calculate the degree of crystallinity, the fibre weight fraction needed to be known. The 0ply samples did not contain fibres, however the 1ply and 4ply samples did and thus the fibre weight fraction first had to be calculated. This was done using a ratio-of-thicknesses method. A micrometre was used to measure the thicknesses of all the weldlines taken from 0ply welds, and thicknesses of all the sample sections taken from 1ply and 4ply welds. The thickness was measured at a point across the surface closest to where the DSC sample was extracted from, while avoiding any areas that had incomplete ED melting, or Kapton film remains, or thermocouples. Figure 3.20 uses red crosses and dotted lines to indicate the regions that were unsuitable for measurement, and blue crosses to indicate the areas that were suitable for measurement.

(a) 0ply weldline **(b)** 1ply/4ply sample section

Figure 3.20: Thickness measurement points. Blue crosses indicate suitable measurement spots, and red crosses indicate avoided spots.

All the measurements were then averaged per ply case and welding parameter set. Using the manufacturer's reported nominal resin weight (34%), equation 3.1 was used to calculate the fibre weight fraction for that particular ply case and welding parameter set. W_f is the fibre weight percentage, t_{sample} is the thickness of the sample section, and $t_{weldline}$ is the average thickness of the weldline.

$$W_f = \frac{(t_{sample} - t_{weldline}) \cdot 0.66}{t_{sample}} \cdot 100\% \tag{3.1}$$

$$\%DOC = \frac{\Delta H_m + \Delta H_c}{\Delta H_f \, (1 - W_f)} \times 100\% \tag{3.2}$$

The final DOC for each sample was calculated using equation 3.2. ΔH_m and ΔH_c are the melting enthalpy and cold crystallisation enthalpy respectively, as was shown in figure 3.18. ΔH_f is the crystallization enthalpy of LM PAEK's 100% crystalline form, with a value of 130 J/g [1]. For un-welded EDs and composite samples, the DOC was calculated using a zero ΔH_c value, because there were no cold crystallisation peaks.

3.9 Thermocouple Data Processing

The thermocouple data was processed in MATLAB in order to visualise the temperature evolution during welding and calculate the cooling rates. The cooling rate was calculated at the mid-point between the T_m and T_g. This is theoretically the point where the re-crystallisation rate for semi-crystalline polymers is at a maximum [46]. For LM PAEK, this is 176 °C [1].

The digital acquisition module logged 10,000 temperature readings for each thermocouple over a period of 10 seconds. If a measurement showed signs of a short-circuited thermocouple (caused by electrical contact between the thermocouple and carbon fibres), or if they were too noisy to calculate a cooling rate, then they were omitted from the results. Examples of omitted results are shown in figure 3.21. The imported data, even if not noisy, was first smoothed using a moving average filter with a span of 50 data points. This made is easier to calculate a smooth gradient of the temperature curve, which represented the cooling rate. The cooling rate values for a small temperature window around the mid-point between T_m and T_g (175-177°C) were averaged to represent the final cooling rate of that weld trial.

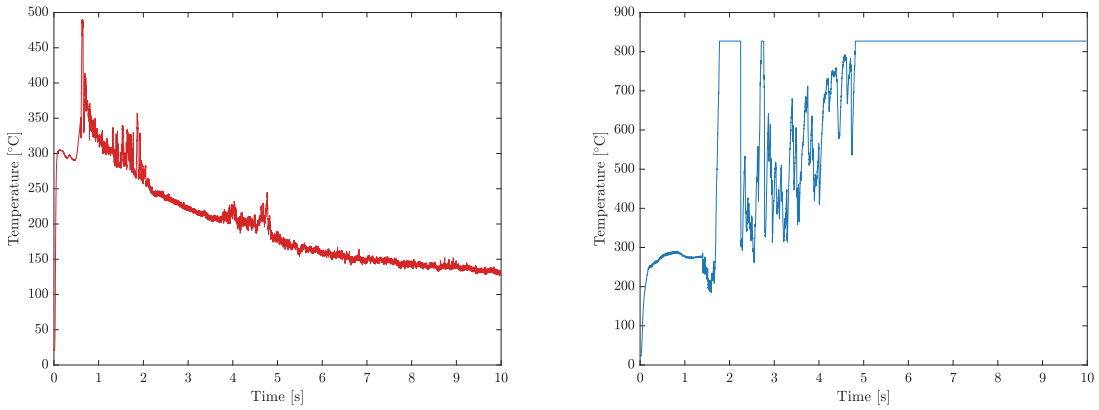

(a) Noisy measurement, 4plyH trial 4 **(b)** Short-circuited thermocouple, 4plyL trial 3

Figure 3.21: Examples of bad data that were omitted

Chapter 4

Experimental Results

This chapter is split into two main sections. The first shows the thermocouple measurements and calculated cooling rates of the welds in graphical form, as a result of the post-processing steps that were outlined in section 3.9. The second section shows the Differential Scanning Calorimetry (DSC) curves that were used to calculate the degree of crystallinity (DOC) of the welded samples, and samples of unwelded energy director (ED) and unwelded composite. In both sections, a summarizing table displays the final averaged results with one standard deviation to represent the scatter of data.

4.1 Thermocouple Measurements

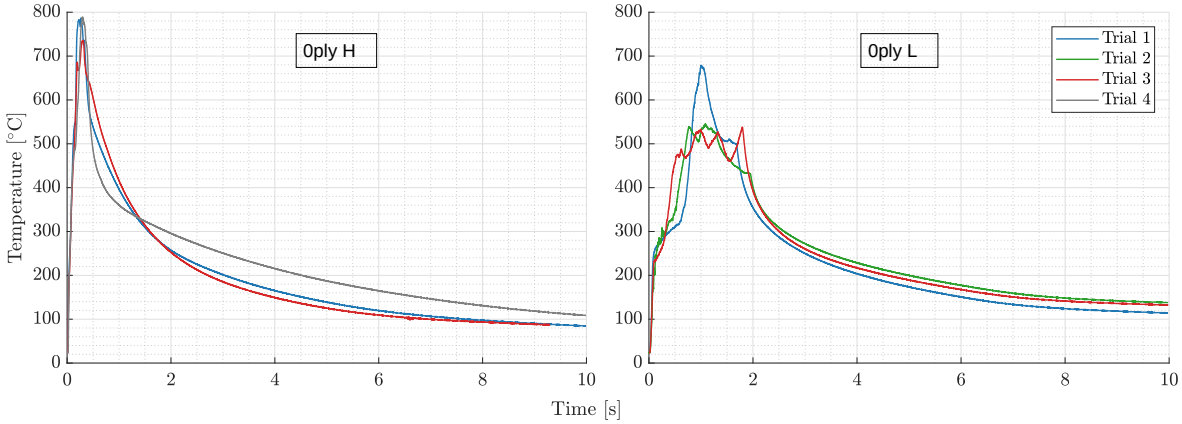

Figure 4.1: Temperature measurements, 0ply H and L

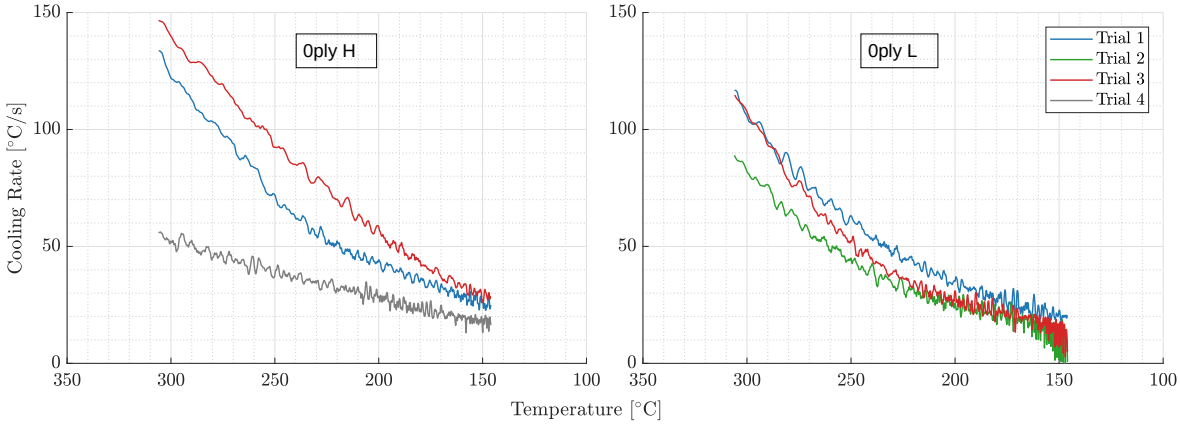

Figure 4.2: Cooling rates, 0ply H and L

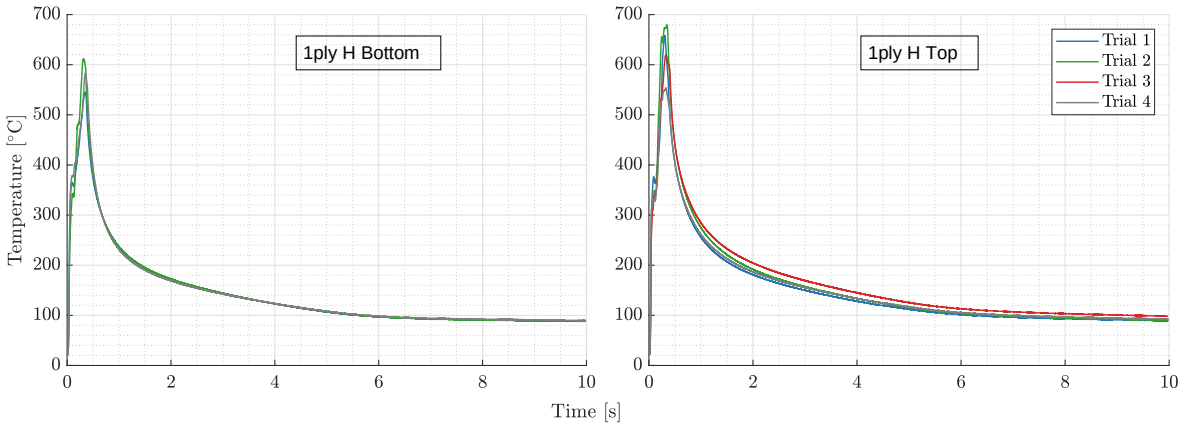

Figure 4.3: Temperature measurements, 1ply H

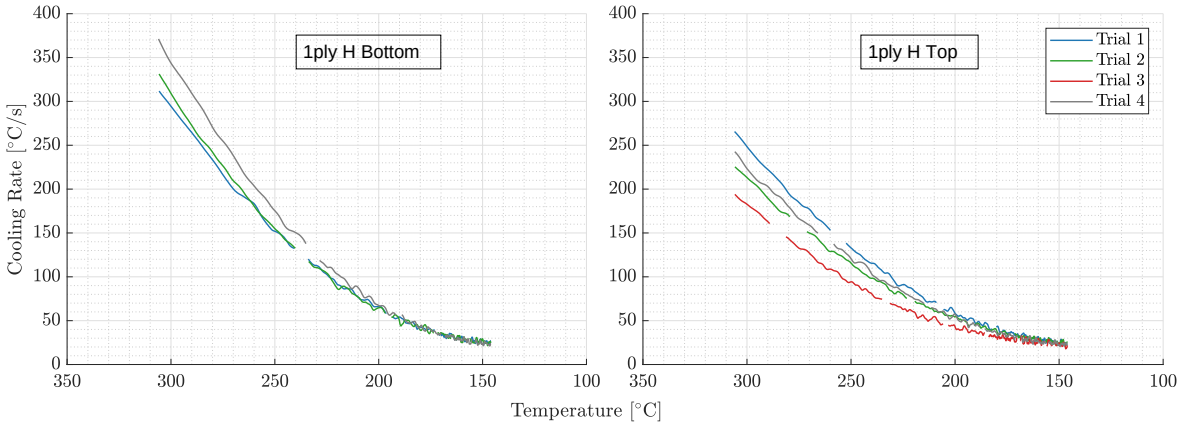

Figure 4.4: Cooling rates, 1ply H

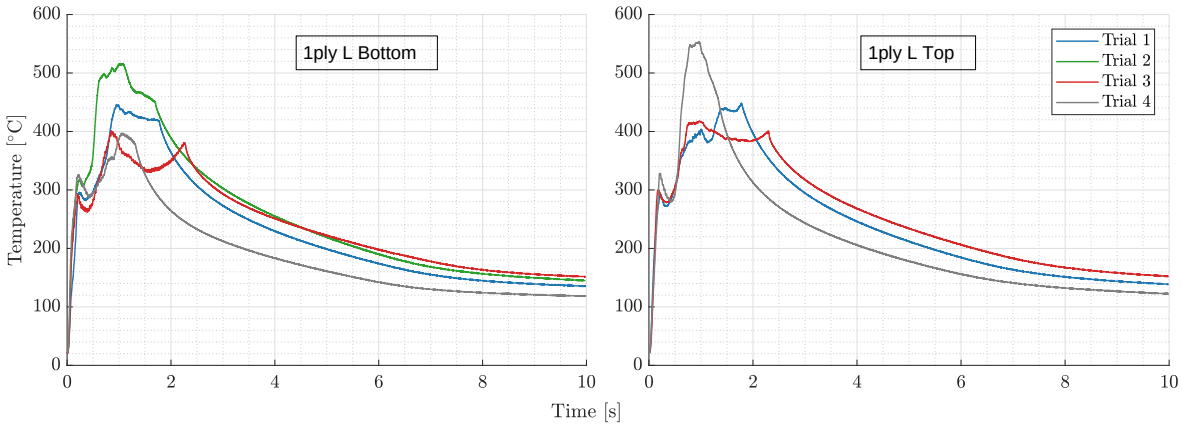

Figure 4.5: Temperature measurements, 1ply L

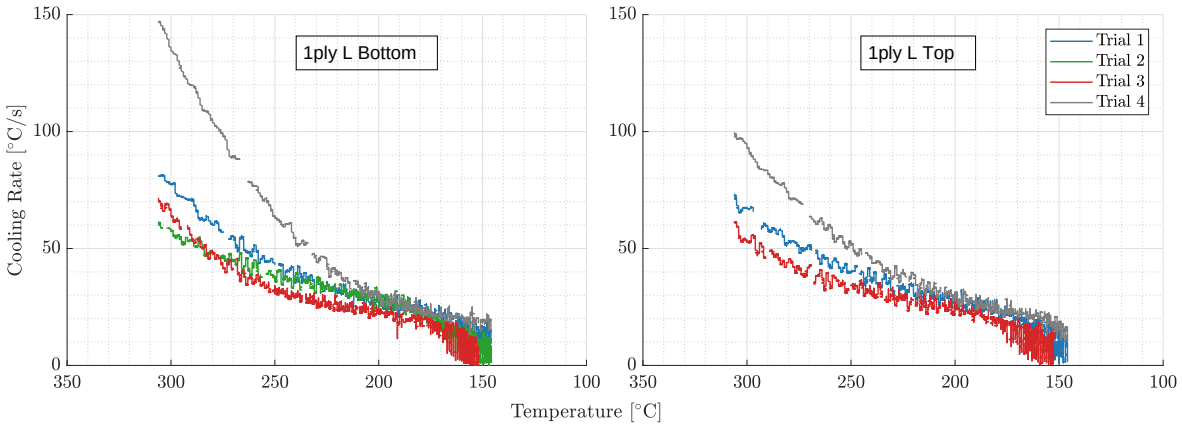

Figure 4.6: Cooling rates, 1ply L

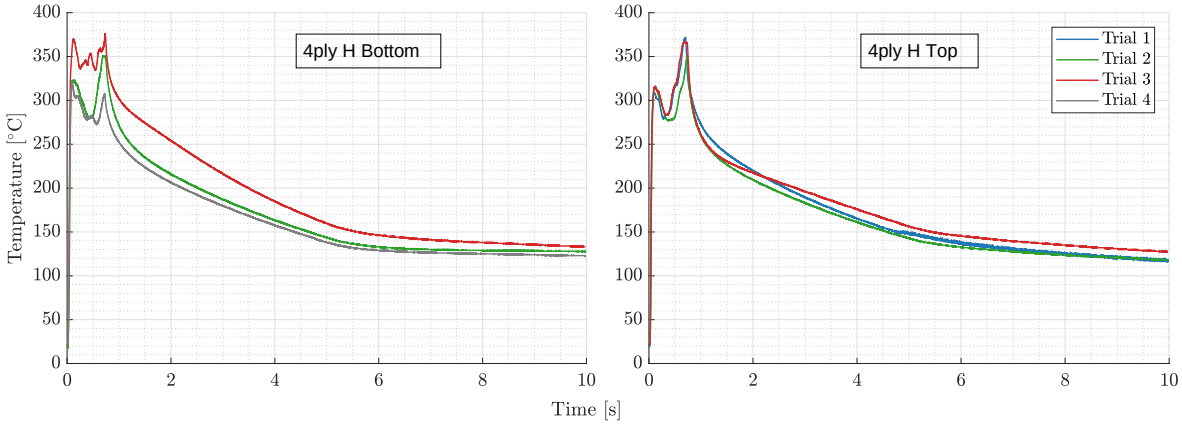

Figure 4.7: Temperature measurements, 4ply H

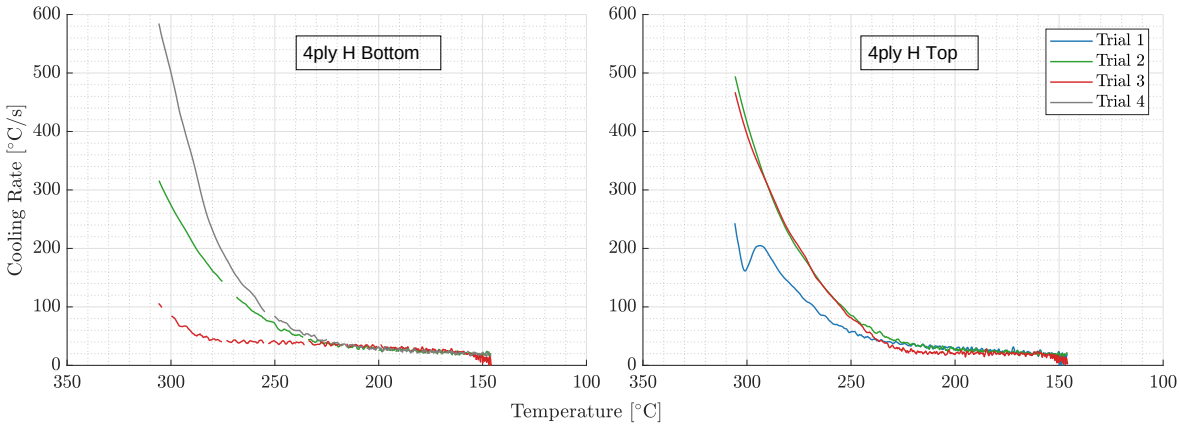

Figure 4.8: Cooling rates, 4ply H

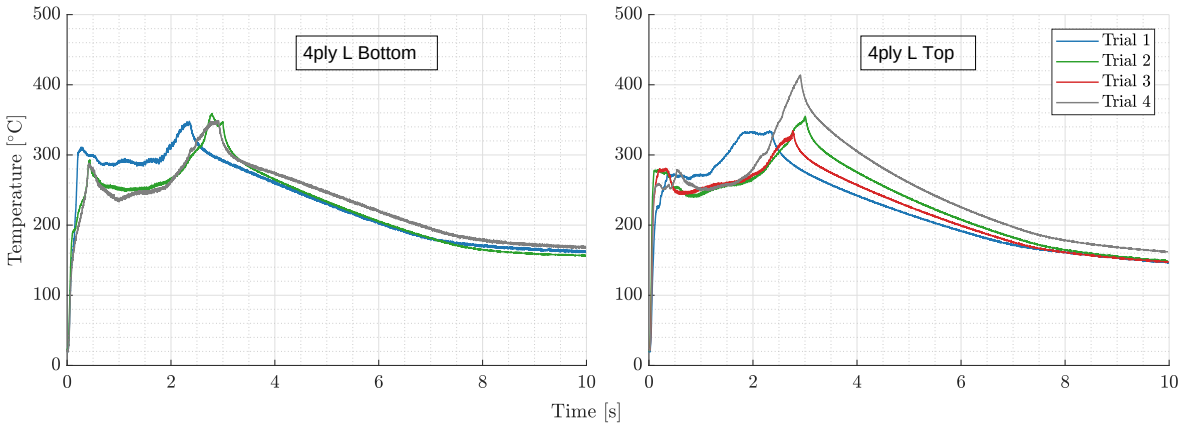

Figure 4.9: Temperature measurements, 4ply L

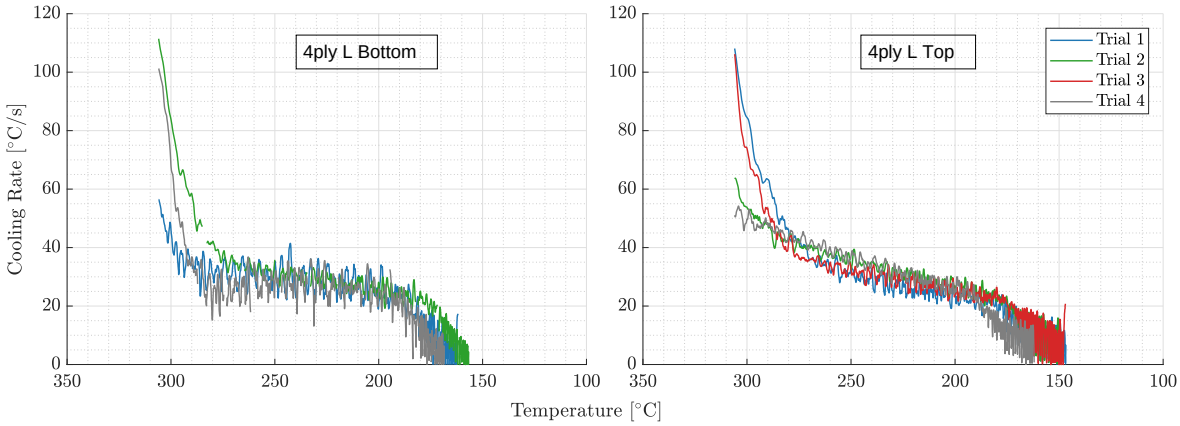

Figure 4.10: Cooling rates, 4ply L

Table 4.1: Summary of Maximum temperatures (Max T) with one standard deviation

		Max T Bottom [°C]	Max T Top [°C]	Average Max T [°C]
0ply	H		770.7 ± 30.0	770.7 ± 30.0
	L		594.5 ± 66.1	594.5 ± 66.1
1ply	H	580 ± 33.2	627.5 ± 54.9	603.8 ± 50.2
	L	440.0 ± 55.3	473.0 ± 70.9	456.5 ± 59.3
4ply	H	349.0 ± 28.1	363.7 ± 10.4	356.3 ± 20.6
	L	352.0 ± 6.1	355.6 ± 27.2	355.6 ± 27.2

Table 4.2: Summary of Cooling Rates calculated at 176°C with one standard deviation

		Rate Bottom [°C/s]	Rate Top [°C/s]	Average Rate [°C/s]
0ply	H		58.5 ± 19.2	58.5 ± 19.2
	L		39.6 ± 3.7	39.5 ± 3.7
1ply	H	108.3 ± 5.9	80.7 ± 10.7	94.2 ± 17.3
	L	35.3 ± 7.6	33.7 ± 4.0	34.5 ± 5.9
4ply	H	38.7 ± 4.0	34.3 ± 6.7	36.5 ± 5.5
	L	28.7 ± 2.5	29.5 ± 2.4	29.1 ± 2.3

4.2 DSC Measurements

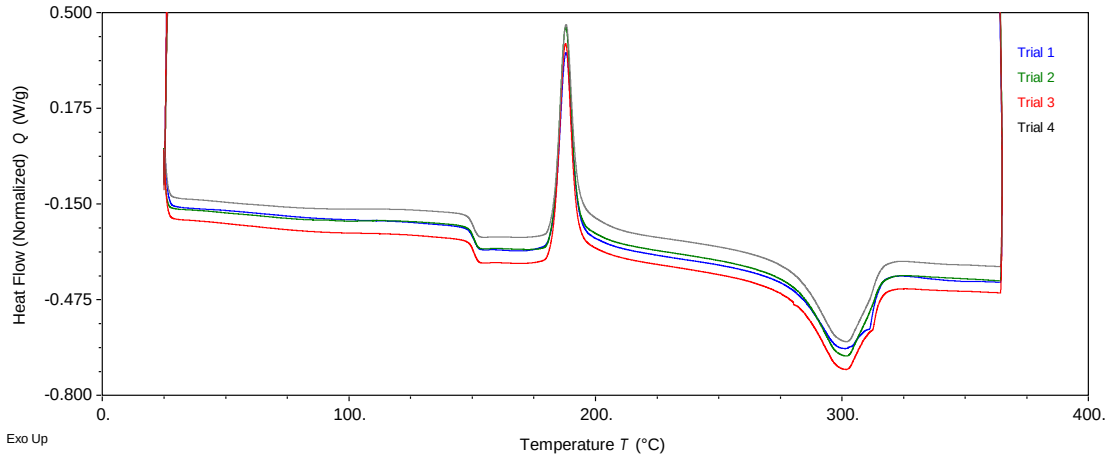

Figure 4.11: DSC heating curves for 0ply H

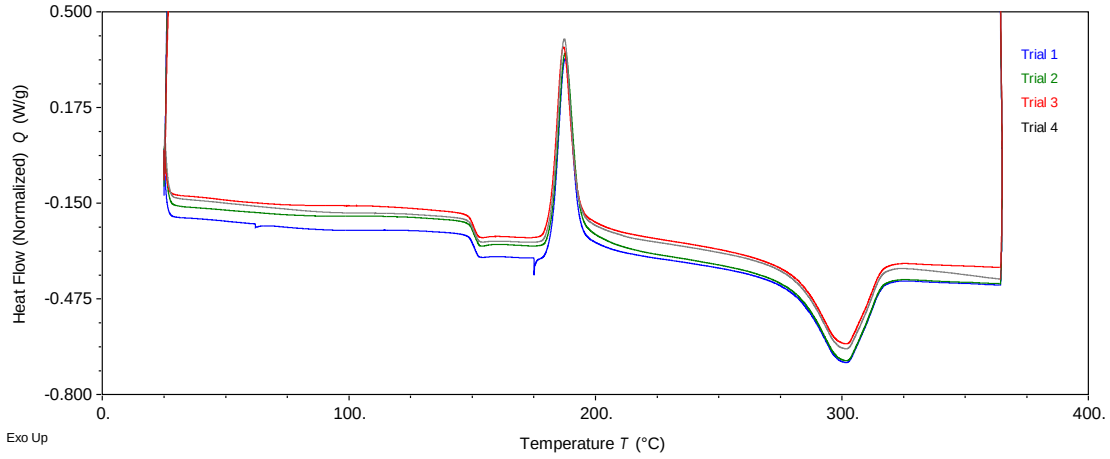

Figure 4.12: DSC heating curves for 0ply L

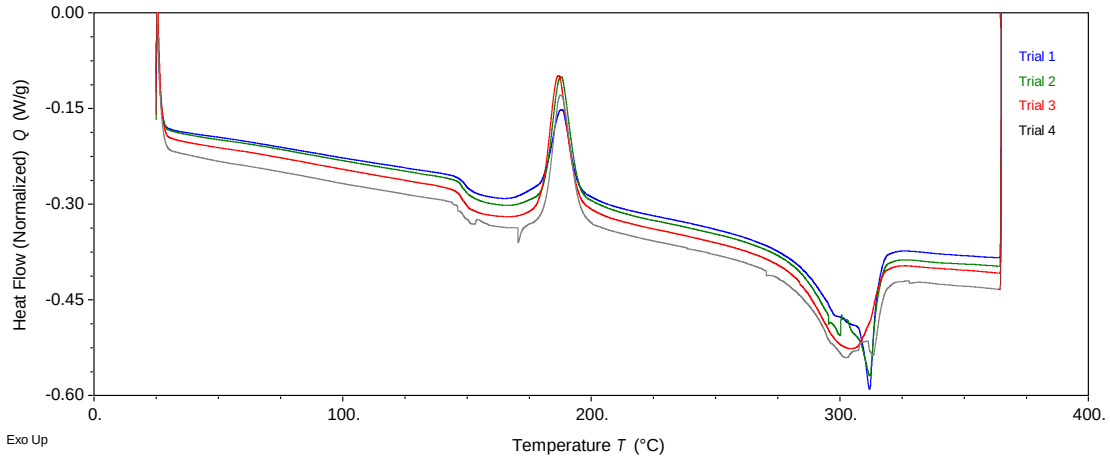

Figure 4.13: DSC heating curves for 1ply H

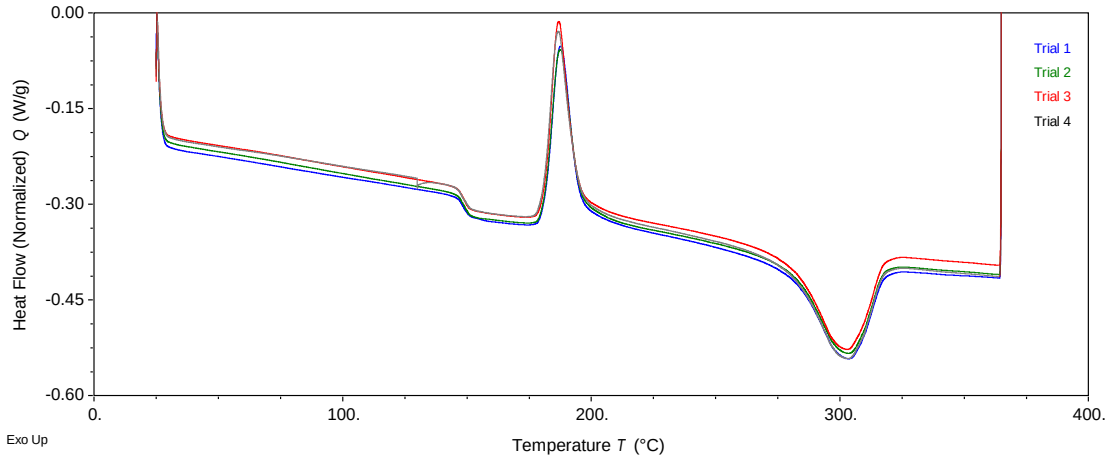

Figure 4.14: DSC heating curves for 1ply L

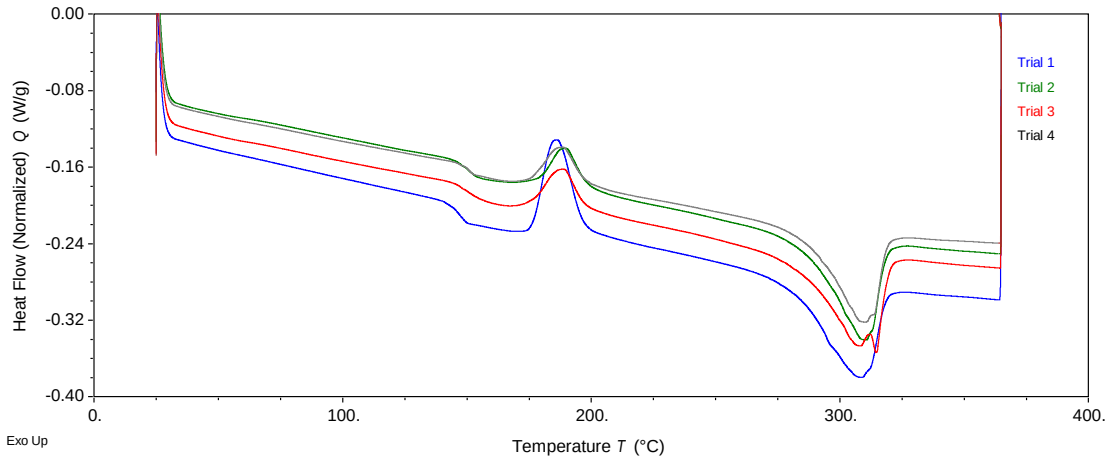

Figure 4.15: DSC heating curves for 4ply H

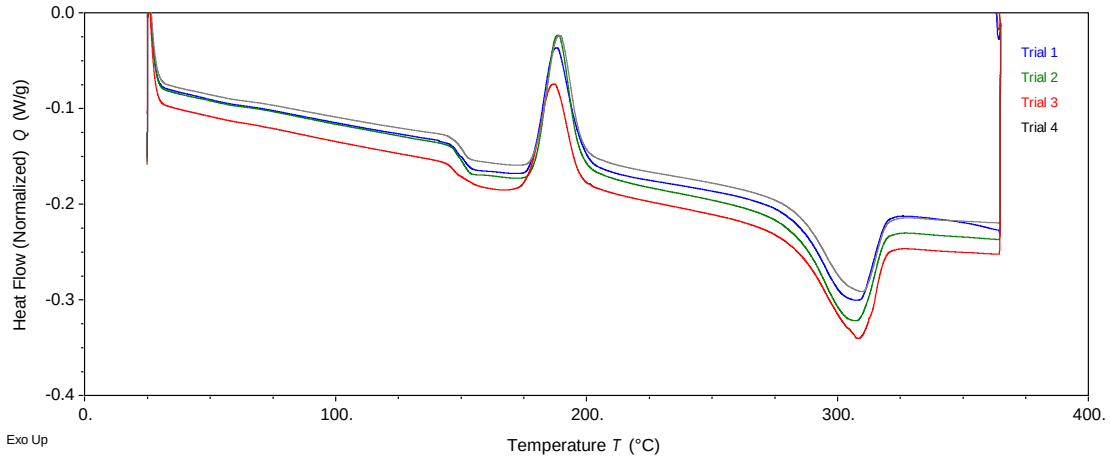

Figure 4.16: DSC heating curves for 4ply L

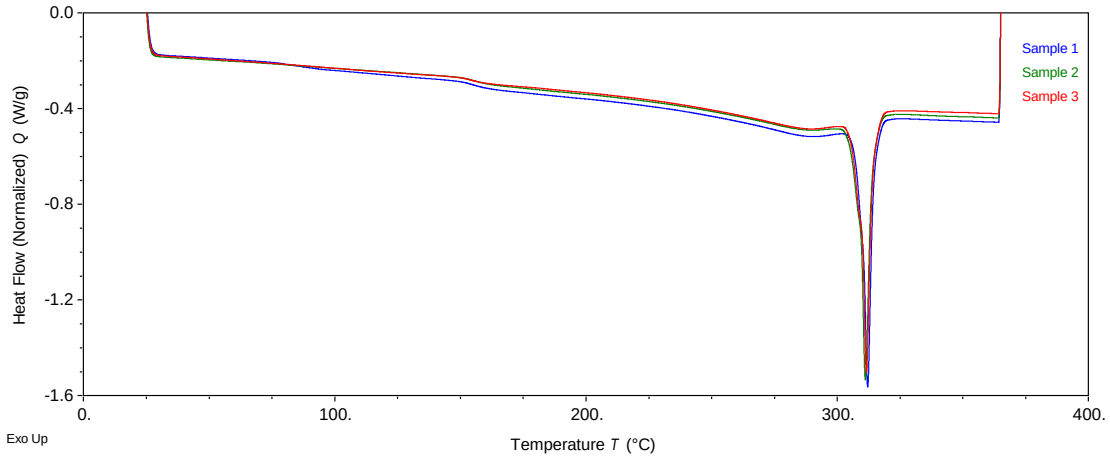

Figure 4.17: DSC heating curves for unwelded ED

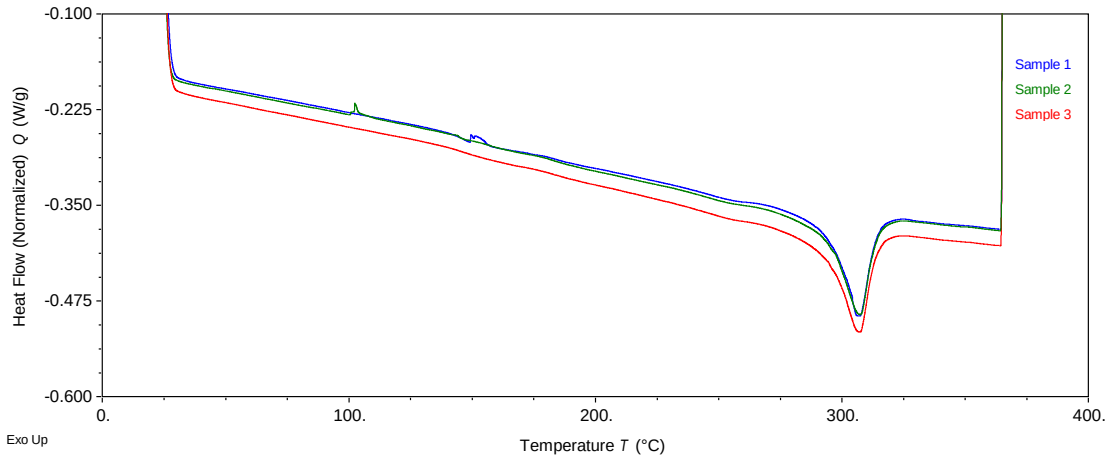

Figure 4.18: DSC heating curves for unwelded composite

4.3 Degrees of Crystallinity

Table 4.3: Thicknesses of weldline ($t_{weldline}$) and sample sections (t_{sample}), with one standard deviation

$t_{weldline}$		H	0.119 ± 0.009 mm
		L	0.111 ± 0.008 mm
t_{sample}	1ply	H	0.502 ± 0.003 mm
		L	0.529 ± 0.015 mm
	4ply	H	1.543 ± 0.025 mm
		L	1.539 ± 0.022 mm

Table 4.4: Estimated fibre weight content of welded samples

	W_f
1ply	51.8%
4ply	61.4%

Table 4.5: Summary of Degrees of Crystallinity, with one standard deviation

		Average DOC [%]
0ply	H	6.8 ± 1.3
	L	5.5 ± 1.2
1ply	H	16.5 ± 4.0
	L	9.1 ± 0.6
4ply	H	17.8 ± 4.1
	L	7.0 ± 1.7
Unwelded ED		45.1 ± 2.5
Unwelded Composite		39.0 ± 3.6

Chapter 5

Discussion

First, the effectiveness of the experimental methodology is assessed. Although it is not part of the results chapter, it was the result of a long development process that had a significant impact on the results. This impact is discussed. Next, the temperature evolution and cooling rates during welding is discussed, and related to the degree of crystallinity. The results suggest that the degree of crystallinity may not be dependent on the cooling rate in the way that was hypothesised. To attempt explaining this, the discussion is extended to investigate the heating phase and the theory behind superheating during welding.

5.1 Effectiveness of Methodology

This section first discusses the main aspects of the methodology development that had the largest impact on the welding process and the material extracted for DSC analysis; the implementation of thermocouples and Kapton films. Additionally, the operation of the hot platen press and the calculation steps for DOC is discussed, since these also had a significant effect on the final results.

5.1.1 Effect of Thermocouples

The thermocouples were necessary to record the temperature evolution during welding, but their manner of implementation likely affected the heating and crystallisation kinetics. It has already been acknowledged in literature that thermocouples can act as energy directors [12, 11].

It is possible that main effect of the thermocouples on heat generation may have to do with them introducing new sources of surface friction. For the 0ply case, the thermocouple sleeve

was taped at the weld interface (figure 3.12a), but the tip was only clamped by the force applied by the sonotrode. This level of clamping gave the thermocouple tip more freedom to vibrate and slide against the ED and adherend surfaces. It is therefore probable that the thermocouple measured the heat generation by surface friction between itself and the neighbouring surfaces, in addition to the surface friction between the ED and adherends. For the 0ply L temperature measurements in figure 4.1, one can observe kinks in the temperature curves between the start and the peak. This might indicate an initial temperature reading dominated by surface friction before viscoelastic friction begins to dominate. Similar kinks in the temperature curves during heating is seen for 1ply H in figure 4.4, and for 1ply L there is even a brief moment of cooling before it heats again to the peak as seen in figure 4.5. For 4ply L welds this brief cooling or plateau is even more exaggerated, as seen in figure 4.9. For the 4ply welds, the greater delay between the initial heating and the peak may be explained by the longer time needed for the heat generated at the weld interface to transfer through the plies.

It is possible that aside from the temperature influence, the crystallisation kinetics were also affected by the physical presence of the thermocouples. During the preliminary testing phase, microscopy was used to observe how the thermocouple interacted with the materials at the weld interface. An example for this is seen in figure 5.1. On the upper left corner of the image, one can see how resin flow has been disrupted around the thermocouple wires, and left patches of high void density. Furthermore, the fibre orientation has been locally forced astray at the thermocouple tip. It is possible that these features would cause variations in the crystallisation kinetics across the surface, although it is not sure how exactly they would be affected. If a sample was taken from an area which contained a lot of voids, then it would not reflect the fibre weight fraction used to calculate the degree of crystallinity.

Figure 5.1: Microscope photograph of a thermocouple tip after welding CF/PEEK 1ply H

The state of the art managed to avoid introducing extra surface friction by embedding thermocouples into the EDs, which could have been replicated for the 0ply case. However, this was not done in order to save time and to make the 0ply case more comparable to the 1ply and 4ply cases. However, embedded thermocouples in 1ply and 4ply coupons were manufactured and welded during the preliminary testing phase. Without the need to insert thermocouples,

this eliminated the extra surface friction in the separated plies. Unfortunately, the majority of measurements (appendix B) were unsuccessful either due to damaged thermocouples or short-circuiting during welding, so a meaningful set of results was not obtained.

There are limited alternatives to using thermocouples to measure temperature. Using fibre optic sensors could be effective, but it is also an intrusive method that may affect temperature or crystallisation kinetics in their own way. The lack of accessibility restricts the use of other non-intrusive methods such as infrared cameras. Thermocouples do have advantages though, being inexpensive and accurate [45], and could be sampled at a very high frequency such that even the fast temperature evolution of USW could be examined in detail.

5.1.2 Effect of Kapton Film

The Kapton films facilitated a way to both insert thermocouples between composite plies away from the weld interface, and to create removable sample sections for DSC analysis which contained carbon fibres. In the previous section, it was already explained how the surface friction was likely influenced by the presence of thermocouples. This also entails the gap in the 1ply and 4ply adherends that was made by the Kapton film to allow insertion of those thermocouples. While the adherend would normally be one monolithic structure, the gap introduces new surfaces that can slide against each other during welding. In addition to this, the thermal properties of Kapton are suspected to also influence the heat transfer within the joint.

Temperature measurements during the preliminary testing phase suggested that Kapton film affects the temperature evolution at its location in the adherend. Coupons with co-consolidated Kapton films were welded and compared to coupons which had their Kapton films removed. Appendix A describes exactly how this was achieved. Table 5.1 shows averaged values of the peak temperatures and cooling rates found in those tests. For the 1ply case, the presence of Kapton films increased the average peak temperature and average cooling rate by 46°C and 37°C/s respectively. The difference was less pronounced for the 4ply case, where the peak temperature increased by 22°C but did not affect the cooling rate. In order to complete the results, the preliminary tests should have ideally been carried out for the L welding parameters and 0ply case as well. Then, it could also be possible to apply an offset to all the results to compensate for presence of the Kapton films. However, these results still provide some preliminary evidence that suggest that the temperature evolution is indeed affected.

If the Kapton film is directly responsible for the discrepancies in peak temperature and cooling rates, then there is a possible explanation. Firstly, it is unlikely that the Kapton film acted as an ED, given that results in literature showed that very thin EDs (0.06 mm) are inefficient at achieving preferential heat generation [47]. Rather, the reason is more likely to be due to changes in heat transfer. If the heat loss to ambient air is ignored, then the main routes of heat transfer away from the weld interface are a combination of through the thickness (adjacent plies), and along the length. Kapton is often used industrially for its thermal insulation capabilities. At room temperature, it has a thermal conductivity of 0.120

Table 5.1: Peak temperatures and cooling rates of CF/PEEK welds found during the preliminary testing phase. Average from 4 trials with one standard deviation.

	With Kapton film	Without Kapton film
1ply H Peak Temperature	595.1 ± 65.6 °C	549.1 ± 30.2 °C
1ply H Cooling Rate	137.1 ± 12.5 °C/s	99.6 ± 1.9 °C/s
4ply H Peak Temperature	432.1 ± 15.7 °C	393.8 ± 34.0 °C
4ply H Cooling Rate	58.0 ± 4.0 °C/s	56.8 ± 5.3 °C/s

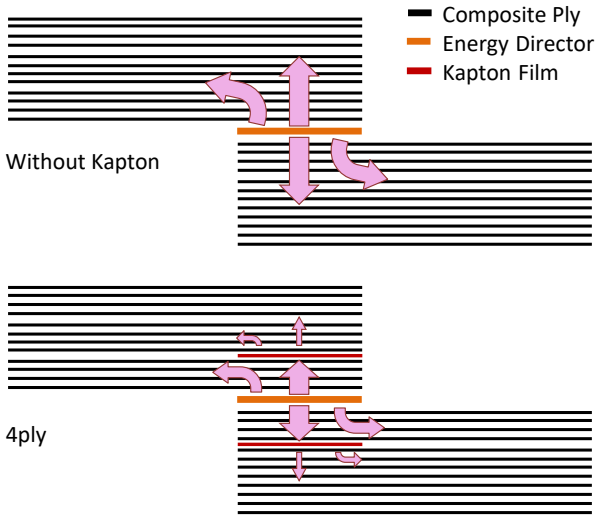

Figure 5.2: Basic idea of how heat flow from the weld interface may be affected by Kapton films. The size of the arrows indicate the magnitude of heat flow.

$Wm^{-1}K^{-1}$ [44]. LM PAEK polymer's thermal conductivity is reported to be twice as high, at 0.240 $Wm^{-1}K^{-1}$ [48], while T700 carbon fibres are 9.588 $Wm^{-1}K^{-1}$ along their length [49]. Therefore, the film acted as an insulator and hindered the transfer of heat through the thickness between the plies that it separated. This suspected hindrance of heat transfer is illustrated using arrows in figure 5.2. Based on this idea, a Kapton film position closer to the weld interface would also further hinder the transfer of heat along the length of the adherend. This may explain why the 1ply welds were affected more than 4ply welds. This would also suggest that the 0ply case was particularly influenced by this phenomenon, although it was not measured so cannot be verified.

The thermal properties of the Kapton also influenced the positioning of the film in the coupons. It was reasoned that having a film positioned between the weld interface and the thermocouple would hinder the heat transfer between those two points. That is why a sample section was chosen that included the ED and all composite plies up to the ply for analysis, such as what is shown in figure 5.3 diagram (a). Even though this configuration was found to interfere with the temperature evolution, it was suspected that isolating the single ply for analysis, such as what is shown in diagram (b), would interfere with the temperature evolution even more. This had implications for the calculation of the DOC. The DOC of the 1ply and 4ply samples were not actually representative of that particular location, but rather

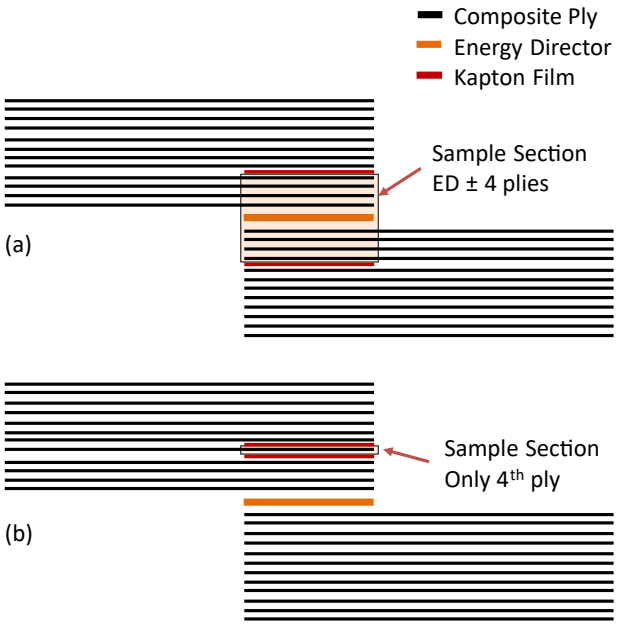

Figure 5.3: (a) The 4ply sample section used in the methodology, (b) The 4ply sample section that was decided against in this methodology.

an average of the ED and all the composite plies up to that location. The averages of the DOC can be approximated as:

$$1ply = (ED + 1^{st}Ply) \,/\, 2 \tag{5.1}$$

$$4ply = (ED + 1^{st}Ply + 2^{nd}Ply + 3^{rd}Ply + 4^{th}Ply) \,/\, 5 \tag{5.2}$$

The DOC at the 1^{st} composite ply can be found by rearranging equation 5.1, but the same cannot be done for the 4^{th} composite ply because equation 5.2 has too many unknowns. The experiments would have be continued for 2ply and 3ply cases in order to complete the data. It is useful to remember that while the 1ply and 4ply temperature results presented in this research are indeed representative of the that particular location, the DOC is not, but can be used as a conservative estimate.

The use of Kapton films was an effective method to insert thermocouples and extract DSC samples, but omitting them would result in a joint that is a better representative of an industrial USW joint. If a method can be developed to successfully embed thermocouples without damaging the thermocouples during consolidation nor have them short-circuit during welding, then Kapton films are not necessary for temperature measurements. For DSC sample extraction, a method could be developed to mill away the composite material surrounding the area wanted for analysis. This would also enable the isolation of a single composite ply in the adherend, without having to include the ED or adjacent plies.

5.1.3 Malfunctioning Hot Platen Press

The hot platen press was not intended to be a factor that affected the development of the methodology, but it malfunctioned in a way that influenced decisions in the final stages of the experimental campaign and may have affected the results. The imperfect functioning of the press' cooling valves led to an uneven heat distribution across the plates during the cooling cycle, as measured by the internal thermocouples.

An uneven cooling distribution has implications for the final quality and properties of the laminate. Firstly, it was very obvious that the laminate was significantly warped, to the extent shown in figure 5.4a where the dotted lines indicate two opposing edges. This is often caused by residual stresses after thermal loading [50]. Secondly, certain regions of the laminate cooling faster than other parts means that those regions will solidify from the melt sooner, and may cause an uneven pressure distribution. This was most likely the reason why it was difficult to press an ED sheet with consistent thickness. This may have also been the reason for excessive squeeze out at some laminate edges, which burst out of the aluminium foil as seen in figure 5.4b. In the same figure, the blue dotted line indicates the orientation of the fibres close to the edge, which is not straight anymore due to the edge squeeze out. On the right edge of the laminate, the white patches seem to be evidence of incomplete resin flow on the surface.

(a) Side-view of a warped laminate

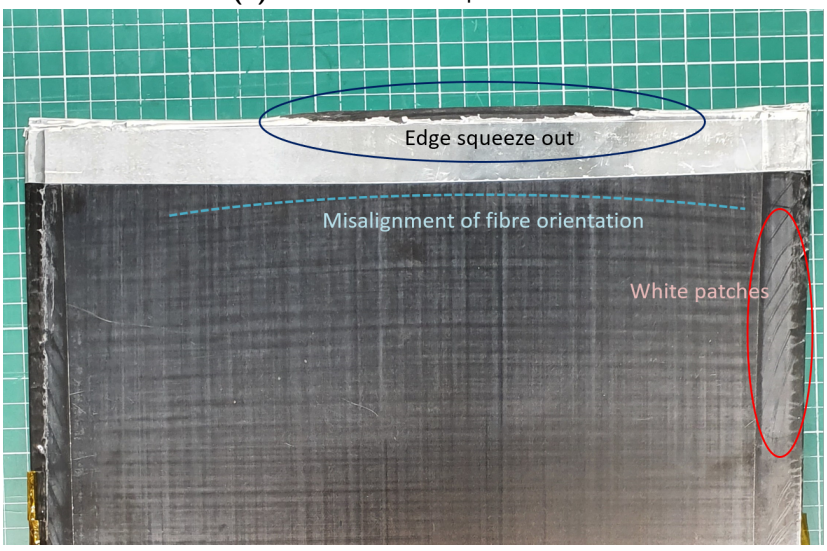

(b) Surface features of a warped laminate

Figure 5.4: Warped laminate due to hot platen press issues

It is unsure how the quality of the laminate might have impacted the results. A warped coupon could affect the force distribution across the weld interface, but there were no remaining

visible signs of warpage after cutting the coupons from the laminate. Additionally, the fibre misalignment and white patches were were most intense at the edges of the laminate while the region used for the weld overlap was at the centre, as indicated in figure 3.3. Other researchers in the laboratory reported that the issues with the press were steadily getting worse over time, so given the uncertainty of the potential impact on the results, it was decided to stop manufacturing laminates for the final steps of the project. The next section explains how this impacted the chosen method to calculate the fibre weight fraction.

5.1.4 Degree of crystallinity calculation step

The main variables that the DOC calculation relies on is the enthalpy of cold crystallisation, H_c, and the enthalpy of melting H_m. Using the TRIOS software from the DSC equipment, it is up to the user to decide how to integrate the respective peaks to calculate the enthalpies. Figure 5.5a shows how the integration was carried out in this research, over a linear baseline. Figure 5.5b shows how the peak could be integrated over a sigmoidal baseline, which results in a much lower enthalpy value. Additionally, if a double melting peak was observed, then both of the peaks were taken into account in the integration, like the example shown in figure 3.19. Although the authors of [48] did not specify how their peaks were integrated, the fact that they found a maximum DOC of 27% for LM PAEK compared to an average DOC of 45.1% in this research implies that their integration methods were different. The DSC data in this research could be re-processed with different methods of integration to see if the results become more comparable. However, the results within this research can still be compared to each other, since the integration method remained consistent.

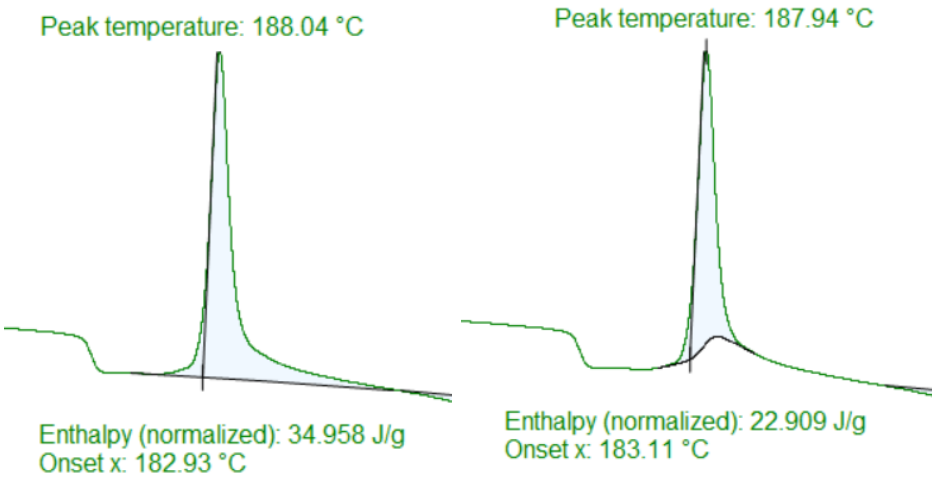

(a) Integration over a linear baseline **(b)** Integration over a sigmoidal baseline

Figure 5.5: Different ways of integrating the cold crystallisation peak of 0ply H trail 1

The DOC is also dependent on the fibre weight ratio. The ratio-of-thicknesses method used to estimate the fibre weight ratio of the 1ply and 4ply samples was dependent on the nominal fibre weight fraction provided by the manufacturer. This fraction is not guaranteed to remain consistent after consolidation or USW, and could vary across different points of the sample

section. This might be especially true considering the signs of incomplete resin flow due to the malfunctioning press discussed in the previous section. The thickness measurements (shown in table 4.3) of the 0ply H and L weld lines varied by 16.8%, the 1ply H and L sample sections by 3.7% and 10.2% respectively, and 4ply H and L sample sections by 13.4% and 14.1% respectively. These degrees of variation reveal the inaccuracy of this method, which should be seen as an estimation rather than an precise calculation.

The chosen method was an alternative to the originally intended acid-digestion method (ASTM D3171-99) which was used during the preliminary testing phase. The malfunctioning hot platen press prevented the manufacturing of the last set of coupons that would have been needed in the acid-digestions. Although the originally intended method would have been a more direct calculation of the fibre weight ratio, it would have been applied to the sample sections of separately welded joints that were not part of the DSC analysis. They would have therefore represented averages again. Assuming that the degree of crystallinity could vary across the sample section, the ratio should be calculated directly on each DSC sample, to be used for that particular sample's DOC calculation. This is theoretically possible using acid digestion, however it is difficult to separate the sample from the DSC sample pan after analysis, and such a low mass will make the calculation overly sensitive to any fibres that are easily lost during the procedure. For some polymers, this is easily done by burning off the polymer matrix using thermogravimetric analysis (TGA), but a quick trial in the laboratory showed that LM PAEK is unable to completely burn off in an environment that does not also burn off the carbon fibres.

5.2 Temperature Evolution and Cooling Rate

The thermocouple measurements that were presented in section 4.1 are discussed here. First, the discrepancies of the temperatures given by the top and bottom thermocouples in 1ply and 4ply welds are addressed. The temperature evolution and cooling rates of the H and L welding parameters of each ply case are subsequently compared. Then, the different ply cases are compared to each other for the H and L welding parameters.

5.2.1 Top Thermocouple vs Bottom Thermocouple

For all weld cases, the top (above the weldline) and bottom (below the weldline) thermocouple recorded the same general heating and cooling path, but for some cases there were distinct differences in the magnitudes of temperature reached and the cooling rates. The discrepancy was greatest for the 1plyH case, shown in figures 4.3 and 4.4. The 1plyH measurements reached a higher peak temperature, but had a slower cooling rate than 1plyL over most of the analysed temperature range. The discrepancy between the measurements for 1plyL, shown in figures 4.5 and 4.6, seems to be less distinct. While trial 4 measured a much higher peak temperature above the weldline than below, trials 1 and 3 reached similar peak temperatures but over slightly differently shaped peaks. The only major discrepancy in cooling rate is also for trial 4, which is again greater for the bottom thermocouple and created more scatter in

its measurement set.

Apart from trial 1, the temperatures of 4plyH measurements in figure 4.7 followed very similar paths. However, the bottom cooling rates in figure 4.8 are very scattered and difficult to compare to the top. When only analysing the midpoint between T_m and T_g, table 4.2 shows that the bottom averaged to a faster cooling rate. For 4plyL temperature measurements in figure 4.9, there is once again some slight differences in the paths followed, but only trial 4 shows a significantly higher peak temperature for the top thermocouple. This creates more scatter in temperature for the top measurements, but interestingly does not reflect in the scatter of the cooling rates in figure 4.10. The cooling rates above the weldline remain higher than below until roughly the midpoint between T_m and T_g.

It is suspected that the discrepancies between top and bottom measurements may be caused by the clamping and welding conditions. The discrepancy might be more noticeable for H welds since the process is much faster, leaving less time for the heat to homogenize across the joint. Since the top thermocouple is closer to the sonotrode, it may receive more vibrational energy that becomes attenuated further down in the joint. Alternatively, it might have more to do with the asymmetrical clamping in the welding fixture. The bottom adherend has more surface contact with the fixture, that could transfer more heat away from the adherend. It was useful to record the temperature of locations both above and below the weldline, so that the definitive calculated cooling rates presented in table 4.2 could be representative of the whole joint.

5.2.2 0ply H vs 0ply L

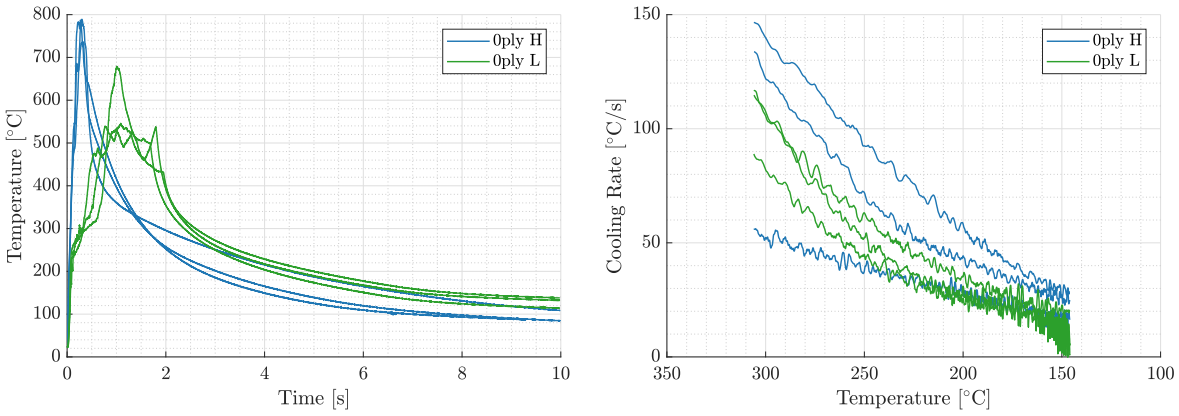

Figure 5.6: Comparison of 0ply H and 0ply L

Figure 5.6 shows how for the 0ply case, welding with H parameters is a fast process that generates a higher temperature with a defined peak that is reached in under half a second. Welding with L parameters is a much slower process that reaches a much lower and delayed peak temperature that occurs over a plateau. While the initial heating rate of L welds is similar to that of H welds, it kinks to a slower rate at about 250°C before increasing again at 300°C until its peak. This change in slope was discussed in section 5.1, and may be attributed

to the thermocouple first measuring the heat from surface friction before the heat generation from viscoelastic friction becomes dominant. The kink probably occurs towards T_m (305°C) because the polymer surrounding the thermocouple tip softens, reducing the friction. Finally, during cooling, L curves consistently stay at a higher temperature than two H curves during cooling. This is probably because its slower heating phase allowed more time for heat to distribute across the joint, creating less of a temperature gradient that would otherwise more quickly transfer heat away from the weld interface.

It is suspected that welding with H parameters creates a higher temperature gradient than L. Immediately after their peaks, H welds decrease in temperature much faster than L welds do after their peaks. However, their cooling rates are much more comparable when isolated to the temperature region between T_m and T_g, as shown in the right-hand plot of figure 5.6. Two out of three H measurements stay consistently higher than L. The one H measurement has the lowest cooling rate at T_m out of all the measurements, but eventually converges to a similar rate at T_g. This spread in results makes it less certain that H welds have faster cooling rates than L, though the results in table 4.2 show that the average rate does still follow that trend.

5.2.3 1ply H vs 1ply L

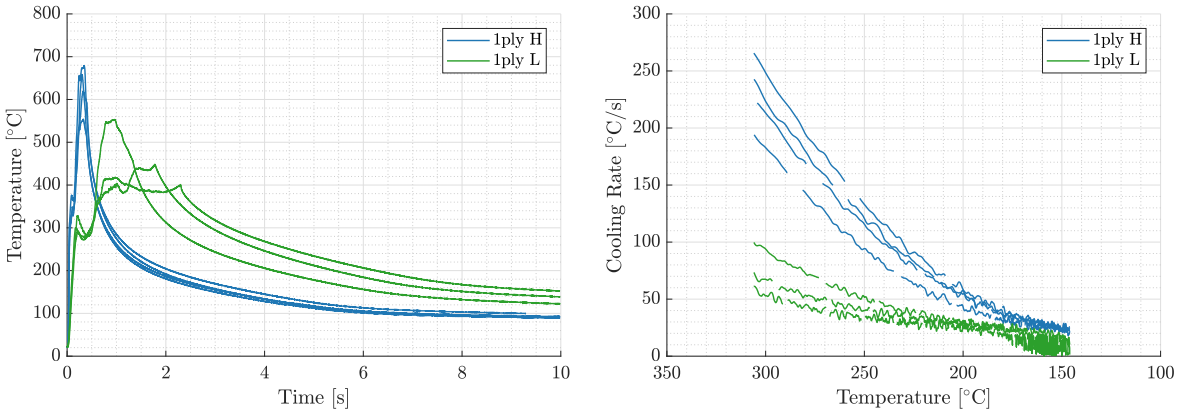

Figure 5.7: Comparison of 1ply H and 1ply L

Figure 5.7 shows that for the 1ply case, the comparison in temperature evolution between H and L welds is very similar to what was seen for 0ply H and L welds, with the exception that the kink in the heating phase observed for L welds has exaggerated here into an initial peak; a brief period of cooling before starting to heat again. Furthermore, it is now noticeable that H welds also undergo the same phenomenon, though on a much shorter time scale. The dip in temperature may be explained by the change of location and environment of the thermocouple. Heat is first generated by the surface friction between the thermocouple, adjacent composite ply, and adjacent Kapton film. Surface friction drops as the composite matrix softens, but now the viscoelastic heat at the weld interface takes longer to reach the thermocouple because it must first transfer through a composite ply. Furthermore, moving the kapton film away from the weldline exposed the first composite ply to the weld interface,

with the fibres in that ply run along the length of the adherend. This could facilitate a faster transfer of heat away from the weld interface, which could emphasise the dip in temperature after the initial peak.

The cooling rates have very different gradients. At T_m, the cooling rates of the H welds are much higher, but they eventually converge to similar values at T_g. Interestingly, the cooling rates of both H and L welds have similar degrees of scatter, while the scatter in the L temperature curves is much higher than that for H curves.

5.2.4 4ply H vs 4ply L

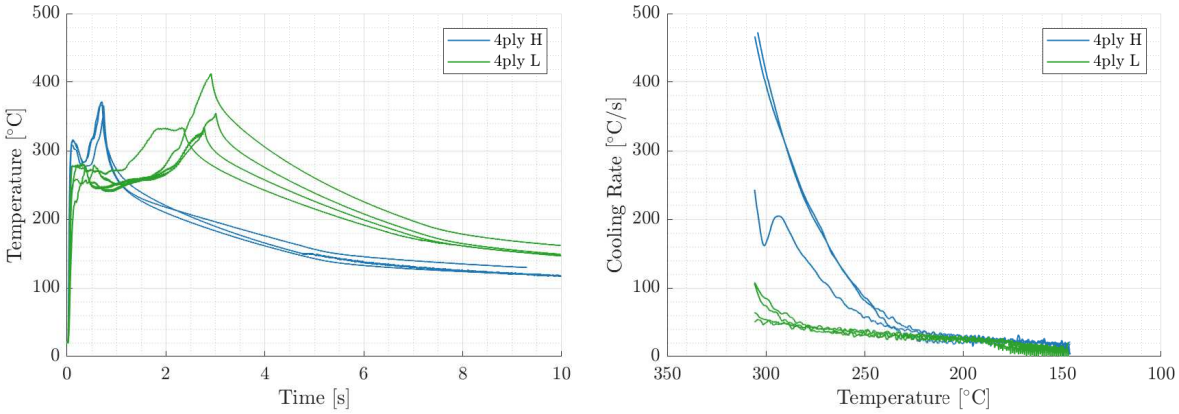

Figure 5.8: Comparison of 4ply H and 4ply L

Figure 5.8 shows that for the 4ply case, the peak temperatures for H and L welds are very similar to each other, though the peak of L welds takes about three times longer to occur. The dip in temperature for both H and L welds are very distinct, such that the curves go through a double peak. The temperature results for L welds are also a lot more scattered.

There appears to be one H measurement that has a much lower cooling rate than the other two. Those other two start their cooling rate at T_m approximately six times higher than the L measurements. There is no conception to what might cause this scatter. Despite the difference, the cooling rates quickly converge to similar values by the midpoint of T_m and T_g.

5.2.5 0ply H vs 1ply H vs 4ply H

Figure 5.9 shows that for welding with the H parameters, locations closer to the weld interface get heated to a higher peak temperature. This relation was expected, since the main bulk of the heat (by viscoelastic heating) is generated at the weld interface. For 0ply and 1ply welds, the final peak occurs at roughly the same time, while for 4ply welds it is delayed after first passing the initial peak. It was expected that the heat generated at the weld interface would take longer to reach locations further away from the interface, however the double peak

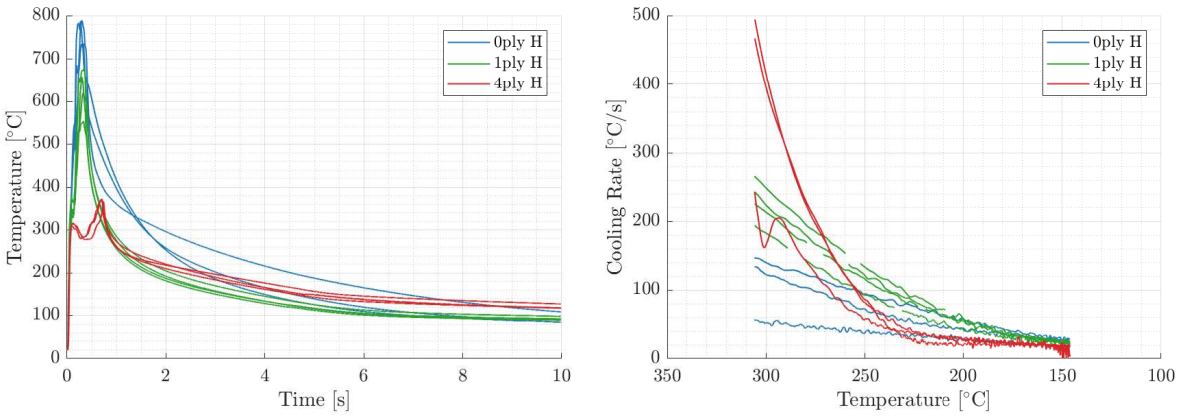

Figure 5.9: Comparison of 0plyH, 1plyH and 4plyH

phenomenon speculated to be caused by the thermocouple and gap in the adherend was not expected.

Interestingly, 4ply welds have the highest cooling rate at T_m. This can be explained by looking at the temperature curves; at T_m, 4ply curves are just coming down from their main peaks where cooling rate is highest, while 0ply and 1ply curves have come far down from their peaks already, giving the cooling rate time to decrease. However, the 4ply cooling rate quickly decreases so that by T_g it has the lowest value. The cooling rate of 1ply welds remain higher than 0ply welds throughout most of the temperature range until it converges to a similar value at T_m. This might have been caused by the composite ply that was in contact with the thermocouple in 1ply welds. The highly thermally conductive fibres in the ply could potentially transfer heat away much faster than 0ply welds which had a Kapton film in between the thermocouple and ply.

5.2.6 0ply L vs 1ply L vs 4ply L

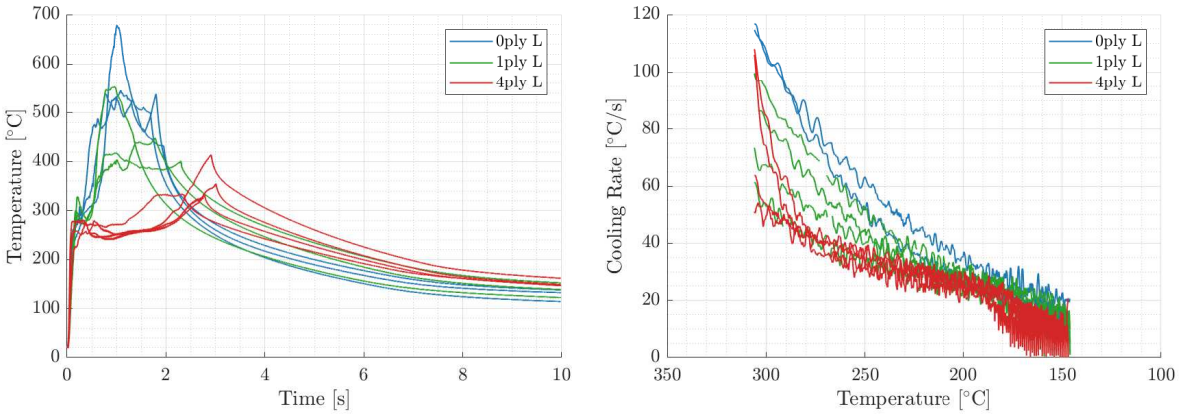

Figure 5.10: Comparison of 0plyL, 1plyL and 4plyL

Figure 5.10 shows that for welding using the L parameters, locations closer to the weld interface get heated to a higher main peak temperature. Most of the 0ply and 1ply temperature plateaus span at least a second in time and occur around a similar time, but most of the 4ply temperature curves have a distinct peak that occur much later in time. As the thermocouple location moves further away from the interface, the dip in temperature before reaching the main point occurs over a large time interval. This is once again likely explained by how it takes longer for the heat generated at the weld interface to reach that location.

The different cooling rates for the L welds do not vary as drastically as they do for the H welds. Throughout most of the T_m to T_g temperature interval, 0ply welds have the highest cooling rate, followed by 1ply, and 4ply welds with the lowest rate. The theory used to explain why 1ply H welds had a higher cooling rate than 0ply H welds obviously cannot be applicable here. It is possible that slower heating of the L welding process spreads heat further away from the joint (lower temperature gradient) thus there are less cooler regions in the adherend for carbon fibres to quickly transfer the heat to. Instead, the cooling rate simply increases as the peak temperature increases.

5.2.7 Relationship between welding parameters, location, and cooling rate

The first research question asks how temperature and cooling rate is distributed through the thickness of the joint. A chart that reflects the summary of maximum temperatures given in table 4.1 is given in figure 5.11. As was hypothesised, welding using the H parameters produced a higher peak temperature than L, with the exception of the 4ply location where they were roughly the same. A chart that reflects the summary of cooling rates in table 4.2 is shown in figure 5.12. As was also hypothesised, welding with the H parameters resulted in higher cooling rates than L for all positions.

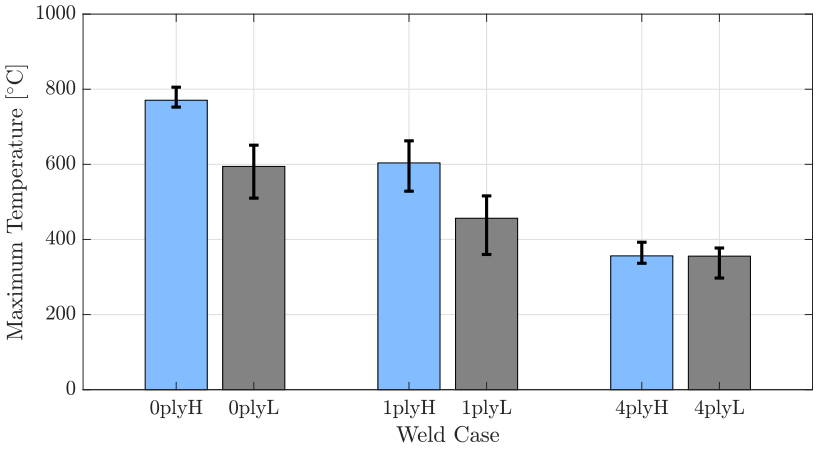

Figure 5.11: Maximum temperatures of welding experiments

Higher peak temperatures were measured closer to the weld interface for both H and L welds, which was also hypothesised. However, the relationship between cooling rate and location was less straight forward. For the L welds, the average cooling rate decreased as the location

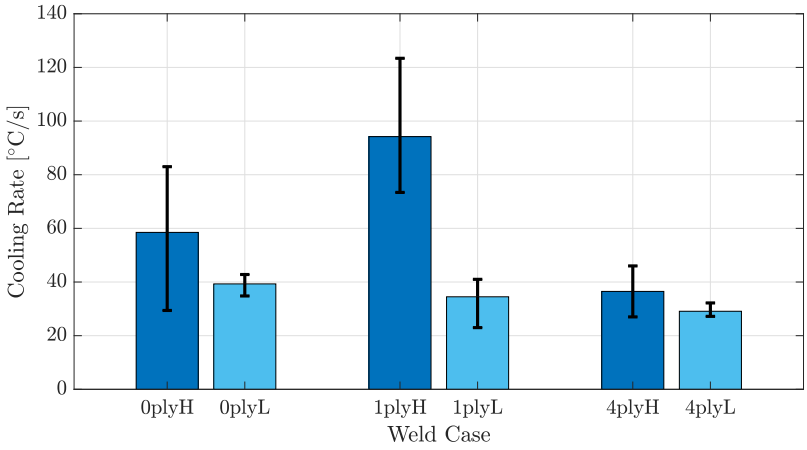

Figure 5.12: Cooling rates of welding experiments

moved away from the weld interface, but the scatter of especially 1plyL makes it an uncertain trend. But for the H welds, the cooling rate as much greater for 1ply welds than the rest. This was not as hypothesised.

5.3 Degree of Crystallinity

The third research question is about how the degree of crystallinity is distributed through the thickness of the joint. A chart that reflects the summary of degrees of crystallinity in table 4.5 is shown in figure 5.13. The first thing to be noticed is that the DOCs of all the welded samples are much lower than the ED or unwelded composite adherend. This was as hypothesised, since the consolidation process of the ED and composite laminates had a very slow cooling phase (7 °C/min) compared to the very fast cooling rates (up to 94.2 °C/s) experienced by the joints during USW. It is also interesting to see that the DOC of ED is slightly higher than that of the composite. For PEEK, [38] found that a fibre fraction of 60% lowered the degree of crystallinity compared to lower fibre fractions, due to the space limitations imposed by the high density of fibres. The same phenomenon might be occurring for LM PAEK.

It was hypothesised that the DOC would increase further away from the weld interface. This trend is observed in the joints welded using the H parameters. There is a greater increase in DOC from 0ply to 1ply welds than there is from 1ply to 4ply welds. This might be attributed to averaging the contents of the sample section, as discussed in section 5.1.2. On the other hand, it may also be due to the carbon fibres acting as nucleation sites. Although the comparison between ED and unwelded composite indicates that the carbon fibres likely reduce the final DOC in slow cooling, they could still accelerate the initial crystal nucleation and growth in fast cooling. The joints welded using the L parameters do not follow the same trend. The DOC increases between 0ply to 1ply welds, but then decreases for 4ply welds. This was unexpected, and no explanation is suggested.

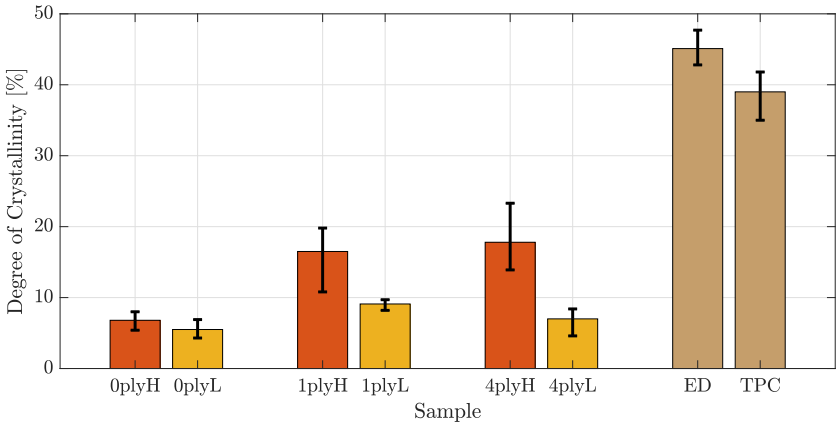

Figure 5.13: Degrees of crystallinity of welded samples, the unwelded ED (labeled ED) and unwelded composite coupon (labeled TPC).

What is even more unexpected, is how all the DOCs of the L welds are lower than those of the H welds. It was hypothesised that welding with H parameters would result in a faster cooling rate that would suppress crystal growth. The faster cooling rates of H welds were confirmed in section 5.2, but the resulting DOC did not decrease as expected. The hypothesis was partially based on the results found in the state of art literature [16], which used PPS as the composite matrix material. The opposite trend may be attributed to the materials' crystallisation behaviours, but it is difficult to find proof of this. The DSC curves of a LM PAEK ED sample and a PPS ED sample are overlaid in figure 5.14. A relevant point may be that LM PAEK's re-crystallisation peak occurs 53°C below its melting peak, while for PPS it is only 34°C. PPS also has higher melting enthalpy and re-crystallisation enthalpy values. Apart from these points and the obvious differences due to a higher melting temperature, there does not seem to be any evidence within these results that the crystallisation behaviour of LM PAEK should be so different to PPS.

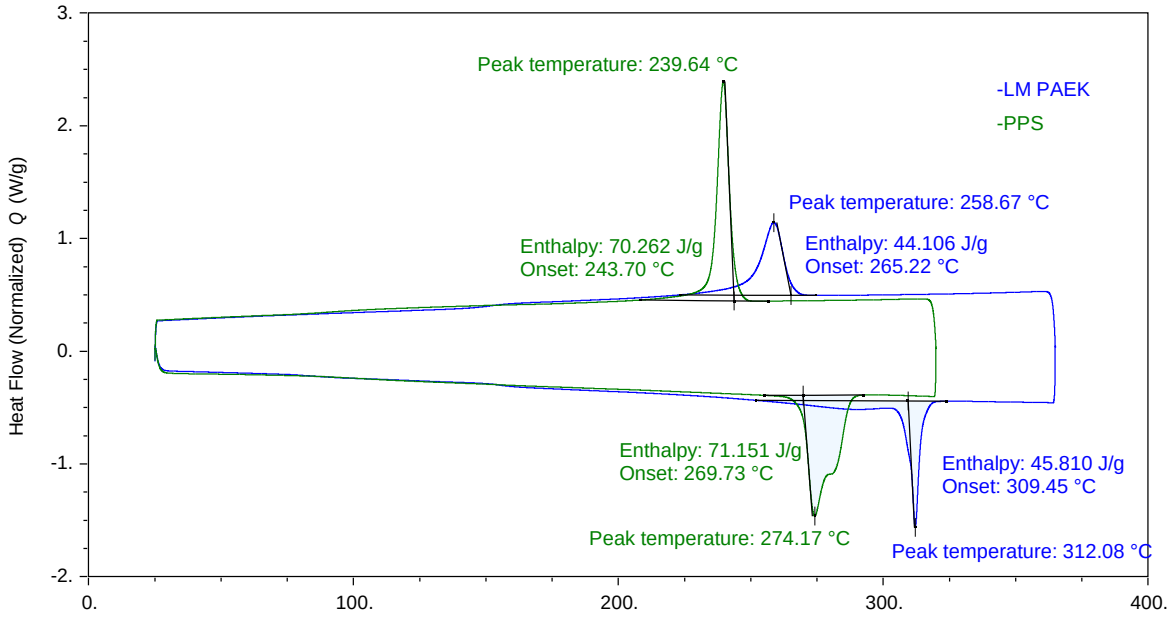

Figure 5.14: DSC curves for LM PAEK and PPS EDs

5.4 Relationship between cooling rates and degree of crystallinity

In this section, the relationship between the calculated cooling rates and DOCs will be further discussed. Table 5.2 provides a summary of the cooling rates and DOCs. Figure 5.15 provides the same summary in graphical form. Once again, it is apparent that there is a greater difference in both cooling rate and degree in crystallinity for the H cases than the L cases. It is also clear that the scatter is much greater for the H cases. Apart from this, there is no noticeable relation trend between DOC and cooling rate. This casts doubts on the role of cooling rate on crystallisation kinetics of LM PAEK composite during USW.

Table 5.2: Summary of Cooling Rates and Degrees of Crystallinity

		Average Rate [°C/s]	Average DOC [%]
0ply	H	58.5 ± 19.2	6.8 ± 1.3
	L	39.5 ± 3.7	5.5 ± 1.2
1ply	H	94.2 ± 17.3	16.5 ± 4.0
	L	34.5 ± 5.9	9.1 ± 0.6
4ply	H	36.5 ± 5.5	17.8 ± 4.1
	L	29.1 ± 2.3	7.0 ± 1.7

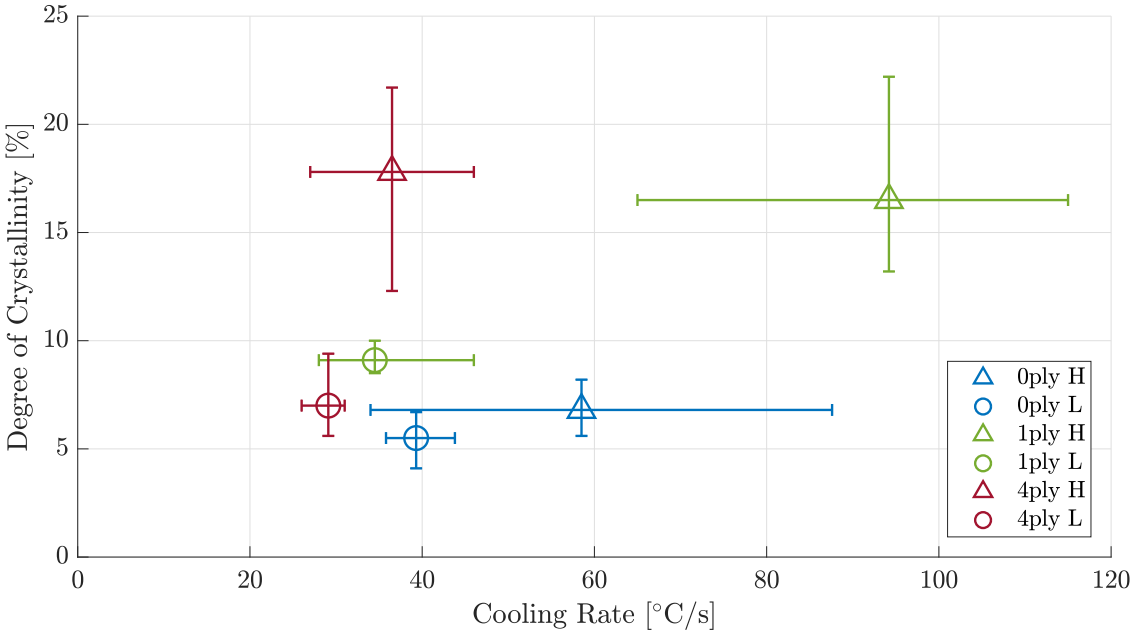

Figure 5.15: Summary of cooling rates and DOCs for all samples

It is possible that using the midpoint between T_m and T_g to define the relevant cooling rate for analysis is too limiting to understand the crystallisation behaviour. It was clearly seen in figures 5.9 and 5.10 that the cooling rates rapidly change over the temperature interval. Furthermore, additional DSC tests in the preliminary testing phase varied the cooling rate between 10°C/min - 200 °C/min, and found that a higher cooling rate reduces the temperature at which the re-crystallisation peak occurs by up to 27°C. This has also been observed for other polymers [51]. This reduction may be more exaggerated for USW since its cooling rates are an order of magnitude higher. If this also affects the temperature at which crystal formation is maximum, then perhaps a different temperature window needs to be analysed for each set of samples. However, since the cooling rates of H welds are still generally higher than L welds over a large temperature range, then it is possible that the final DOCs are not dependent on the cooling rates. Instead, it is suspected that the DOC is less dependent on the crystallisation behaviour as it is on the melting behaviour. This is discussed in the next section.

5.5 Relating heating phase to the degree of crystallinity

It is suspected that the final DOCs are more dependent on the melting behaviour during the heating phase rather than the crystallisation behaviour during the cooling phase. It is possible that the heating phase of USW is so fast that a portion of the crystals do not have enough time to melt before the cooling phase begins. Welding using H parameters is a faster process than L, so would leave a higher portion of unmelted crystals. The basis for this phenomenon is known as superheating; polymer crystals can be heated to well above their melting temperature without immediate melting if heat is supplied faster than the time

needed for the crystal to melt [52, 53, 54]. It is also possible that after the heating phase, the cooling rate is above the critical rate of crystallisation suppression for LM PAEK. This would suppress re-crystallisation, and the unmelted crystals would define the final DOC.

Superheating of polymers has been modelled in [54] to find power-law heating rate dependences. However, it is difficult to apply to this research because USW creates a very brief moment of superheating with temperatures that go well beyond the melting temperature. Without a theoretical relation between the degree of superheating and crystal melting rate, several variables that were suspected to affect crystal melting were plotted against the DOCs:

- Heating rate until T_m
- Integration of heating phase
- Time spent above T_m
- Integration of phase above T_m

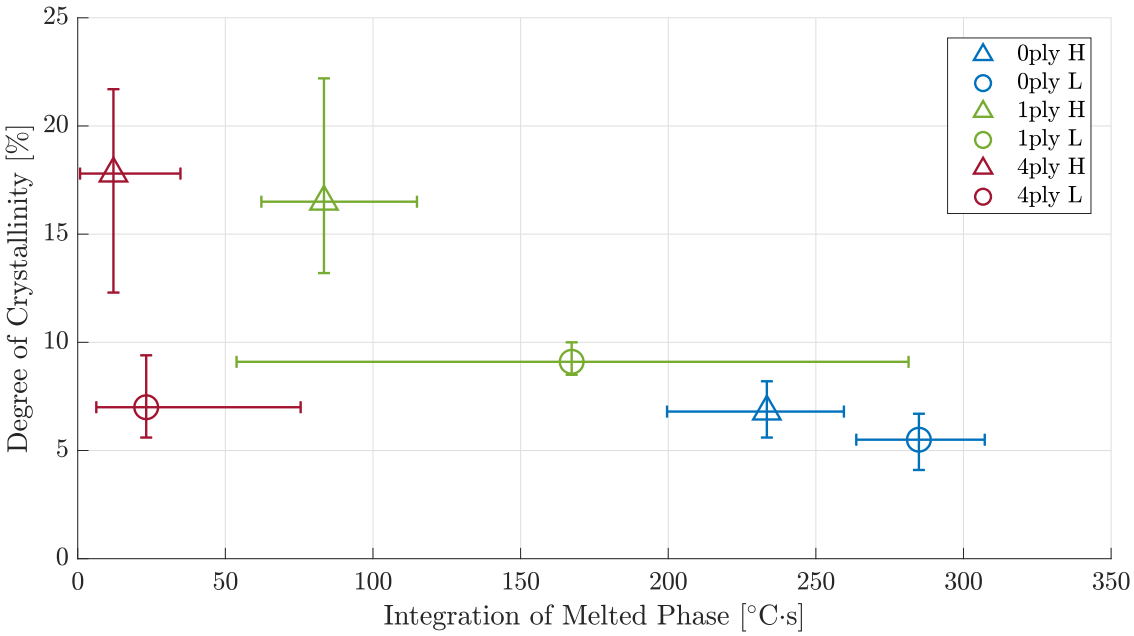

Figure 5.16: Integral under the melted phase plotted against DOC

The variable that produced the clearest trend was the integration of all the parts of the temperature curves above T_m. An integration of this part combines both the temperature and the time, and therefore better represents the total energy added to the respective location in the joint. The relation is plotted in figure 5.16, which generally shows that the DOC decreases for an increasing integration of the molten phase, with the exception of 4ply L. However, when considering the scatter, it could be argued that the trend is only observable for the H cases whereas the L cases stay within too similar of a DOC with each other. Furthermore, the scatter for the 0py H and L cases also put them in a very similar DOC to each other, that could discredit the idea that the trend starts at the 0ply L point. The trend could potentially

become more defined if the samples analysed in DSC were representative of only the material from that location in the joint, instead of including the ED and all the compose plies up to that location. It is predicted that the true DOC of 1ply and 4ply would increase, though it is not known by how much. While figure 5.16 provides some evidence that superheating might be responsible for the final DOC, it cannot be confirmed until more tests are completed and more data collected.

There is still no clear explanation for why the final DOC of the LM PAEK weldline (0ply) shows no clear relation with its cooling rate whereas the final DOC of PPS does. It is possible that the results in the state of the art [16] were also affected by superheating to some degree, though it was not discussed by the researcher. The crystallisation behaviours of the two materials must be studied in more detail for further comparison. Finally, it is not clear from this analysis whether the carbon fibres in LM PAEK composite contribute any effect to the final DOC.

Chapter 6

Conclusions & Recommendations

The aim of this MSc. thesis was to investigate how the ultrasonic welding (USW) process affects the degree of crystallinity (DOC) at the weldline and adjacent plies in carbon fibre reinforced LM PAEK joints. This was done by first developing a methodology that could measure the temperature at different locations through the thickness of the joint during welding, and then extract a sample for DSC analysis. This was accomplished using a system of co-consolidated Kapton films, which was analysed critically to identify its impact on the results. The relationship between the calculated DOCs and the temperature evolution during the cooling phase and heating phase was then researched, revealing some unexpected results. First the conclusions will be given, which address the research questions. Then recommendations for future research will be given.

6.1 Conclusions

The methodology was developed in such a way that thermocouples could easily be inserted into the desired locations through the thickness of the composite joint prior to welding, and then allow an extraction of a sample for DSC analysis after welding. The embedded Kapton films was able to isolate the energy director (ED) for analysis, or include the adjacent composite plies so that the effect of the carbon fibres could be investigated. However, the methodology is suspected to have interfered with the results in multiple ways. A gap (delamination) was created in the adherends for the 1ply and 4ply cases to introduce the thermocouples, so the temperature measurements were likely affected by the extra surface friction between the composite ply and the Kapton film at the gap, and between those materials and the thermocouples. The Kapton films likely acted as thermal insulators and hindered heat transfer. Additionally, the results may have been influenced by the malfunctioning cooling valves of the hot platen press, which affects the consistency of the composite coupons and EDs. Finally, the calculation steps for the DOC likely affect the accuracy of the results, which makes them hard to compare to literature but are still suitable to be compared within the same research

framework.

The thermocouple measurements provided a mixture of expected and unexpected results. It is generally observed that moving further away from the weld interface lowers peak temperature reached and raises the time needed to reach that peak. Welding with high force and amplitude (H) also creates a higher and faster peak temperature compared to welding with low force and amplitude (L). This is consistent with results in literature concerning the weld interface, though the difference in peak temperature also diminishes as location moves further away from the weld interface. H welds also featured higher cooling rates than L welds. For L welds, the cooling rates decreased further away from the weld interface. However, against expectations, the highest cooling rate for H welds occurred at the first composite ply.

The DOC of the joint is reduced from the original DOC of the unwelded composite and ED at least until the 4th ply away from the weld interface. Apart from this expected result, the rest of the DOC results were very different from what was hypothesised. While the DOCs of H welds increased further away from the weld interface, the DOCs of L welds did not vary greatly between each other. Furthermore, all the DOCs of L welds were lower than H welds. This is the opposite of what was expected and observed in literature for PPS, which found that the DOC is reduced for higher cooling rates. The DSC analyses of LM PAEK and PPS were compared to each other, but no evidence could be found that could explain such a difference in crystallisation behaviour. It is possible that calculating the cooling rate at the midpoint between T_m and T_g is an incomplete temperature window for analysis.

It is suspected that the DOC is defined more by crystal melting during the heating phase rather than re-crystallisation during cooling. There was no relation noticed between the DOC and cooling rate when combining all the results. However, there is a noticeable trend if the DOCs are plotted against the integration of the temperature curves in the molten phase. For most of the results, it appears that higher values of this integration resulted in lower DOCs. This could imply that the LM PAEK crystals are being superheated; the heating phase occurs so fast that a portion of crystals do not have the time to melt. Higher temperatures over a longer time impart more energy to the joint, melting more crystals, but the cooling rate may be so high that re-crystallisation is suppressed. However, this trend is most strongly noticed for H welds. Since the scatter of L welds makes it possible to argue that the DOCs do not vary between their ply cases, it cannot be said for sure that they are also part of the trend. Finally, it is uncertain whether the carbon fibres play a role in this phenomenon.

6.2 Recommendations

Firstly, it would be useful to continue the experiments using the methodology defined in this research to complete experiments for 2ply and 3ply cases. This would make the data more complete, and help strengthen the analysis. The experiments could even continue beyond the 4th ply, to investigate how many plies are affected by the USW process. Once this is complete, changes to the analysis and experimental methodology are suggested to address all the limitations addressed in the section 5.1 and to further understand the phenomenons

observed in this research:

- **Compare the cooling rates at different temperatures:** Since it is unsure if the mid-point between T_m and T_g is really representative of the maximum crystallisation rate during the USW process, a sensitivity analysis of the cooling rate with respect to temperature could provide new information or trends.
- **Embed thermocouples into adherends & EDs:** The thermocouple tips would create less surface friction if they were embedded into the surrounding materials. Embedding them into composite is especially difficult because they will be subjected to consolidation conditions and may become more prone to short-circuiting during welding. Further development of the methodology must find a way to mitigate this.
- **Omit Kapton films in sample removal system:** This will result in a welded joint that is more representative of an industrially welded joint, but will require a more sophisticated method. It could be possible to use a computer numerical control machining tool to machine away parts of the weld until only the section wanted for analysis is left. This would be a very sensitive procedure, and care must be taken to ensure that the friction caused by machining does not generate a degree of heat that could interfere with the DOC measurement.
- **Use a more accurate method to calculate the fibre weight fraction:** This could be improved by acid-digestion as originally intended, although ideally the fibre weight fraction of each sample should be calculated individually.
- **Use Wide Angle X-Ray Diffraction to measure crystallite sizes:** this will give new insight into the crystallisation kinetics, since the DOC may only be part of the story. This was also done in the state of the art.
- **Use Flash DSC to investigate crystallinity after fast heating and cooling phases:** Normal DSC machines cannot reflect of the order of magnitude of heating and cooling rates experienced by the joints during USW. A flash DSC should be used to analyse LM PAEK, which can then be compared to the flash DSC results from literature.

Bibliography

[1] Toray Advanced Composites & Victrex. Processing guidelines for TC1225 T700/PAEK UD Tape.

[2] Tencate Advanced Composites. Tencate CETEX TC1225, 2018.

[3] Ginger Gardiner. PEEK vs . PEKK vs . PAEK and Continuous Compression Molding. *CompositesWorld*, pages 2–3, 2018.

[4] Roger Vodicka. Thermoplastics for Airframe Applications A Review of the Properties and Repair Methods for Thermoplastic Composites. Technical report, 1996.

[5] Qiyi Chu, Yong Li, Jun Xiao, and Dajun Huan. Processing and characterization of the thermoplastic composites manufactured by ultrasonic vibration – assisted automated fiber placement. *Journal of Thermoplastic Composite Materials*, 31(3):339–358, 2018.

[6] A Maffezzoli, J M Kenny, and L Nicolais. A macrokinetic approach to crystallization modelling of semicrystalline thermoplastic matrices for advanced composites. *Journal of Materials Science*, 28:4994–4995, 1993.

[7] W O O I L Lee and George S Springer. A Model of the Manufacturing Process of Thermoplastic Matrix Composites Ifacture. *Journal of Composite Materials*, 21(November):1017–1055, 1987.

[8] C Ageorges, L Ye, and M Hou. Advances in fusion bonding techniques for joining thermoplastic matrix composites : a review. *Composites: Part A*, 32(2001):839–857, 2000.

[9] Chris Red. Thermoplastics in Aerospace Composites Outlook, 2014-2023 : CompositesWorld, 2014.

[10] H. Potente. Ultrasonic Welding - Principles & Theory. *Materials & Design*, 5(November):228–234, 1984.

[11] Irene Fernandez Villegas, Lars Moser, Ali Yousefpour, Peter Mitschang, and Harald E.N. Bersee. Process and performance evaluation of ultrasonic, induction and resistance welding of advanced thermoplastic composites. *Journal of Thermoplastic Composite Materials*, 26(8):1007–1024, 2013.

[12] Irene Fernandez Villegas. In situ monitoring of ultrasonic welding of thermoplastic composites through power and displacement data. *Journal of Thermoplastic Composite Materials*, 28(1):66–85, 2015.

[13] Irene Fernandez Villegas. Strength development versus process data in ultrasonic welding of thermoplastic composites with flat energy directors and its application to the definition of optimum processing parameters. *Composites Part A: Applied Science and Manufacturing*, 65:27–37, 2014.

[14] M Natesh, Liu Yun, S Arungalai Vendan, K A Ramesh Kumar, Liang Gao, Xiaodong Niu, Xiongbin Peng, and Akhil Garg. Experimental and numerical procedure for studying strength and heat generation responses of ultrasonic welding of polymer blends. *Measurement*, 132:1–10, 2019.

[15] Michael Troughton. *Handbook of Plastics Joining: Chapter 2 - Ultrasonic Welding*. William Andrew Inc., New York, 2nd ed. edition, 2009.

[16] Nikos Koutras, J Amirdine, I Fernandez Villegas, N Boyard, and R Benedictus. Characterisation of Crystallinity at the Interface of Ultrasonically Welded Carbon Fibre PPS Joints. *Composites Part A*, 125(105574), 2019.

[17] Irene Fernandez Villegas. Welding Lecture Part B, 2017.

[18] Irene Fernandez Villegas. Welding Lecture Part A, 2017.

[19] Chapal Kumar Das, Asish Malas, Parthajit Pal, Sven Friedrich, and Michael Gehde. Ultrasonic Welding of Amorphous and Semi Crystalline Materials. *Advanced Materials Research*, 716:271–275, 2013.

[20] Kaifeng Wang, Daniel Shriver, Yang Li, Mihaela Banu, S Jack Hu, Guoxian Xiao, Jorge Arinez, and Hua-tzu Fan. Characterization of weld attributes in ultrasonic welding of short carbon fiber reinforced thermoplastic composites. *Journal of Manufacturing Processes*, 29:124–132, 2017.

[21] Kaifeng Wang, Yang Li, Mihaela Banu, Jingjing Li, Weihong Guo, and Haris Khan. Effect of interfacial preheating on welded joints during ultrasonic composite welding. *Journal of Materials Processing Tech.*, 246:116–122, 2017.

[22] Genevieve Palardy, Huajie Shi, Arthur Levy, Steven Le, and Irene Fernandez. A study on amplitude transmission in ultrasonic welding of thermoplastic composites. *Composites Part A*, 113(April):339–349, 2018.

[23] Francisco Sacchetti, Wouter J B Grouve, Laurent L Warnet, and Irene Fernandez Villegas. Effect of cooling rate on the interlaminar fracture toughness of unidirectional Carbon/PPS laminates. *Engineering Fracture Mechanics*, 203(February):126–136, 2018.

[24] K S Suresh, M Roopa Rani, K Prakasan, and R Rudramoorthy. Modeling of temperature distribution in ultrasonic welding of thermoplastics for various joint designs. *Journal of Materials Processing Technology*, 186(2007):138–146, 2006.

[25] Frank Senders, Martijn van Beurden, Genevieve Palardy, and Irene F Villegas. Zero-flow: a novel approach to continuous ultrasonic welding of CF/PPS thermoplastic composite plates. *Advanced Manufacturing: Polymer and Composites Science*, 2(3-4):83–92, 2016.

[26] RINCO. Standard 50 Series, 2019.

[27] DUKANE. Ultrasonic Welders, 2003.

[28] M Barroso Romero, I Fernandez Villegas, and H E N Bersee. Optimizing ultrasonic welding of carbon-fibre-reinforced polyetherimide. *JEC Composites Magazine No 70*, (February):54–58, 2012.

[29] Robert J. Young and Peter A. Levell. *Introduction to Polymers*. CRC Press, Boca Raton, third edition, 2011.

[30] M Erhun and Suresh G Advani. A Predictive Model for Heat Flow During Crystallization of Semi-Crystalline Polymers. *Journal of Thermoplastic Composite Materials*, 3(April):90–109, 1990.

[31] Hui Quan, Zhong-ming Li, Ming-bo Yang, and Rui Huang. On transcrystallinity in semi-crystalline polymer composites. *Composite Science and technology*, 65(June):888–1021, 2005.

[32] M J Folkes, G Kalay, and A. Ankara. THE EFFECT OF HEAT TREATMENT ON THE PROPERTIES OF PEEK AND APC2. *Composite Science and technology*, 46:77–83, 1993.

[33] Lulgl Torre, Alfonso Maffezzoll, and Jose M Kenny. A Macrokinetic Approach to Crystallization Applied to a New Thermoplastic Polyimide (New TPI) as a Model Polymer. *Journal of Applied Polymer Science*, 56:985–993, 1995.

[34] F Sonmez and H Thomas Hahn. Modelling of Heat Transfer and Crystallization in TPC Tape Placement.pdf. *Journal of Thermoplastic Composite Materials*, 10:197–240, 1997.

[35] S. Y. Hobbs. *Polymer Microscopy*, volume 19. 1980.

[36] George Odian. *Principle of Polymerization*, volume 58. Wiley-Interscience, fourth edition, 2004.

[37] N. E. Zafeiropoulos, C. A. Baillie, and F. L. Matthews. Study of transcrystallinity and its effect on the interface in flax fibre reinforced composite materials. *Composites Part A: Applied Science and Manufacturing*, 32(3-4):525–543, 2001.

[38] Eric J H Chen and Benjamin S Hsiao. The effects of transcrystalline interphase in advanced polymer composites. *Polymer Engineering & Science*, 32(4):280–286, 1992.

[39] Marco Regis, Marco Zanetti, Michele Pressacco, and Pierangiola Bracco. Opposite role of different carbon fiber reinforcements on the non-isothermal crystallization behavior of poly(etheretherketone). *Materials Chemistry and Physics*, 179:223–231, 2016.

[40] Suchitra Multur. Thermal Analysis of Composites Using DSC. *Advanced Topics in Characterization of Composites*, pages 11–33, 2004.

[41] W O O I Lee, Margaret F Talbott, and George S Springer. Effects of Cooling Rate on the Crystallinity and Mechanical Properties of Thermoplastic Composites. *Journal of Reinforced Plastics and Composites*, 6:2–12, 1987.

[42] PerkinElmer. Differential Scanning Calorimetry (DSC) (Frequently asked questions), 2013.

[43] Mettler-Toledo. The Future of Thermal Analysis, 2019.

[44] DuPont^{TM}. Kapton ® HN, 2019.

[45] International Electrotechnical Commission. Thermocouples - Part 1: EMF specifications and tolerances.

[46] J E Spruiell, C J Janke, S W Case, and K L Reifnider. A review of the measurement and development of crystallinity and its relation to properties in neat PPS and its fiber reinforced composites. Technical Report August, 2004.

[47] Genevieve Palardy and Irene Fernandez Villegas. Ultrasonic welding of thermoplastic composites with flat energy directors: Influence of the thickness of the energy director on the welding process. In *ICCM International Conferences on Composite Materials*, number July, pages 19–24, 2015.

[48] Jérémie Audoit, Lisa Rivière, Jany Dandurand, Antoine Lonjon, Eric Dantras, and Colette Lacabanne. Thermal, mechanical and dielectric behaviour of poly(aryl ether ketone) with low melting temperature. *Journal of Thermal Analysis and Calorimetry*, 135(4):2147–2157, 2019.

[49] Toray Composite Materials. Carbon Fiber T700S, 2018.

[50] J. Sinke, Y. Wang, M. Abouhamzeh, and R. Benedictus. Process induced warpage in laminated shells. In *ICCM International Conferences on Composite Materials*, volume 2013-July, pages 2575–2582. International Committee on Composite Materials, 2013.

[51] Leonard C. Thomas. Use of multiple heating rate DSC and modulated temperature DSC to detect and analyze temperature-time-dependent transitions in materials. *American Laboratory*, 33(1), 2001.

[52] E Hellmuth and B Wunderlich. Superheating of linear high-polymer polyethylene crystals. *Journal of Applied Physics*, 36(10):3039–3044, 1965.

[53] Akihiko Toda, Masamichi Hikosaka, and Koji Yamada. Superheating of the melting kinetics in polymer crystals: A possible nucleation mechanism. *Polymer*, 43(5):1667–1679, 2002.

[54] Huanhuan Gao, Jing Wang, Christoph Schick, Akihiko Toda, Dongshan Zhou, and Wenbing Hu. Combining fast-scan chip-calorimeter with molecular simulations to investigate superheating behaviors of lamellar polymer crystals. *Polymer*, 55(16):4307–4312, 2014.

Appendix A

Preliminary Concepts Methodology

As explained in chapter 3, the development of the methodology included the trial and error of several concepts.

1. Embedded Kapton films that stayed within the coupons during welding
2. Embedded Kapton films that were removed from the coupons prior to welding
3. Embedded thermocouples that could be connected to measure the temperature at the welding area

The concepts were tested using uni-direction carbon fibre Polyetheretherketone (UD CF/PEEK) composite, since carbon fibre Low Melting Polyaryletherketone (LM PAEK) composite had not yet been supplied. Since LM PAEK is reported to have very similar mechanical and thermal properties to PEEK [48], it was considered appropriate to transfer the methodology developed for one material to the other.

The first concept was the final methodology used in this research, and is described in chapter 3. The other two concepts will be described in this appendix. Only the 1ply and 4ply cases were tested, for the H welding parameters. The temperature measurements are given in appendix B.

A.1 Material Definition

UD CF/PEEK was provided by Toray Advanced Composites, in the form of a rolled unidirectionl pre-preg sheet, 305 mm wide. PEEK neat polymer was provided by Victrex, as sheets of 0.25 mm thick film. These sheets were cut and used directly as energy direcors

(EDs) without any further processing. The film's properties are assumed to be identical to the polymer matrix of the composite, since Victrex also supplies the polymer matrix to Toray Advanced Composites. The properties for the composite and polymer are summarised in table A.1. The higher processing temperature required a slightly different laminate pressing cycle, as shown in figure A.1.

Table A.1: Properties of CF/PEEK Composite and Neat Polymer [1]

T_g	143°C
T_m	343°C
Processing Temperature	385°C
Resin Content (wt)	34%

The same polyimide (Kapton) films and thermocouples were used as those used in the final methodology.

A.2 Material Related Differences in Methodology

Due to the higher processing temperature of PEEK compared to LM PAEK, a slightly different hot platen press cycle was used, as shown in figure A.1.

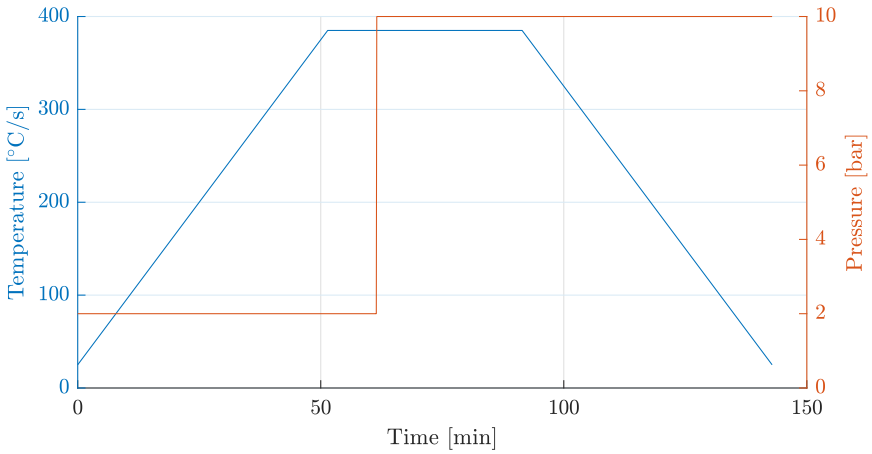

Figure A.1: PEEK Laminate press cycle

A different optimal welding displacement was also used. The welding parameters are defined in table A.2.

Table A.2: PEEK Welding parameters

	H (high)
Frequency	20kHz
Holding Time	4s
Trigger/welding/hold Force	1000 N
Amplitude	86.2 μm
Displacement	0.09 mm

A.3 Removed Kapton

The manufacturing steps for this concept was mostly the same as for the final methodology described in sections 3.3, except for a few key differences. Firstly, the Kapton films were embedded on the sides of the laminate instead of the centre, so that both 1ply and 4ply coupons could be manufactured in a single laminate. Secondly, both sides of the Kapton film were coated with three layers of Marbocote release agent, so that they would not adhere to the neighbouring composite plies. This affected the quality of the consolidated laminate on the 1ply side, as shown in figure A.2. The outer composite ply (that will be closest to the weld interface) has deformed and become split at the location of the Kapton film. After cutting, the ply was no longer curved, but still contained splits on some coupons as seen in figure A.3a. On the 4ply side, this was not an issue.

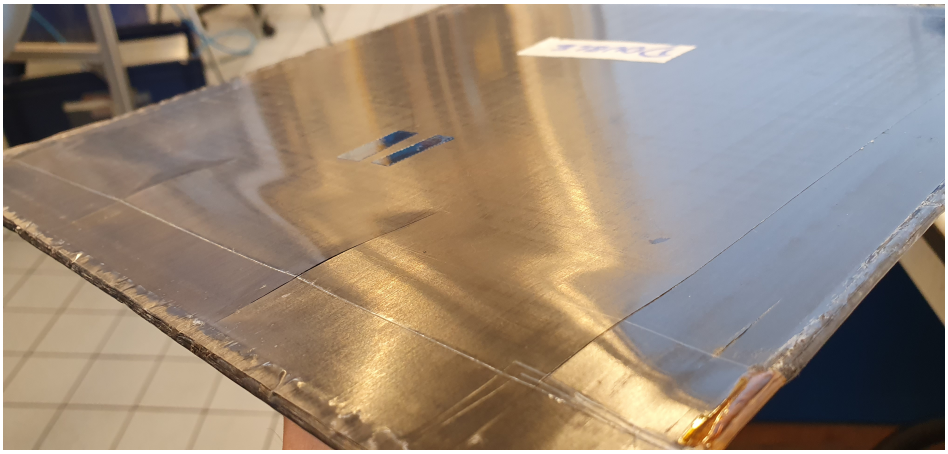

Figure A.2: Laminate embedded with Kapton film coated with release agent on both sides

The welding procedure was also almost the same as that in section 3.5, except for one key difference. The Kapton film was removed from the coupons prior to welding, as shown in figure A.3b. The release agent made the removal very easy, but the separated plies had to be cleaned because a lot of debris got inside during the cutting process. The rest of the welding steps remained the same, and signs of the splits were not visible anymore after welding.

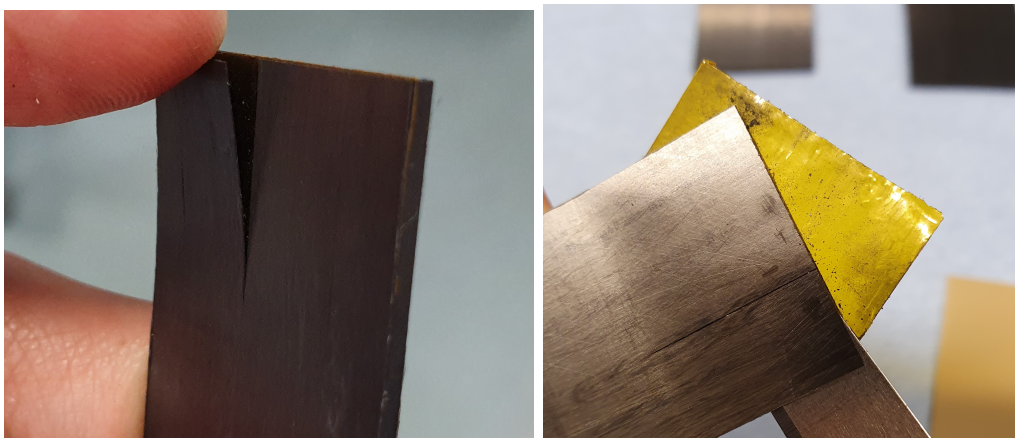

(a) Split outer ply **(b)** Removing the Kapton

Figure A.3: PEEK removed Kapton concept, 1ply coupon

A.4 Embedded Thermocouples

The manufacturing steps for this concept differed greatly from those for any of the concepts involving Kapton films. At the locations where the Kapton films would normally be placed, the thermocouples were placed directly. They were positioned so that the tip would be in the centre of the weld interface, and the rest of the wire trailed away towards the free end of the coupon. They were fixed into their positions using Kapton adhesive tape. The positioning of the thermocouples on the pre-preg sheets prior to consolidation is shown in figure A.4a, while a close-up of how they are taped is shown in figure A.4b.

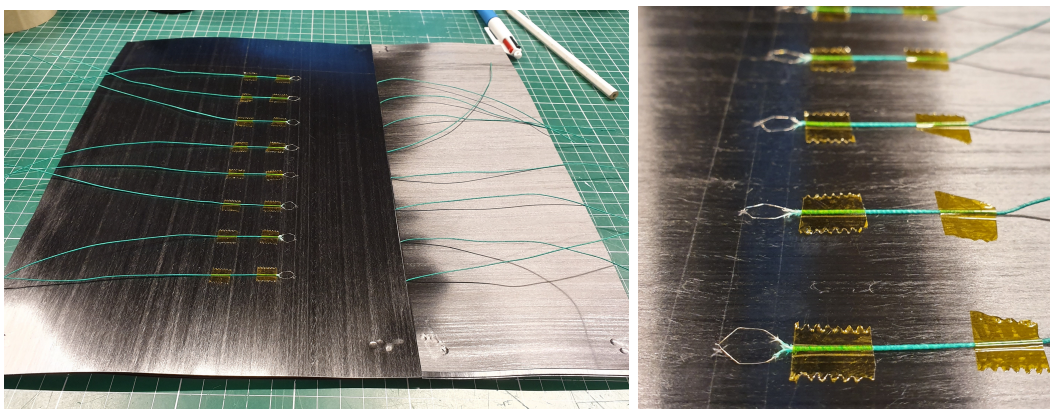

(a) Positioning on laminate **(b)** Closeup of taping

Figure A.4: Embedded thermocouple laminate before consolidation

The pre-preg sheets were cut and stacked in such a way that the thermocouple wire trailing away from the tip would exit the coupon at mid-point of the coupon's length. Because of all the loose wires, a lot of attention had to be given during the cutting process in order to avoid cutting any of the wires. Figure A.5a shows the laminate after consolidation, and figure A.5b shows the cut coupons.

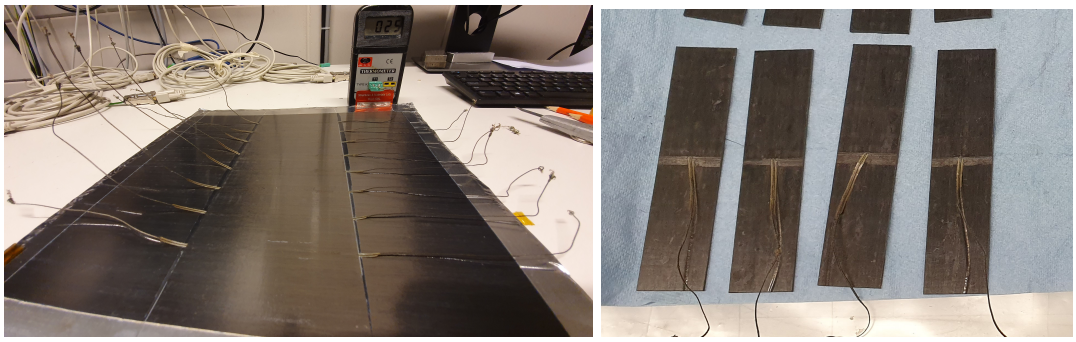

(a) Consolidated laminate **(b)** Cut coupons

Figure A.5: Embedded thermocouple consolidated laminate and coupons

The thermocouples were visibly damaged from the pressing process. The prolonged heat caused the glass-braid insulation to unravel or decompose, as shown in figure A.6. This made it difficult to the connect the thermocouples to their terminals, as the colour code was not visible anymore and extra care was needed to separate exposed metal so that they would not short-circuit.

(a) **(b)**

Figure A.6: Damaged thermocouples in embedded thermocouples coupons

During welding, more smoke was produced than usual, and there were signs of heat generation in areas of the adherends next to the weld interface. An example is shown in figure A.7, where the leftover tape that was used to secure the ED had small melted patches. Underneath the tape, the composite plies protruded slightly in the same location. This is suspected to be due to the Kapton tapes within the adherends used to secure the thermocouples in place. The tapes may act as additional EDs, and adhesive layers may have decomposed and outgassed due to the high heat.

Figure A.7: Heat generation away from weld interface

Appendix B

Preliminary Concepts Results

The temperature measurements and cooling rates of the preliminary welding trials are presented here. The cooling rates are shown between the T_m and T_g of polyetheretherketone (PEEK). The composite's properties are listed in appendix A. However, the cooling rates have not been calculated for the embedded thermocouple welds, because of the lack of successful measurements. A summary of the results comparing embedded Kapton to removed Kapton is shown in table 5.1.

B.1 Embedded Kapton

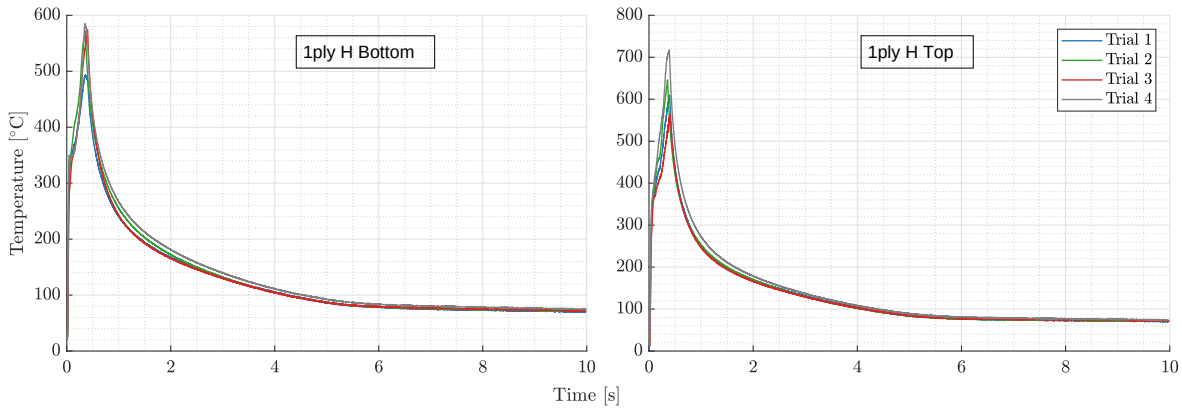

Figure B.1: Temperature measurements, embedded Kapton 1ply

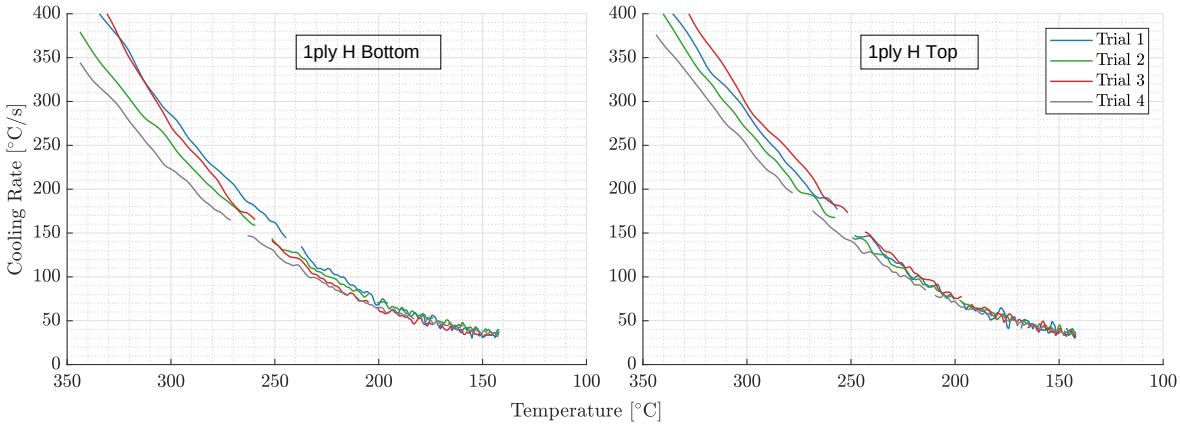

Figure B.2: Cooling rates, embedded Kapton 1ply

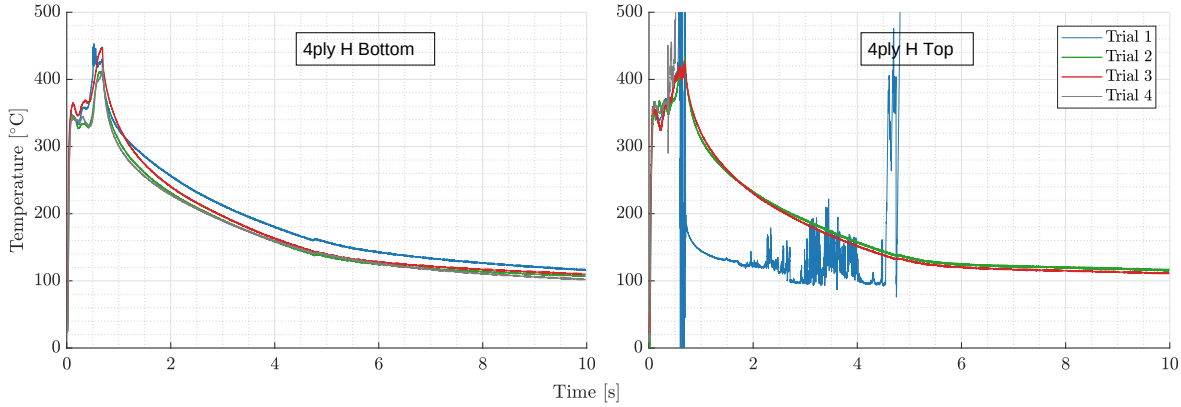

Figure B.3: Temperature measurements, embedded Kapton 4ply

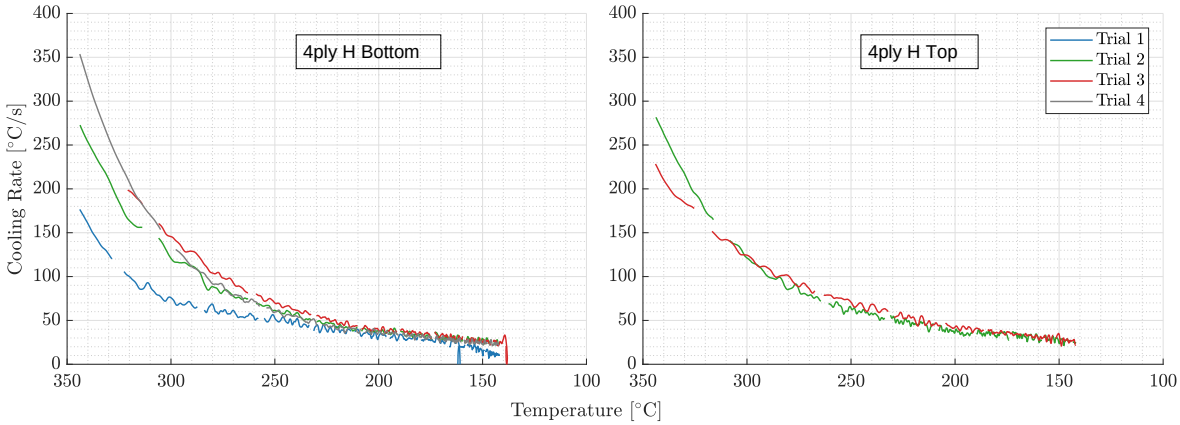

Figure B.4: Cooling rates, embedded Kapton 4ply

B.2 Removed Kapton

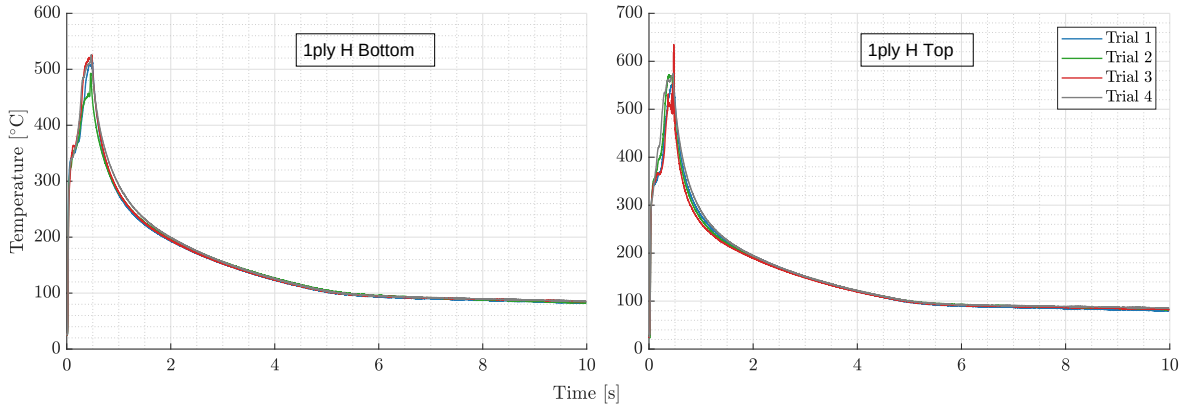

Figure B.5: Temperature measurements, removed Kapton 1ply

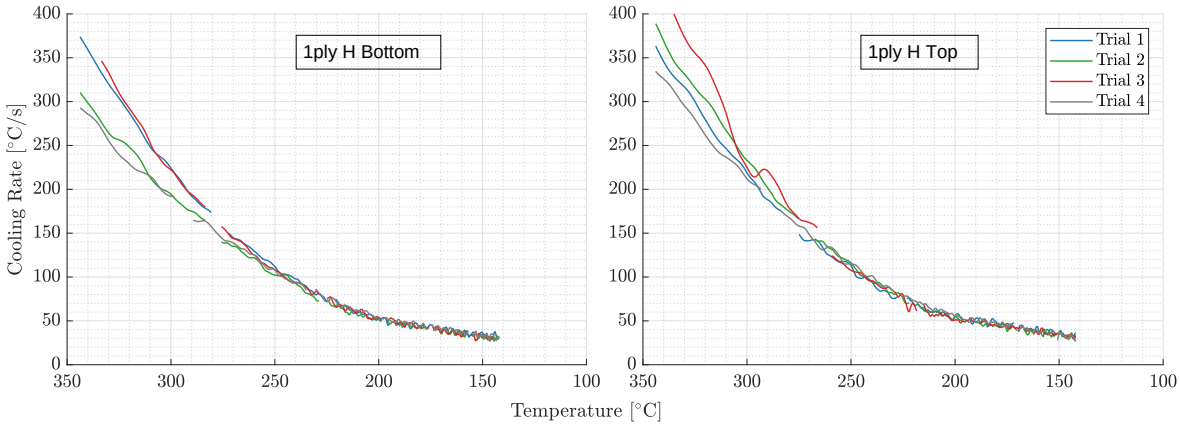

Figure B.6: Cooling rates, removed Kapton 1ply

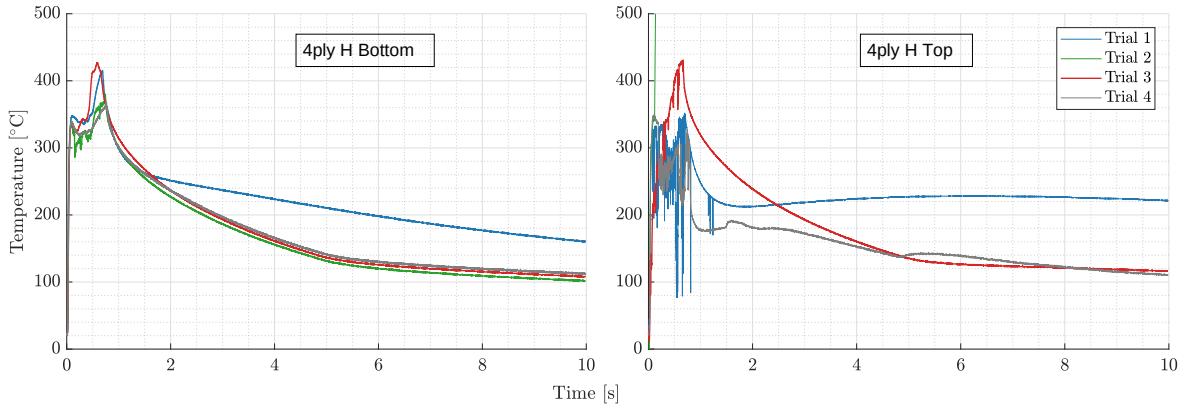

Figure B.7: Temperature measurements, removed Kapton 4ply

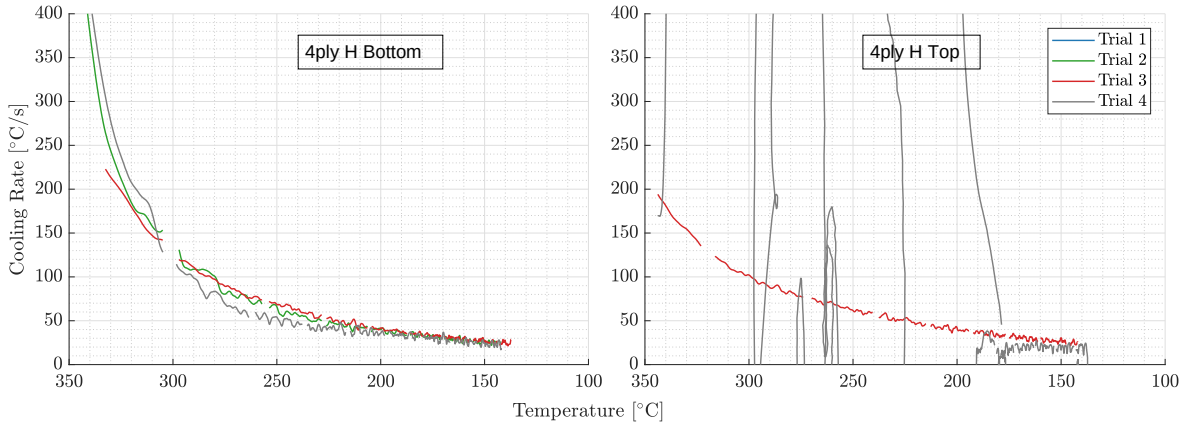

Figure B.8: Cooling rates, removed Kapton 4ply

B.3 Embedded Thermocouples

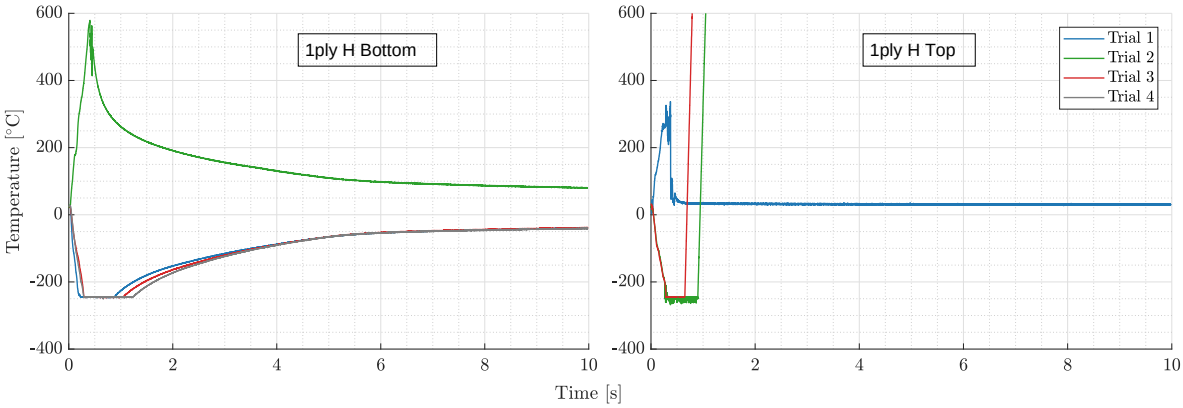

Figure B.9: Temperature measurements, embedded thermocouple 1ply

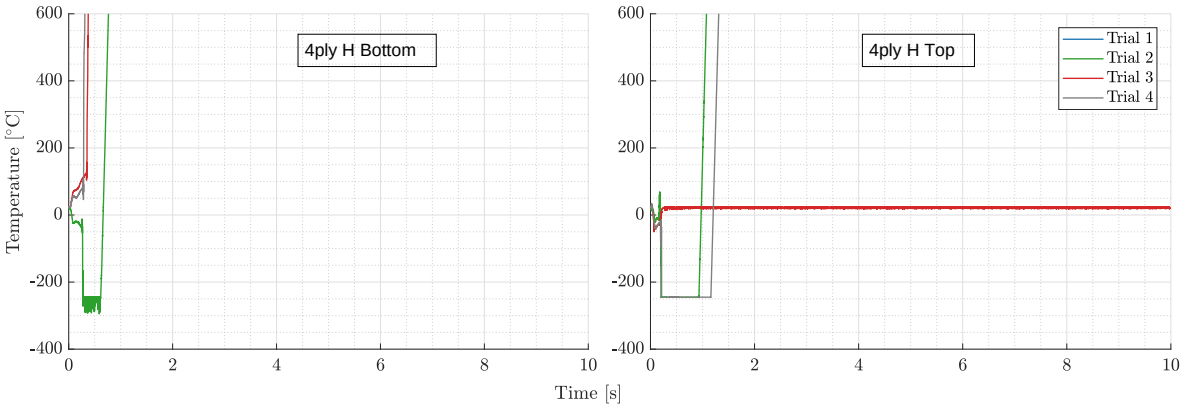

Figure B.10: Temperature measurements, embedded thermocouple 4ply